# NOVEL UWB ANTENNA DESIGNS WITH DOUBLE NOTCH FOR WLAN BAND REJECTION

## A DISSERTATION

*Submitted in partial fulfillment of the*
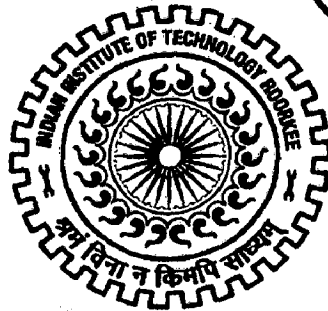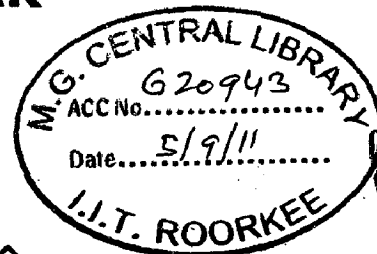*requirements for the award of the degree*
*of*

**MASTER OF TECHNOLOGY**

in

**ELECTRONICS AND COMMUNICATION ENGINEERING**
**(With Specialization in RF & Microwave Engineering)**

By

**S.THEEPAK**

**DEPARTMENT OF ELECTRONICS AND COMPUTER ENGINEERING**
**INDIAN INSTITUTE OF TECHNOLOGY ROORKEE**
**ROORKEE -247 667 (INDIA)**
**JUNE, 2011**

# Candidate's Declaration

I hereby declare that the work, which is being presented in the dissertation entitled, "NOVEL UWB ANTENNA DESIGNS WITH DOUBLE NOTCH FOR WLAN BAND REJECTION", which is submitted in the partial fulfillment of the requirements for the award of degree of *Master of Technology* in *RF & Microwave Engineering*, submitted in the Department of Electronics and Computer Engineering, *Indian Institute of Technology*, Roorkee (INDIA), is an authentic record of my own work carried out under the supervision of **Dr. S.N.Sinha**, HOD, Department of Electronics and Computer Engineering, Indian Institute of Technology, Roorkee.

I have not submitted the matter embodied in this dissertation for the award of any other degree or diploma.

Date: June 30, 2011

Place: Roorkee

(S.Theepak)

Enroll. No: 9533012

# Supervisor's Certificate

This is to certify that this dissertation entitled, "NOVEL UWB ANTENNA DESIGNS WITH DOUBLE NOTCH FOR WLAN BAND REJECTION", which has been submitted by S.Theepak is record of his own work carried out by him under my supervision. I also certify that the above statement made by the candidates is correct to the best of my knowledge and belief.

Date:   June 30, 2011
Place:   Roorkee

(Dr. S.N.Sinha)
HOD
E&CE Department
IIT – Roorkee
Uttaranchal – 247667
India

In this dissertation, we present several designs for a microstrip line monopole antenna and CPW fed monopole antenna.

First, a monopole antenna to cover the entire UWB band of 3.1-10.6GHz is designed. Different types of tapers are investigated to achieve the impedance match over the desired band. A parametric study of various dimensional parameters is carried out on CST Microwave Studio with the aim of understanding their effect on antenna characteristics. The operating principle of the antenna is studied based upon the H-field distribution over the antenna.

The UWB antenna interferes with WLAN frequency of 5.2 GHz (5150-5350 MHz) and 5.8 GHz (5725-5825 MHz). So UWB antenna with single notch centered at 5.5GHz and covering 5.1-5.8GHz is developed. The inherent disadvantage in this method is that frequency between 5.1GHz and 5.8GHz cannot be used for transmission. To avoid this, UWB antenna with double notches at 5.2GHz and 5.8GHz has been developed.

For UWB antenna with single notch, a T-shaped parasitic strip is introduced in the ground plane to reject the WLAN frequencies. Two cases of this antenna have been investigated by varying the distance between the parasitic strip and ground plane. When the distance between parasitic strip and ground plane is more, notch is sharp giving rise to increased ringing. In the second case where the distance is less, notch bandwidth increases and there is substantial reduction in the ringing.

Next, two band-rejection notches at 5.2GHz and 5.8GHz are introduced by combining two traditional band-notching techniques. In microstrip line fed monopole antenna, by combining a T-shaped parasitic strip in the ground plane and a CSSRR in the radiating patch, a double notch has been achieved. In CPW fed monopole antenna by combining a slot in the patch and a CSSRR on both side of the ground plane, a double notch has been achieved.

Performance of the proposed antenna has been investigated in both frequency and time domain. It is found that the antenna exhibits omnidirectional radiation in H-Plane, with a gain of 2-4dB except at the notch frequencies. It also exhibits low-level ringing and pulse distortion, making it suitable for UWB communication systems.

The antenna parameters have been optimized with CST MICROWAVE STUDIO and an NH9338 substrate of thickness 1.524mm and relative permittivity of 3.38 has been used in simulation as well as for the fabrication of the antenna.

# Table of Contents

# Table of Contents

# *Figures*

# Tables

# Introduction

## 1.1 Introduction

UWB systems transmit with very low power levels achieving power spectral density of -41.3dbm/MHz [1]. This low PSD facilitates the UWB spectrum to be overlaid on the spectra of other wireless systems without interference. In addition, UWB is unlicensed and can allow high data rates, thus claiming more attention in the wireless world.

The contemporary 3G technology and the near future 4G technology requires high data rates. The data rate, C of an Additive White Gaussian Noise (AWGN) channel as given by Shannon-Nyquist criterion is shown in equation 1.1 [2].

$$C = B \times log_2(1 + SNR) \qquad (1.1)$$

where B denotes the channel Bandwidth and SNR denotes the signal to noise ratio of the channel. In order to increase the data rate, the designer can boost up power and bandwidth. Since the PSD is limited to -41.3dBm/MHz, only bandwidth can be enhanced to provide with high data rates.

The Federal Communications Commission (FCC) allocated the 3.1-10.6GHz spectrum for UWB radio communication in February 2002. This huge bandwidth supports the high data rate. The FCC defines the term UWB as a communication system whose emissions have a fractional bandwidth ($B_f$) greater than 0.2 or occupy greater than 1.5GHz of spectrum [3].

$$B_f = \frac{B}{F_c} = 2 \times \left(\frac{F_h - F_l}{F_h + F_l}\right) \qquad (1.2)$$
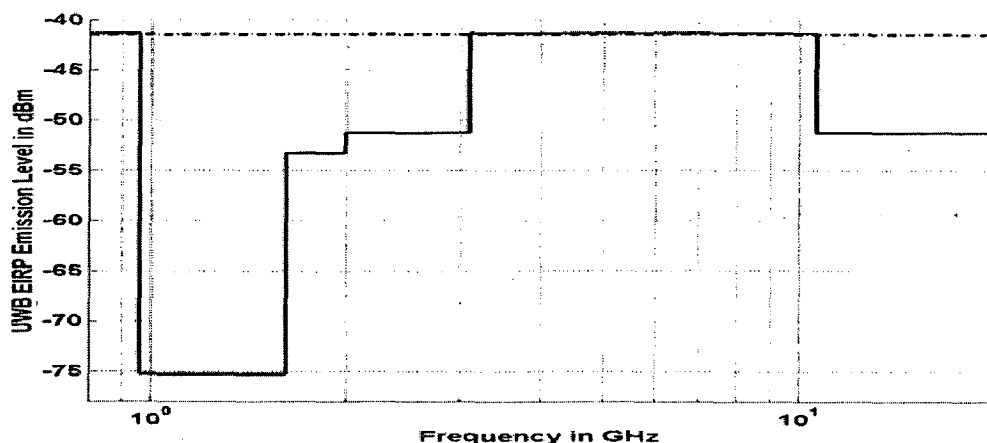


Figure 1.1 UWB Spectral Mask defined by the FCC [1]

where $F_c$ is the center frequency, $F_h$ is the highest frequency, $F_l$ is the lowest frequency and B is the total bandwidth. This bandwidth is measured between -10db points in the PSD curve of the radiated signal. The UWB spectral mask shown in Figure 1.1 has been defined by the FCC, allowing a maximum PSD of -41.3dBm/MHz in the UWB frequency band, to ensure peaceful coexistence of UWB and other wireless systems.

One problem with UWB systems is that their operation may interfere with WLAN operating bands which exist at 5.2 GHz (5150-5350 MHz) and 5.8 GHz (5725-5825 MHz). To overcome this problem a number of UWB Monopole antennas have been developed which reject the 5.1-5.8GHz frequency band. The common methods used to achieve band-notched characteristics include use of slots, such as, Inverted U-shaped [4] and complementary split ring resonator [5], in the patch and inserting a parasitic strip in the ground plane [6,7]. The main disadvantage of these schemes is that use of a single band-rejection notch results in the loss of precious spectrum of 700MHz, while the two WLAN bands use only 200MHz and 100MHz, respectively. Further, no information is available on the time-domain behaviour of most of these antennas, which is of considerable importance in UWB communication systems.

## 1.2 Motivation and challenges in UWB antenna design

The unsuitability of the conventional antenna design for UWB is explained below. Firstly, when the resonant antenna works at its resonant frequency, most of the power is radiated. But if the resonant antenna is fed with non-resonant frequency, a large portion of input power will reflected back to the feeding line.

Secondly, frequency independent antenna like log-periodic and spiral antennas offer large bandwidth (B.W,) but different frequency components are radiated from different parts of the antenna structure [8]. The phase center of the antenna keeps shifting, which causes dispersion. The conventional antenna design approach fails for wide impedance bandwidth. Thus new approach is needed to achieve wide impedance bandwidth.

Radiation pattern and gain must be stable over operating bandwidth. The UWB antenna needs extra characterization from the conventional antenna parameters such as high radiation efficiency since, the transmit power is very low. The dielectric and conductor losses should be kept low. Added to that, linear phase is required over the operating bandwidth to cause minimum pulse distortion.

The UWB antenna must be compact enough to fit inside the portable devices. The limitation of conventional antennas and the unique requirement of ultra-wideband antennas,

as described above, have put design challenges before the antenna designers which need to be overcome.

While only frequency domain behaviour of the antennas is important for narrow-band signal, the time domain behaviour becomes equally important for UWB antennas. Since UWB systems operate with very wide bandwidth, the antennas act as pulse shaping filters and have an important impact on system design which should take into account the characteristics of both source pulses and the transmitted and received pulses.

## 1.3. Historical review

While UWB technology may represent a hot research area at present, it certainly is not a new concept. Hertz found that an electric current oscillating in a conducting wire would radiate. He generated radio waves using spark gap apparatus in 1886. Hertz also tried to generate sine wave of particular frequency, but due to lack of proper technology his equipment radiated damped sinusoidal impulses that would be considered UWB by modern standards [9]. Of Hertz's antenna design, the parabolic reflector can be regarded as UWB and he laid the foundation to create UWB antenna. Hertz had used a wavelength of 66cm. In 1895, Jagadish Chandra Bose used spark gap apparatus to generate wavelength as short as 5mm [10]. He demonstrated in public on how to ring a bell using EM waves. Bose invented the first horn antenna which he called "collecting funnels" and is shown in Figure 1.2.
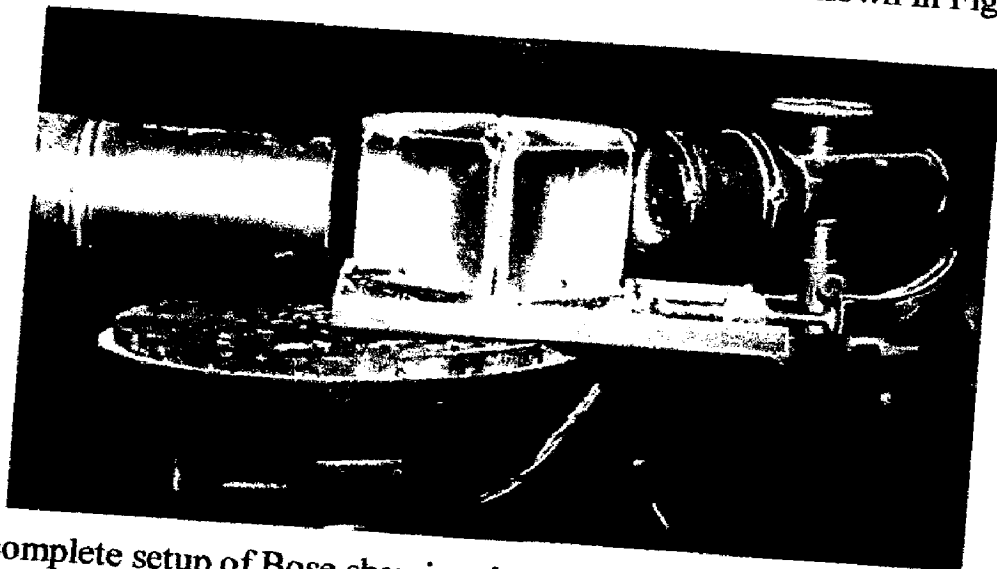


Figure 1.2 A complete setup of Bose showing the transmitting in the left and receiving Horn antenna in the right [10]

In 1939, Philip Carter rediscovered the Lodge's biconical antenna and conical antenna [9]. He incorporated tapered feed to Lodge's original antenna. Lindenblad gave a gradual impedance transformation to sleeve dipole to make achieve impedance matching. Later it was

3

used in television transmission. The radio corporation of America wanted to broadcast multiple channels from single location which used an array of Lindenblad's coaxial horn [9].

Schelkunoff investigated antennas with large shape like spherical antenna [9]. The large shape distributes current over a large area and so have low reactive energy. So antenna impedance is purely resistive and does not vary with frequency. The fundamental UWB principle- 'if the antenna is thick, change in reactance is small' is given by R.W.P King [9].

Rumsey found that if the shape of the antenna was completely specified by angles, its performance will be independent of frequency such as the infinite biconical dipole [8]. To make infinite structures more practical, the designs usually require that the current on the structure decreases with distance away from the input terminals [11]. After a certain point the current is negligible, and the structure beyond that point to infinity can be truncated and removed. The lower cutoff frequency is that for which the current at the point of truncation becomes negligible. The upper cutoff is limited to frequencies for which the dimensions of the feed transmission line cease to look like a "point".

Mushiake discovered that the product of input impedances of a planar electric current antenna (plate) and its corresponding 'magnetic current' antenna (slot) was a real constant [12]. Therefore, an antenna built in a complementary structure of electric and magnetic currents exhibits real constant impedance. This theory, referred as 'Mushiake's relation', has led to the development of a large family of self-complementary antennas with constant input impedance. Mushiake's relation has relaxed the condition for achieving ultrawide impedance bandwidth. However, it doesn't guarantee constant radiation patterns over the operation bandwidth.

## 1.4. Problem statement

The primary aim of this dissertation is to investigate novel designs for compact UWB antennas with good frequency domain and time domain performance. The entire problem considered in this dissertation can be broken up into the following parts:-

1. To design compact UWB monopole antennas using both microstrip line and coplanar waveguide feeds. This shall involve study of different impedance matching techniques to obtain size reduction and good time-domain behaviour.

2. To introduce band-rejection notches at 5.2GHz and 5.8GHz WLAN bands without affecting the frequency and time domain behaviour over rest of the UWB band

3. To verify the designs through extensive experimental investigations.

## 1.5 Organization of Dissertation

This dissertation is organized in five chapters as follows:

Chapter 2:      Various methods to increase the impedance bandwidth and to introduce notch in the UWB antenna have been studied. UWB antennas have been classified as monopole antennas, slot antennas, self complementary antennas and band notched antennas. Band notched antennas are again classified as single notch and double notch.

Chapter 3: In this chapter designs for microstripline-fed monopole antennas with and without notch have been proposed and studied in both frequency and time domain. The operating principle of the microstripline-fed monopole antenna without bandnotch has been explained with magnetic field distribution over the antenna.

Chapter 4: In this chapter designs for CPW-fed monopole antennas have been proposed and studied in both frequency and time domain. The operating principle of the CPW-fed monopole antenna without bandnotch has been explained with magnetic field distribution over the antenna.

Chapter 5: This chapter concludes about the research that has been done in this dissertation. Suggestions for future work are also given in this chapter.

# 2. Review of printed UWB antennas

Recent developments in UWB planar technology have been reviewed. Various methods to increase the impedance bandwidth and to introduce notch in the UWB antenna have been investigated. The UWB antenna can be classified based on geometry, radiation characteristics, feeding, notching method, self complementary, monopole, dipole and slot antennas. Based on geometry it can be classified as two-dimensional and three dimensional. For portable devices antenna size should be small and lightweight so planar antennas are preferable. Based on the application requirement, the radiation characteristics can be directional or omnidirectional. For directional radiation pattern, tapered slot antenna like Vivaldi antenna can be used.

## 2.1 UWB printed monopole antennas

The monopole achieves desired impedance bandwidth with omnidirectional radiation pattern and can be made compact. Initially the size of monopole was big and it was around 35×30mm [13]. Later bandwidth enhancement techniques like steps in the patch, notch in ground plane, slit in radiating patch and inserting slot in ground plane helped to achieve impedance matching at compactness. The effect of ground plane in UWB monopole has been explained with surface current distribution and the ways to reduce ground effect at lower frequencies have been discussed.

### 2.1.1 Rectangular monopole antenna with steps in the patch
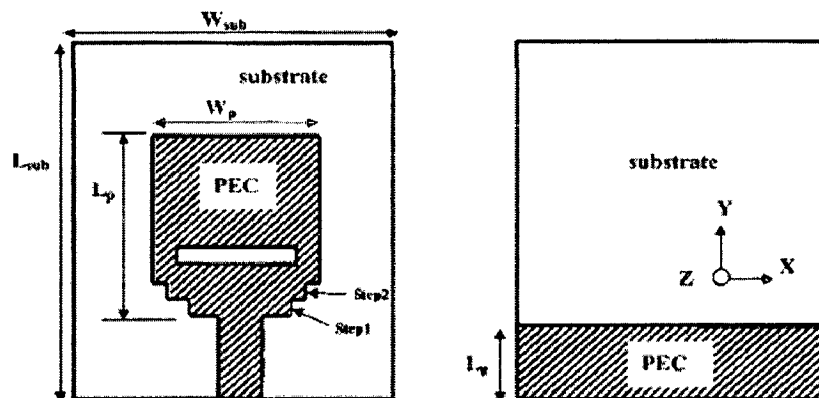


Figure 2.1 Geometry of rectangular monopole antenna [13]

The UWB antenna shown in Figure 2.1 consists of a rectangular patch with two steps, a single slot on the patch, and a partial ground plane. The impedance matching is enhanced by employing the following three techniques. The first technique comprises of the two steps in the radiating patch that is used to fine tune the impedance matching. The other techniques are the partial ground plane and the single slot on the patch. The operating bandwidth is from 3.2-12GHz and group delay variation is less than 0.5ns. The size of the antenna is 30×35mm.

## 2.1.2 Printed circular disc monopole antenna
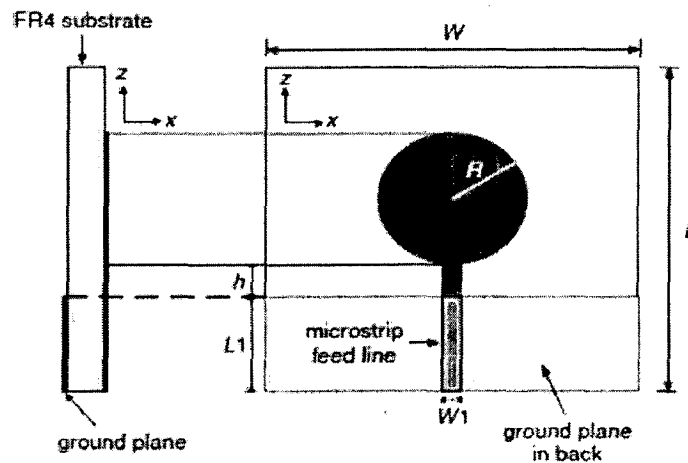


Figure 2.2 Geometry of printed circular disc monopole [14]

From the simulation results, it is observed that the operating bandwidth of the monopole shown in Figure 2.2 is critically dependent on the feed gap $h$ and ground plane width $W$. Both these parameters modify the input impedance of the antenna. By optimizing $h$ and $W$ impedance matching can be obtained over a wide bandwidth. The operating bandwidth is from 2.78-9.78GHz and the radiation pattern is similar to the traditional monopole. The size of the antenna is 42×50mm.

## 2.1.3 Impedance bandwidth enhancement techniques for monopole antenna

Impedance-matching is improved by introducing a pair of notches at the two lower corners of the square planar monopole [7]. By modifying the dimensions of the notches, the impedance bandwidth of the antenna can be enhanced. The dimensions of the antenna have an effect on the coupling between the planar monopole and the ground plane which can fine tune the impedance profile.
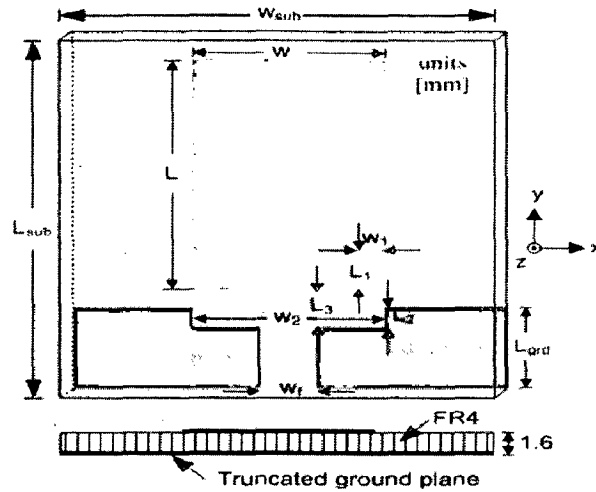
Fig. 2.3 Geometry of microstrip-fed monopole antenna with notch in the ground Plane [15]

The size of the monopole is further reduced by introducing notches at the ground plane to 16×18mm as shown in Figure 2.3. The operating bandwidth of the antenna is from 3.1-11GHz and monopole like radiation pattern is obtained. The ground plane with notch describes the broadband characteristics of the antenna as it provides matching between the patch and the feedline over the operating bandwidth. The notch creates a capacitive load that neutralizes the inductive nature of the patch. This counterbalances the reactive part and produces a nearly resistive input impedance [16].
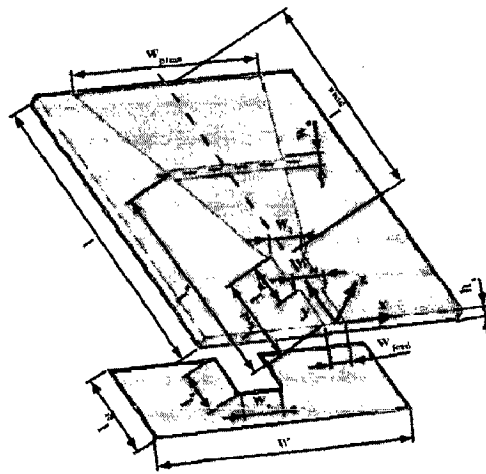


Figure 2.4 Geometry of tapered monopole antenna with slot in the radiating patch [17]

The bandwidth of monopole antenna can be further improved by inserting a slot in the radiating patch [17] as shown in Figure 2.4. The antenna shown has been implemented in Rogers RO3210 with dielectric value of 10.2 and has a dimension of 25×28.5×1.27mm. The effect of antenna performance in the presence of human hand has been observed to degrade the antenna performance.
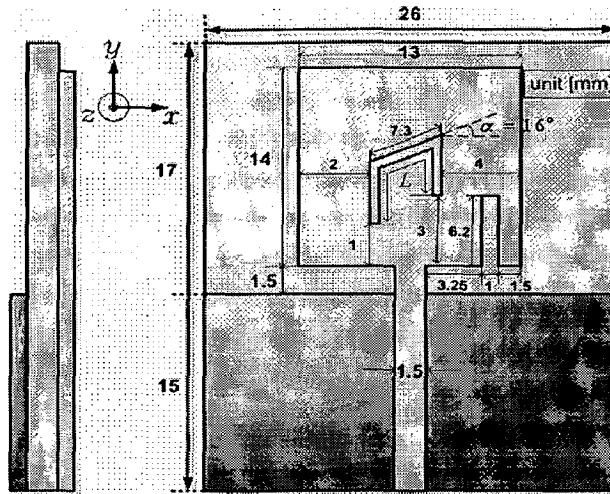
Figure 2.5 Geometry of an antenna with a narrow slit [18]

The narrow slit shown in Figure 2.5 in the radiating patch leads to an additional surface current path. The change in slit height causes a change in the current path. This causes the additional resonances to occur [18]. By optimizing the height of the slit, the largest impedance bandwidth can be achieved. The size of the antenna is 26×32mm and operating bandwidth is from 3-11GHz. Omnidirectional radiation pattern and gain of 5dB with a variation of 2.3dB is obtained other than notch band.
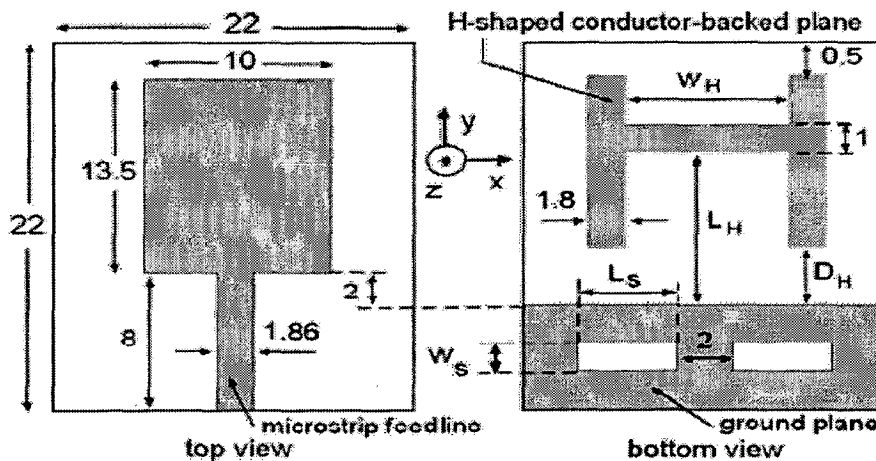


Figure 2.6 Geometry of the antenna with Defected Ground Plane (DGS) [19]

By inserting slots in the ground plane as shown in Figure 2.6, an additional current path is introduced. This slot affects the inductance and capacitance of the input impedance profile of the antenna. By changing the width and height of the slot, the reactive part can be neutralized, leading to improved bandwidth. The resonant frequency of the DGS structure is controllable by modifying the shape and size of the slot. The antenna has compact dimension of 22×22mm and operating bandwidth from 3.1-14GHz. Gain of the antenna is observed to varying around 4db.

9

## 2.1.4 UWB monopole with reduced ground effect
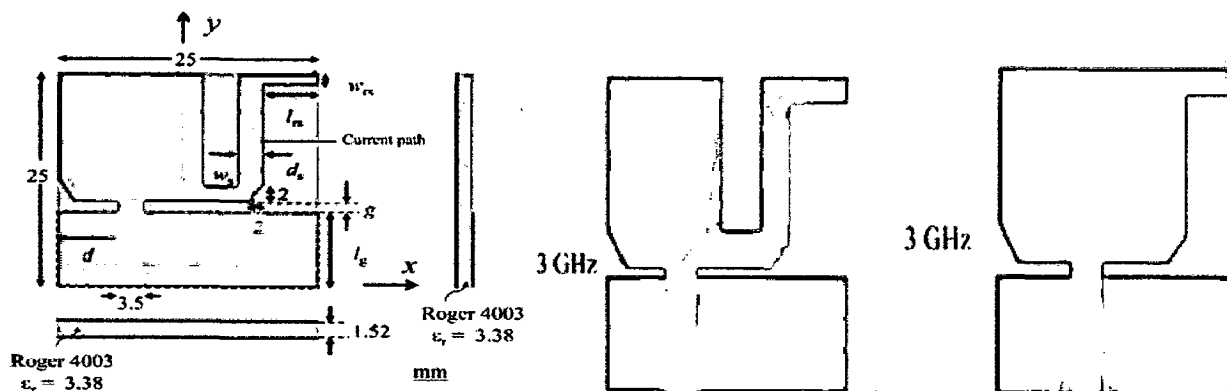


Figure 2.7 (a) Geometry of the antenna with notch in the radiator (b) Surface current distribution the antenna with notch in the radiator (c) Surface current distribution the antenna without notch in the radiator [20]

At 3GHz the surface current distribution for an antenna without the notch in the radiator is shown in Figure 2.7 (c). In Figure 2.7 (c) it is clear that electric current is concentrated around the feed line and so ground plane does not affect the impedance matching. In Figure 2.7 (b) for an antenna with a notch in the structure, it is seen that the surface current is concentrated at the notch. Thus ground plane does not affect the impedance matching at low frequencies [20]. The notched antenna has suppressed the ground plane effect at low frequencies over the conventional designs without notch. The size of the antenna is 25×25 and operating bandwidth is 2.9-11.6GHZ. The antenna provides three-dimensional omnidirectional radiation pattern with radiation efficiency of 75-95%.

## 2.1.5 Miniature hook-shaped monopole antenna
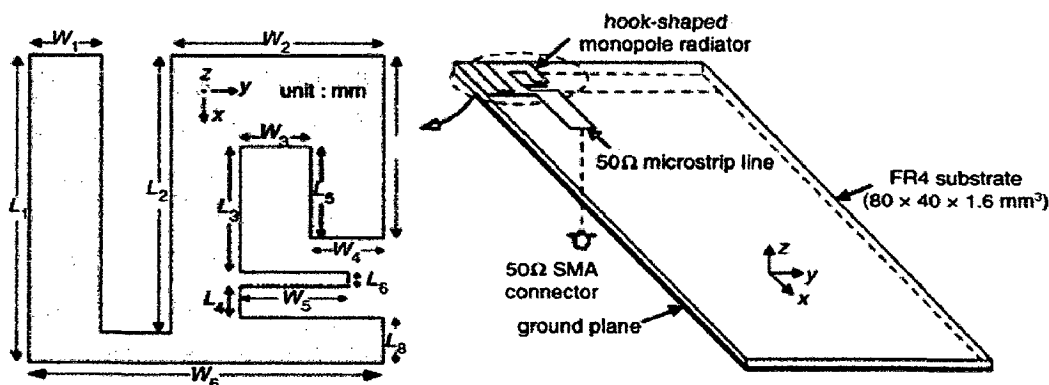


Figure 2.8 Hook shaped monopole antenna [21]

The UWB antenna consists of a hook shaped radiator with dimensions 10×10×1.6mm and operating bandwidth is from 3-10.7GHz. The multi-branch structure of

the antenna generates various resonant modes needed for broadband operation [21]. The resonant lengths of the antenna are about quarter-wavelength long. The lowest operating frequency $f_r$ is given in Equation 2.1 and L1 is given by Equation 2.2 [21].

$$f_r = \frac{c}{4L_1 \times \sqrt{\frac{\varepsilon_r + 1}{2}}} \tag{2.1}$$

$$L_1 = \frac{(L_2 + L_7 + W_2) + (L_3 + L_4 + L_5 + L_6 + W_3)}{2} \tag{2.2}$$

where c is the speed of light in free space, $\varepsilon_r$ is the dielectric constant and L1 is the average length of estimated outer and inner current paths. The gain of the antenna is 3-5dB. The group delay variation is less than 0.5ns.

## 2.2 Slot antennas

Slot antennas can be used when application requires less near field coupling. Vivaldi antenna is end-fire travelling wave tapered slot antenna. Circularly polarized slot antenna has been developed to reduce polarization mismatch losses. Multilayer Frequency selective surface reflectors are used along with slot antenna to increase the gain of the slot antenna.

By Booker's principle complimentary slot antenna can be derived from a planar dipole antenna. Booker derived the relationship between the impedance of a slot antenna and the impedance of its complimentary dipole. In order to get a slot antenna with an impedance of 50ohm, dipole antenna with 710ohm is designed [22]. By choosing the appropriate taper for the slot line of the Barne's antenna as shown in Figure 2.9, excellent matching can be obtained [22,23].
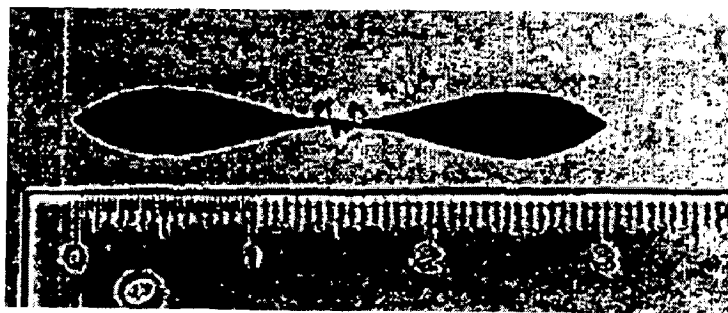


Figure 2.9 Barne's UWB magnetic slot antenna [23]

Slot antennas have reduced cable currents. Some applications require antenna with lesser near-field coupling. Magnetic antennas have less near-field coupling, as relatively large magnetic fields tend not to couple more strongly with near-by objects [23].

11

## 2.2.1 Tapered slot antenna
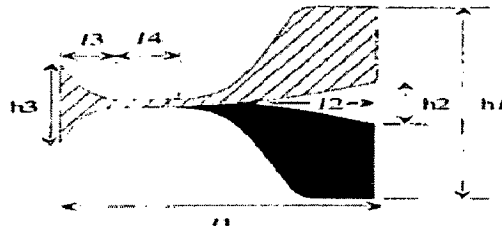


Figure 2.10 Geometry of Vivaldi antenna [24]

The Vivaldi antenna shown in Figure 2.10 is end-fire travelling wave antenna and at different frequencies, different parts of the antenna radiate. The operating bandwidth is limited only by the transition from the feeding transmission line to the slot line of the antenna, and by the finite dimensions of the antenna. Gazit has introduced the antipodal Vivaldi antenna to increase the bandwidth and has resolved the microstrip to slotline transition problem[25]. But it has very high level of cross polarization in the upper part of the frequency band [24]. The balanced antipodal Vivaldi antenna presented in Figure 2.10 has wide bandwidth with reduced amount of cross polarization. The impedance bandwidth is from 1.3-20GHZ and size of the antenna is 74×100mm.

## 2.2.2 A printed dipole antenna with tapered slot feed
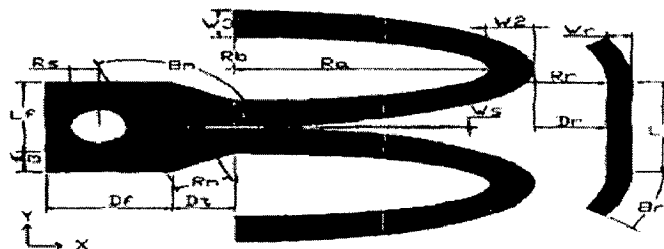


Figure 2.11 Geometry of UWB antenna With tapered slot feed [26]

The tapered slot antenna has inherent ultra-wide bandwidth and the dipole has omni-directional radiation in H-plane. The above two mentioned antennas are combined to form a novel antenna which shares ultra-wide bandwidth and omni-directional pattern. To obtain a quasi-omni-directional pattern, the direction of the outer half of the dual exponentially tapered strips are reversed [26] and elliptical shapes are used to smoothen the transition near the aperture. The strip in front of the aperture introduces an extra resonance in the low frequency range and acts as a reflector that spreads energy more evenly around. The geometry of UWB antenna with a microstrip line to slotline transition is shown in Figure 2.11.

## 2.2.3 Broadband cross-shaped microstrip-fed slot antenna
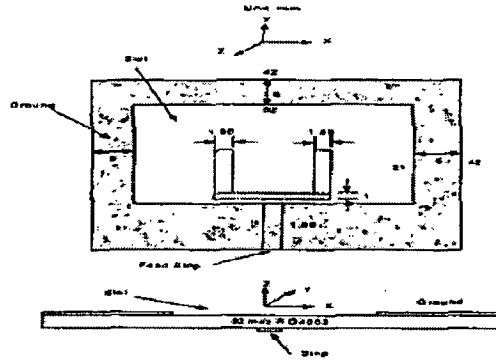


Figure 2.12 Geometry of wide slot antenna [27]

In Figure 2.12 a wide slot antenna with fork shaped microstrip feed is shown. The operating bandwidth is 2.5-11.3GHz. The wide slot has a quasi omnidirectional radiation pattern in azimuthal plane and radiation is vertically polarization. The 50ohm microstrip feed line with a fork-shaped tuning stub structure is printed on the opposite side of the substrate. The dimension of the fork-like tuning stub affects the coupling. Ultra wideband can be achieved by varying the coupling between the microstrip feed line and the printed wide slot which is realised by optimizing the dimensions of feed line [28]. The first resonant frequency depends on the antenna size. The placement of tuning stub can expand the upper frequency of bandwidth to higher frequencies. By optimizing stub size and shape, a wide impedance bandwidth can be achieved [29].

## 2.2.4 Circularly polarized

If Circularly polarized UWB antenna is used in transmitters and receivers, the loss due polarization mismatch can be reduced.

## 2.2.4.1 CPW-Fed circularly polarized square slot antenna with inverted-L strips
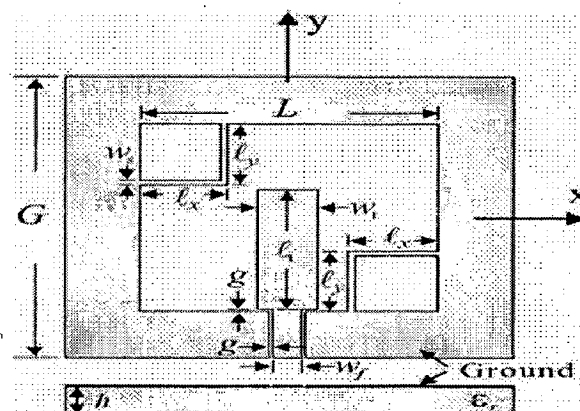


Figure 2.13 square slot antenna loaded by a pair of inverted-L grounded strips [30]

The Circularly polarized operation of the antenna is due to the two grounded inverted-L metallic strips placed around two opposite corners of the square slot [30] as shown in Figure 2.13. The inverted- L metallic strips will generate right- and left-hand circularly polarized (RHCP and LHCP) radiations in the +z and -z directions, respectively. Opposite-handed CP radiations can be generated if the two inverted-L strips are placed around the other two corners of the square slot. An axial ratio of < 3dB is achieved over 2-3GHz and fractional bandwidth of 52%. The measured gain is of 4dB with variation of 1dB.

## 2.2.4.2 Broadband CPW-fed circularly polarized square slot antenna
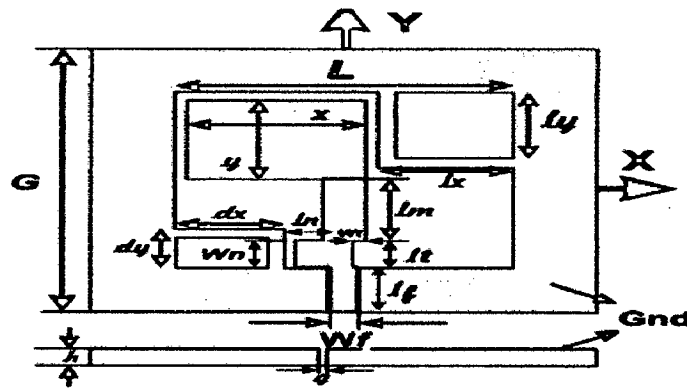


Figure 2.14 Geometry of the circularly polarized square slot antenna [31]

Two unequal-sized inverted-L strips positioned on two opposite corners are capable of generating a resonant mode for exciting two orthogonal E-vectors [30]. Improved Axial ratio Bandwidth (ARBW) can be obtained by optimizing the feed line with a rectangular patch and the inverted-L strips [31]. The above change in structure for improved ARBW, affects the impedance bandwidth and an improved impedance matching can be obtained by two tuning stubs embedded in the feeding structure. The ARBW of 2GHz is achieved and impedance bandwidth is 2.6-13.1GHz. The size of the antenna is quite high 60×60×0.8mm. The maximum gain is found to be 4.2dBi.

## 2.2.5 Enhanced gain by multilayer frequency-selective surface reflector
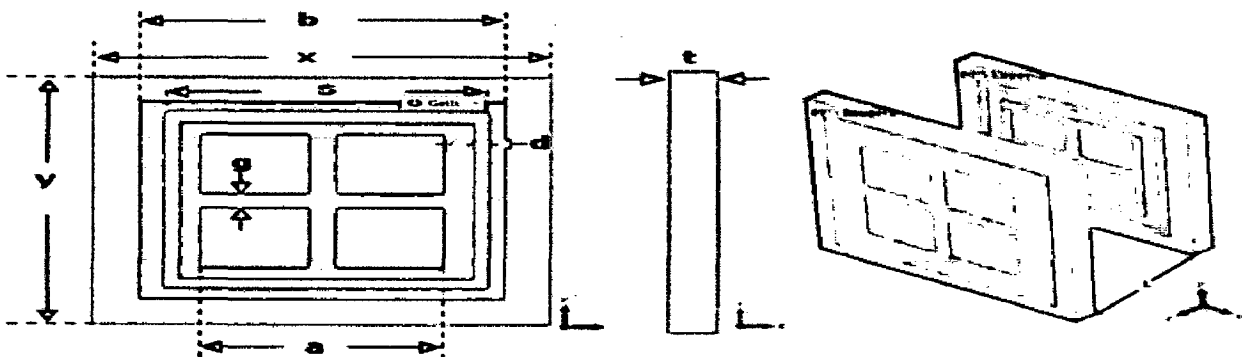


Figure 2.15 (a) Unit cell of second layer FSS [21]          (b).Multilayer FSS [21]
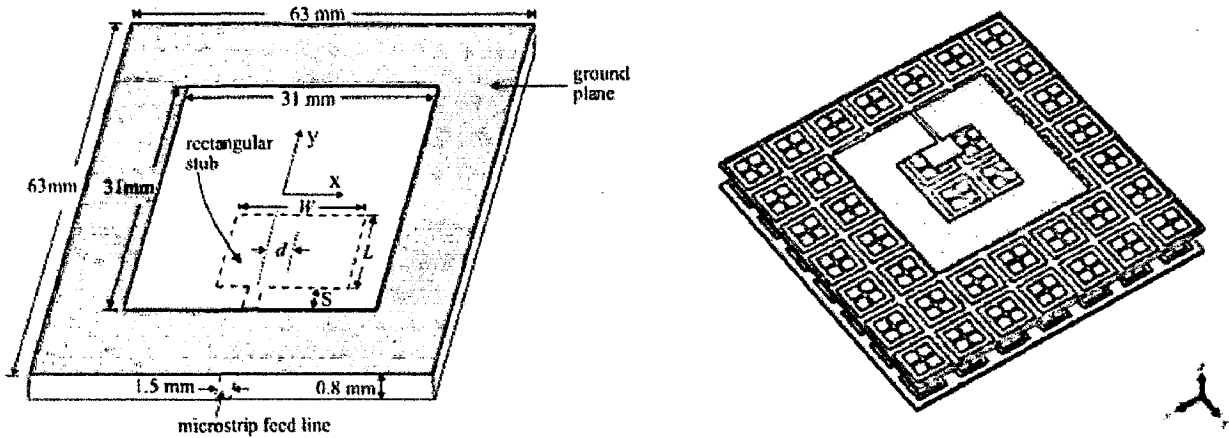
. Figure 2.16 (a) UWB square slot antenna[33]   (b) UWB square slot on FSS reflector[32]

Frequency Selective Surfaces (FSSs) shown in Figure 2.15 (a) and (b) allow significant control of the phase of reflection and transmission characteristics over a wide frequency band [32]. This can improve the gain and radiation properties of antennas. The stacked FSS shown in Figure 2.15 (b) can be mounted closer to slot antenna as shown in Figure 2.16 (a) without disturbing the impedance bandwidth. The unit cell of second layer FSS consists of cross dipole and first layer has additional slit. The FSS layer works from 4GHz to 12 GHz and the antenna is well matched from 3GHz-18.36GHz even after the insertion of FSS layer. The gain increases in the entire frequency band with maximum gain reaching 10.98dBi from the slot antenna gain of 6dBi without FSS.

## 2.3 Self complementary antennas

Babinet's Equivalence Principle [11] in optics states that when the field behind the screen with an opening is added to the field of complementary structure, the sum is equal to the field when there is no screen. Later booker generalized Babinet's principle by including polarization. The relation between the input impedance of a slot antenna $Z_S$ and that of a complementary wire antenna $Z_C$ is given by Equation 2.3 [34].

$$Z_S Z_C = \eta^2/4 \qquad (2.3)$$

In 1940s, Yasuto Mushiake derived a relation without any restriction to the slot or wire, to the design of arbitrarily-shaped complementary planar structures [12]. An antenna built in a complementary structure of electric and magnetic currents, exhibits real constant impedance. This theory, has led to the development of a large family of self-complementary antennas. However, it does not guarantee constant radiation patterns over the operation bandwidth.
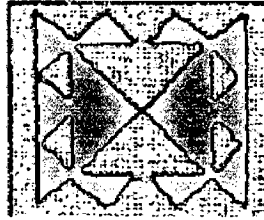
Figure 2.17 Self-complementary Sierpinski gasket[35]

The self-complementary ultra-wideband antennas shown in Figure 2.17 are implemented on low-loss resin materials. The self-complementary antenna impedance is matched to a 50ohm system by a 3-stage Chebyshev transformer over the UWB band.

## 2.3.1 Quasi self-complementary antenna
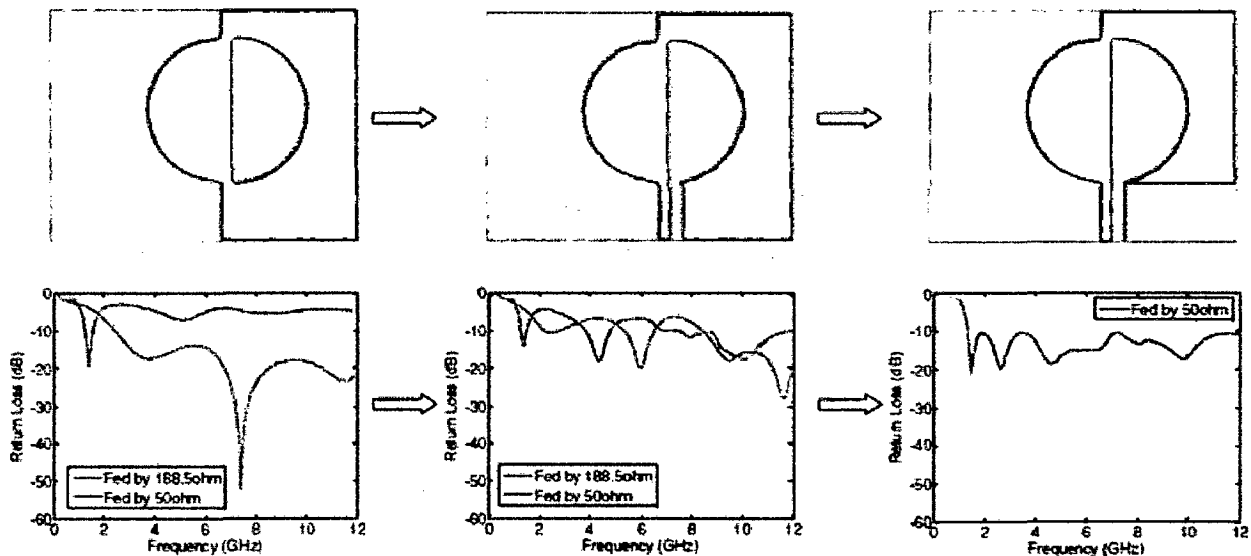


Figure 2.18 Impedance matching evolution of the quasi-self-complementary antenna [36]

The issue with a self complementary antenna is that, it needs an impedance matching network to match 188.5ohm to 50ohm. In Figure 2.18 (a) no matching section is attached to the self complementary structure. The antenna is fed by $188.5\Omega$ and $50\Omega$ characteristic impedances separately for observing S11. The return loss curves in Figure 2.18 (a) indicate that the antenna is matched to 188.5ohm and not to 50ohm. With a central strip of the matching section adhered to the half circular disc in Figure 2.18 (b), the impedance matching to the 50 $\Omega$ feed becomes better, however, the matching to the 188.5 $\Omega$ feed gets degraded. Finally, with the entire CPW-like matching section attached in Figure 2.18 (c), the return loss curve shows a good impedance matching to the 50 $\Omega$ feed over the UWB band. So impedance transformer is avoided by this method.

16

## 2.3.2 Miniature quasi self-complementary and tapered slot antenna
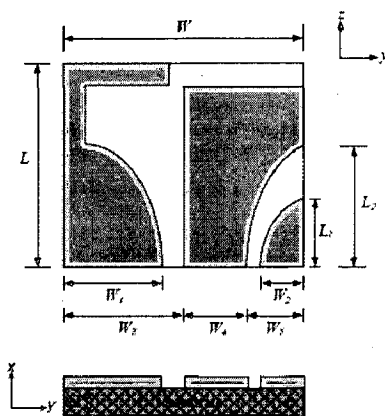


Figure 2.19. Geometry of miniature UWB antenna [37]

The antenna shown in Figure 2.19 has compact size of 19mm×16mm. Two miniaturisation techniques have been utilised i.e. the quasi-self-complementary structure and the tapered slot [37]. The tapered slot is formed by the arc of ellipses. The dimensions of the tapered slot are optimized to enhance the operating bandwidth. The impedance bandwidth is from 3GHz to 12GHz.

## 2.4 UWB band notched antennas

UWB antennas based on filtering of WLAN can be categorized as single notch, double notch and without filtering.

### 2.4.1 Single notch

The single notch is achieved by cutting U-slot in the patch, by narrowband resonating structure, spurline, $\lambda/4$ stub, parasitic strip in the ground plane, L-branches in ground plane and microstrip open-loop resonator.

### 2.4.1.1 Notching with inverted U-slot in the patch
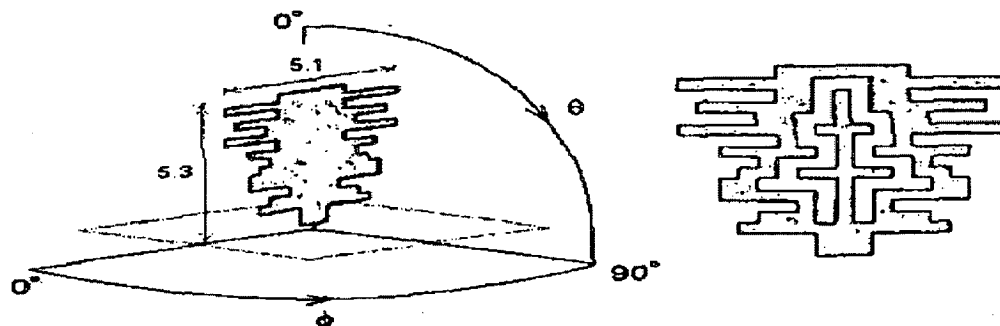


Figure 2.20 Geometry of the antenna with and without notch function [38]

17

The band-notching feature is created by removing portions of metal from the metal monopole as shown in Figure 2.20. The antenna's input impedance is nearly equal to zero at the notch frequency and it acts as an open-ended quarter wave transmission line. The currents flowing on either side of the gap are exactly out of phase at notch frequency. The notch frequency can be adjusted by changing the effective length of the gap.

### 2.4.1.2 By narrowband resonating structure
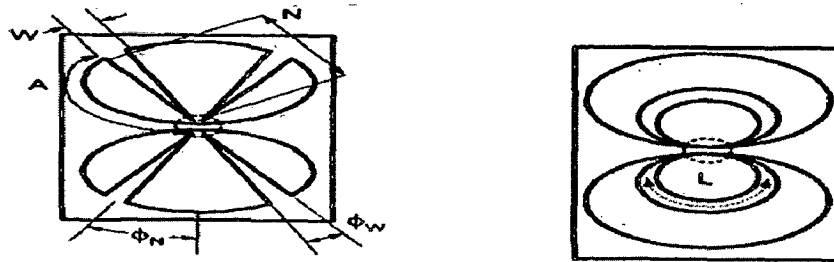


Figure 2.21 (a) Triangular notch in the antenna [39]     (b) Elliptical notch in the antenna[39]

By introducing narrowband structure in the antenna, certain frequency can be rejected. The notch frequency for Figure 2.21(a) is given by the A+N, where A+N is the half wavelength [39]. For the elliptical notch dipoles shown in Figure 2.21(b), the notch frequency is at which L is a half wavelength. The resonant frequency of half wave resonator is given by Equation 2.4 [40].

$$f_r = \frac{c}{2l}\sqrt{\frac{2}{\epsilon_r+1}}$$  (2.4)

where $c$ is the velocity of light, $l$ is the length of the resonator and $\epsilon_r$ is the relative permittivity of the substrate. The accuracy of resonant frequency calculation has been improved by extending the technique of Janaswamy and Schaubert [40].

### 2.4.1.3 Notching with spurline and with λ/4 stub
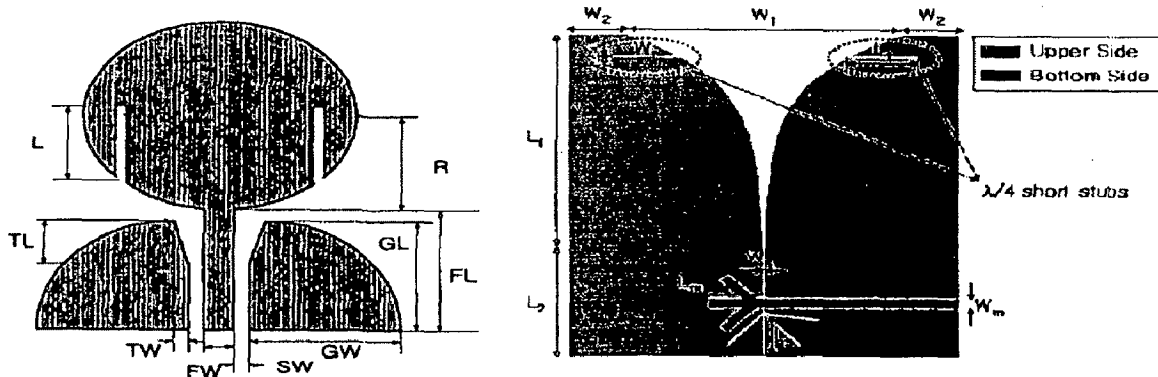


Figure 2.22 (a) Circular monopole with slits[41] (b) Tapered slot antenna with λ /4 stubs[42]

The two slits are inserted into the circular monopole as shown in Figure 2.22(a) for WLAN notching. The slit is the modified form of the spur line and acts as a band-stop filter [41]. The frequency band of 5.15-5.825GHz has been rejected. In another method , $\lambda$ /4 short stubs are inserted into tapered slot radiator .At Notched frequency, real part of the impedance is very high as 265 ohms, while the imaginary part is almost zero [42]. Thus $\lambda$ /4 short stubs act as a band-stop filter. The frequency band of 5.05-5.93GHz has been rejected.

## 2.4.1.4 Notching by parasitic strips in the ground plane
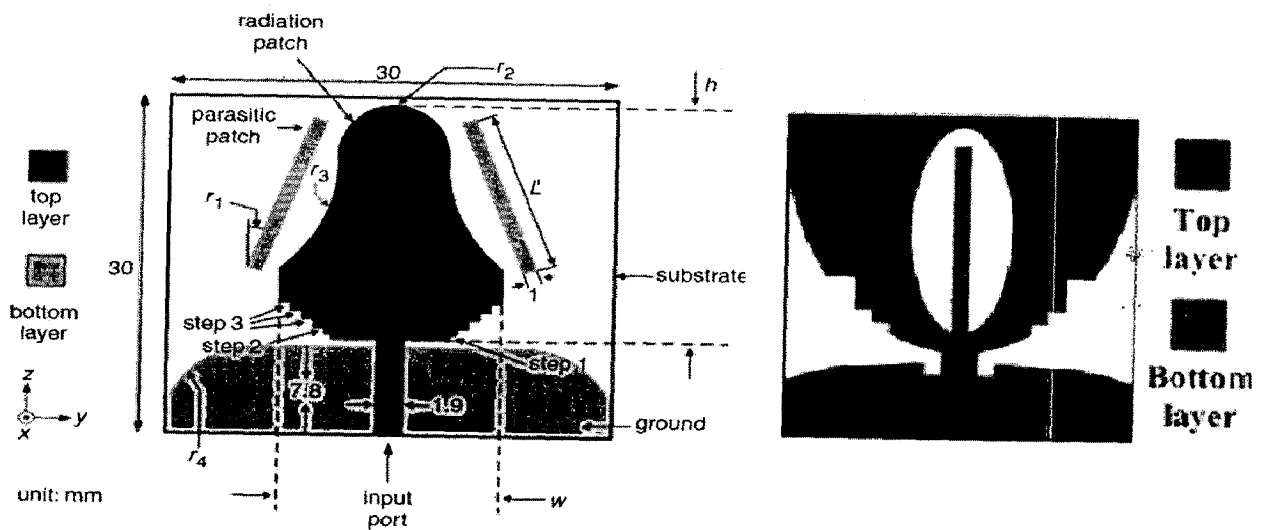


Figure 2.23 Notching with (a) Two Parasitic strip [43]    (b) Single Parasitic strip [6]

Notching is done by attaching two parasitic patches to the bottom layer of the antenna as shown in Figure 2.23(a). At the notching frequency, parasitic patch lengths correspond approximately to a quarter-wavelength. At the notch frequency, the current flows are more dominant around the parasitic patch, and they are oppositely directed between the parasitic patch and the radiation patch [43].

The single parasitic strip as shown in Figure 2.23(b) acts as a filter and improves impedance matching [6]. The distance between the parasitic strip and ground plane affects the impedance matching. The initial length of the parasitic strip is designed as quarter-wavelength of the notching frequency.

19

## 2.4.1.5 Notching by two T-shaped stub in the elliptical slot in the patch
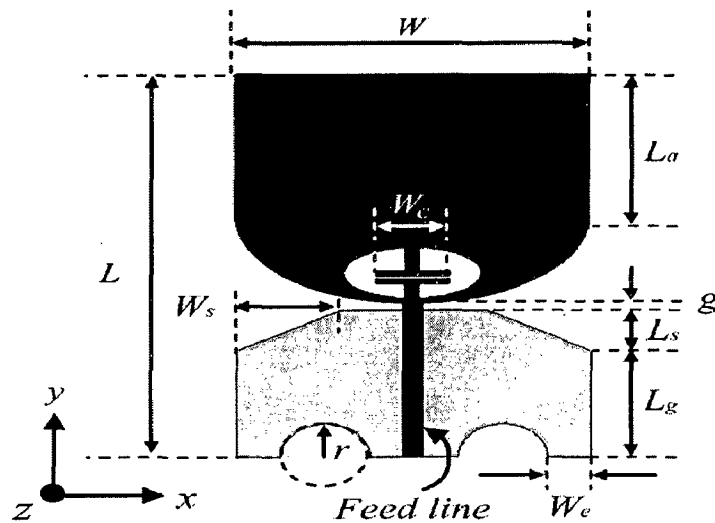


Figure 2.24 Geometry of an antenna with T-shaped stubs in the slot [44]

The notching is done by two T-shaped stubs as shown in Figure 2.24 which is equivalent to a parallel LC circuit [44]. The T-shaped stubs are placed inside an elliptical slot cut in the radiation patch. This approach provides a steeper rise in VSWR curve at the notch frequency.

## 2.4.1.6 Notching Using L-branch in the ground plane
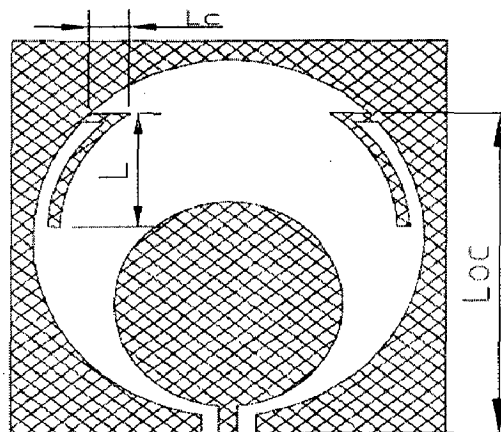


Figure 2.25 Geometry of the Antenna with L-Branch [45]

The L branch length can be easily changed to get different band-notching frequency. In this antenna, the L branch is connected to the ground and it is different from other frequency rejecting techniques likes U-slot, T -branch in the radiating element as point connecting to the ground can change in big range. L + Lc is about one quarter wave length of the band-notched frequency [45]. It provides notching at 5.8GHz.

## 2.4.1.7 Band-notched UWB antenna by incorporating a microstrip open-loop resonator
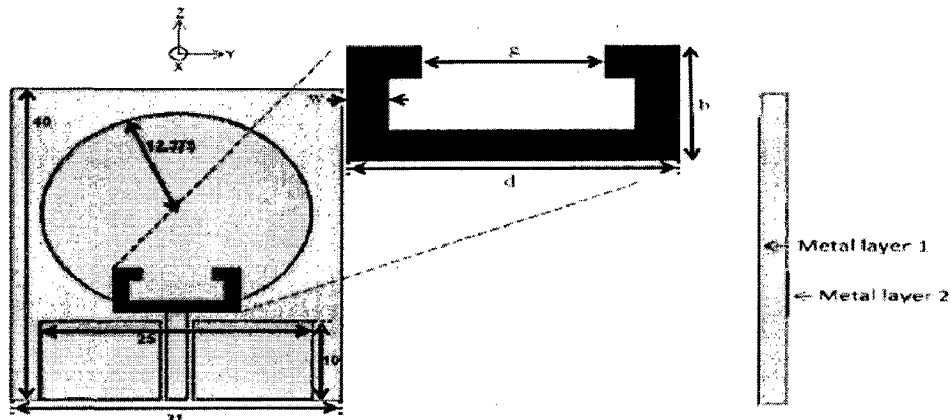


Figure 2.26 Geometry of UWB Antenna with Microstrip Open-Loop Resonator [46]

The filter design methods and the UWB antenna design methods have been growing tremendously in separate manners. So the filter and UWB antenna design are designed separately and combined together. A microstrip open loop resonator is combined with UWB antenna as shown in Figure 2.26. This antenna provides notching at 5.1GHz. Radiation pattern are consistent over operating bandwidth.

## 2.4.1.8 Novel coupling bandnotched filter
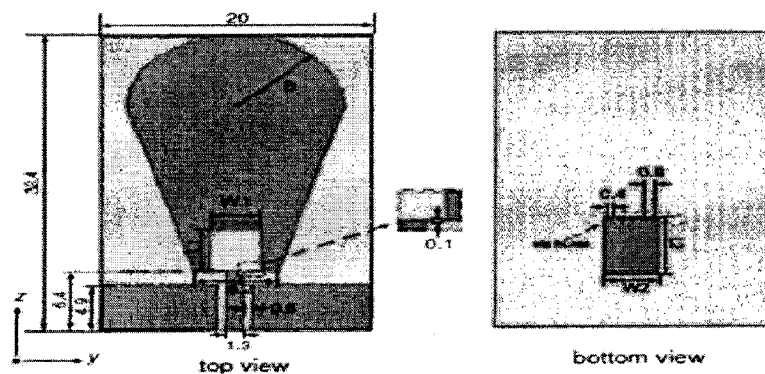


Figure 2.27 Geometry of UWB antenna with coupling bandnotched filter [47]

An UWB monopole antenna with a novel coupling bandnotched filter is shown in Figure 2.27. The filter consists of a smaller rectangle slot in the metallic radiation patch and a bigger rectangle added on the back ground plane. By a row of metallic via holes, the top and bottom metallic layers are connected. The filter is equivalent to a series LC circuit which is connected across the feed line and the radiation patch in parallel [47]. The frequency band of 4.84-6.12GHz has been notched. Excellent transient response is achieved.

21

## 2.4.2 Double notch

Most of the above discussed techniques of a single-notch antenna have a wide notch-band width that covers the whole 5–6-GHz band with notch frequency around 5.5 GHz. The useful frequencies between the 5.2- and 5.8-GHz WLAN bands are thus wasted. This provides motivation to design a dual-notch antenna to reject the 5.2- and 5.8-GHz interference bands. The strong coupling between the 5.2GHz and 5.8GHz resonator has to be overcome.

### 2.4.2.1 Double notch using electromagnetic-bandgap structures
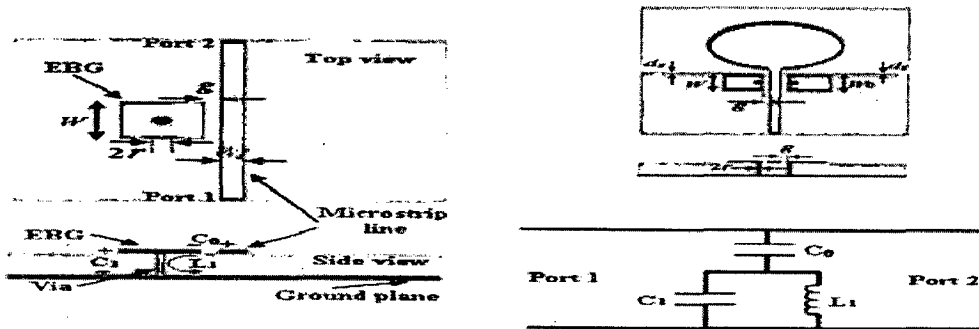


Figure 2.28 (a) Centre-located vias mushrom-type EBG (b) Equivalent model (c) Two edge-located vias mushroom-type EBG on either side of the microstrip feedline [48]

EBG structures are placed on different sides of the microstrip fed line, creating a weaker coupling between the two EBG structures. By using two edge-located vias, mushroom-type electromagnetic bandgap (ELV-EBG) structures at different sides of the microstrip line with different size, WLAN frequency can be rejected. The fabrication is complex and the notched frequency deviation percentage is from 5.3% to 6.4% [48].

### 2.4.2.2. Double notch with co-directional spilt ring resonator
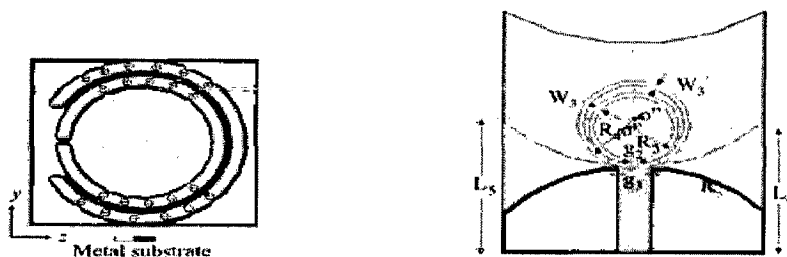


Figure 2.29 (a) Co-directional SRR [49]      (b) Antenna with co-directional SRR [49]

When the inner ring is placed along the same direction as the outer ring as shown in Figure 2.29 (a), the capacitance coupling between the rings decreases drastically [49]. Thus, the co-directional SRR can exhibit dual distinct fundamental magnetic resonance frequencies for each ring. Measured dual notched bands are 4.85-5.35 GHz and 5.65–6.08 GHz.

# 3. Microstripline-fed monopole antennas with Klopfenstein taper

In this chapter, we present several designs for a microstripline-fed monopole antenna.

First, a monopole antenna to cover the entire UWB band of 3.1-10.6GHz is designed. Different types of tapers are investigated to achieve the impedance match over the desired band. A parametric study of various dimensional parameters is carried out on CST Microwave Studio with the aim of understanding their effect on antenna characteristics.

The operating principle of the antenna is studied based upon the H-field distribution over the antenna. It is observed that at the low frequency end of UWB spectrum, standing wave dominates. When the frequency is increased, a hybrid mode of travelling wave and standing wave appears over the antenna. As the frequency is increased towards the high-frequency end of UWB spectrum, travelling wave dominates except at the top of the antenna structure.

Secondly, a monopole antenna with a band-rejection notch covering the frequency range of 5.2-5.8GHz is designed. The effect of notch bandwidth on antenna performance has been discussed. The tradeoff between notch bandwidth and ringing effect is highlighted with the simulated results.

Next, two band-rejection notches at 5.2GHz and 5.8GHz are introduced by combining two traditional band-notching techniques. By combining a T-shaped parasitic strip in the ground plane and a Complementary Single Split Ring Resonator (CSSRR) in the radiating patch, a double notch has been achieved. As opposed to the conventional single band-rejection notch antennas, the frequency band between 5.2 and 5.8GHz can also be used for transmission. Performance of the proposed antenna has been investigated in both frequency and time domain.

The antenna parameters have been optimized with CST MICROWAVE STUDIO and an NH9338 substrate of thickness 1.524mm and relative permittivity of 3.38 has been used in simulation as well as for the fabrication of the antenna.

## 3.1 Antenna without band-notched function
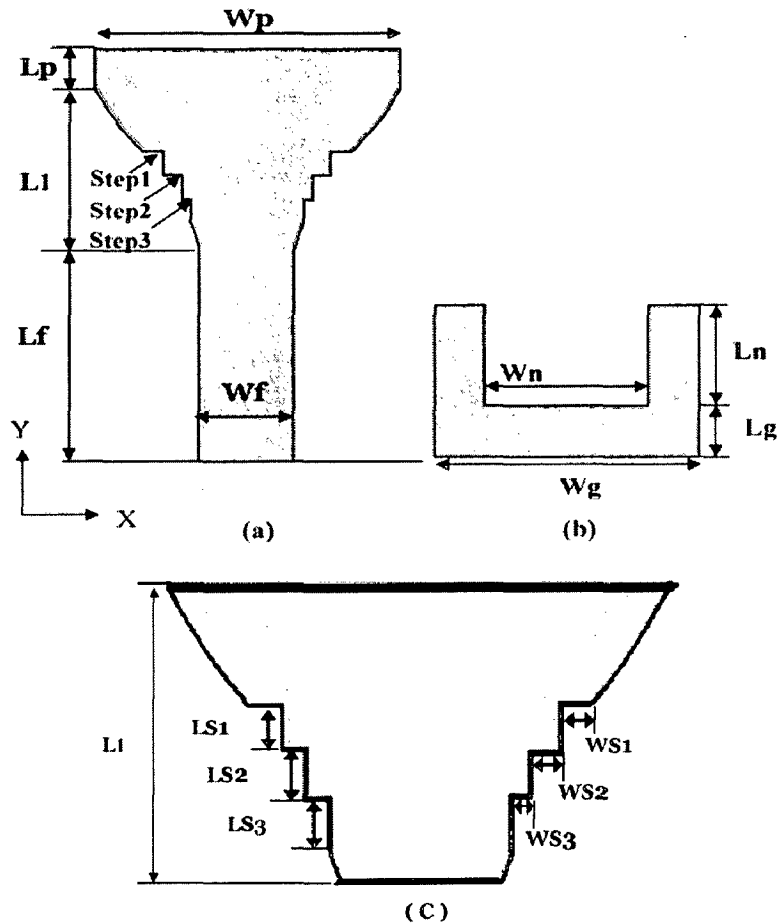


Figure 3.1 Geometry of the antenna without band-notched function (a) front side (b) back side (c) Klopfentstein taper with steps

Figure 3.1 shows the proposed antenna without band notch function. The radiating structure consists of a rectangular patch of size Lp×Wp and a tapered transition of length L1. Different types of tapers like linear, exponential and Klopfenstein taper were examined to connect the rectangular patch and the feed line, so as to improve the matching of the antenna over the operating bandwidth. Steps have been introduced in the taper as shown in Figure 3.1 (c). LS1, LS2, and LS3 denote the length of step1, step2 and step3 respectively. WS1, WS2 and WS3 denote the width of step1, step2 and step3 respectively. Lf and Wf denote the length and the width of the feed line, respectively. The NH9338 substrate of thickness $h$ =1.524 mm and $\varepsilon_r$ = 3.38 has been used. The width of the microstrip feed line Wf is fixed at 3.463mm in order to achieve 50 Ω impedance. The combined length of Ln with Lg gives the length of the ground plane. Wg denotes the width of the ground plane. Ln and Wn denote the width and the length of the notch of the ground plane ( Figure 3.1 (b)).

24

Keeping the width *Wp* constant and increasing *L1*, it is observed that the greater the value of *L1*, the smoother is the transition. However if we continue to increase *L1*, the electric coupling between the lower side of the patch and the upper side of the ground becomes poor, affecting the overall impedance matching.

## 3.1.1 Design analysis

The resonant length of a microstrip patch can be obtained by using simple relations of the effective relative dielectric constant represented as a function of the substrate parameters and the operating frequency [11]. As the patch has a partial ground plane on the other side of the substrate, the Equation of the effective dielectric constant is modified. The modified Equation is analogous to the Equation of a microstrip structure with infinite ground plane, but with a different multiplication coefficient A for the term h /W. Eqns 3.1-3.5 [50] were used to obtain an initial estimate of length Lp and width Wp of the antenna.

$$\varepsilon_{eff} = \frac{\varepsilon_r+1}{2} + \frac{\varepsilon_r-1}{2}\left[1 + A\frac{h}{W}\right]^{\frac{-1}{2}} \qquad (3.1)$$

where $\varepsilon_r$ is the permittivity of the substrate and h is the height of the substrate and $A$ is the new multiplication coefficient. The remaining Equations used to design a patch antenna are given below.

$$Wp = \frac{c}{2f}\sqrt{\frac{2}{\varepsilon_r+1}} \qquad (3.2)$$

$$L_{eff} = \frac{c}{2f\sqrt{\varepsilon_{eff}}} \qquad (3.3)$$

$$Lp = L_{eff} - 2\,\Delta L \qquad (3.4)$$

$$\Delta L = 0.5h \qquad (3.5)$$

where *c* is the speed of light in free space. By simulating different patches with different substrate parameters, one can determine an appropriate value for the multiplication coefficient *A* which is found to be 11.25 [50]. In the present design, the operating frequency *f* Equation (3.2) and (3.3) is assumed to be the center frequency of the UWB range (6.85 GHz). For this operating frequency and afore-mentioned substrate parameters, the dimensions of the patch would be *Wp* =14.79mm and *Lp* =12.56mm. Two variations are introduced on this patch to enhance its operating bandwidth. The first one is to introduce a taper between the radiating patch and the microstrip feed line. The second modification is to insert a U-shaped notch in the ground plane.

The impedance matching can be done with tapers like linear, exponential and Klopfenstein taper [51]. After investigating various types of tapers, the Klopfenstein taper was found to give the best impedance match over the desired bandwidth. The Klopfenstein taper has been drawn with the RF utilities given in MATLAB [52]. The program matches load impedance $Z_{load}$ to the characteristic impedance of the feed line Zo, using Klopfenstein taper. The impedance corresponding to Wf and Wp are 50$\Omega$ and 20.9$\Omega$, respectively. Wp and Wf correspond to Z0 and Zl respectively, in the program. The number of sections N to approximate the taper was taken to be 100. The passband ripple R (dB) is taken to be -30dB. The MATLAB code for Klopfenstein taper is given in Appendix. The output of the program consists of impedance variation as a function of distance as shown in Figure 3.2.
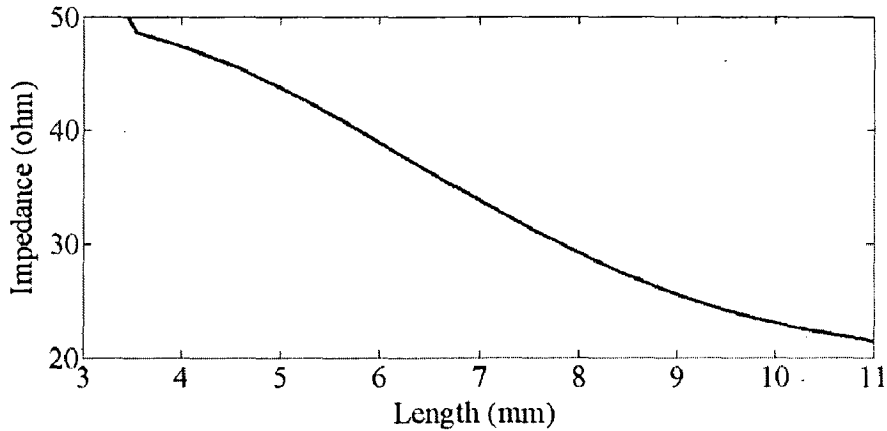


Figure 3.2 Variation of impedance with respect to the length for Klopfenstein Taper

Later, the impedance value given by the output of program is converted to corresponding length of microstrip line by using Eqns 3.6-3.8[51].

$$\frac{W}{d} = \begin{cases} \frac{8e^A}{e^{2A}-2} & \frac{W}{d} < 2 \\ \frac{2}{\pi}\left[B - 1 - \ln(2B - 1) + \frac{\epsilon_r-1}{2\epsilon_r}\left\{\ln(B - 1) + 0.39 - \frac{0.61}{\epsilon_r}\right\}\right] & \frac{W}{d} > 2 \end{cases} \quad (3.6)$$

$$\text{where,} \quad A = \frac{Z_0}{60}\sqrt{\frac{\epsilon_r+1}{2}} + \frac{\epsilon_r-1}{\epsilon_r+1}\left(0.23 + \frac{0.11}{\epsilon_r}\right) \quad (3.7)$$

$$B = \frac{377\pi}{2Z_0\sqrt{\epsilon_r}} \quad (3.8)$$

where $W$ is the width of the microstrip line and A and B are constants given by Eqn 3.7 and 3.8, respectively. A MATLAB code is written for Eqn 3.6 and input to the program is impedance. The output of the program is the width of the microstrip line and it is shown in Figure 3.3.
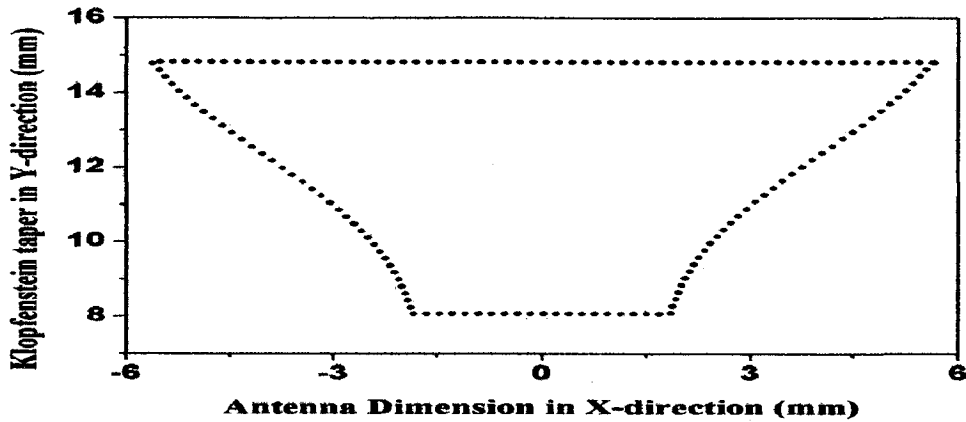
Figure 3.3 Klopfenstein taper structure connecting feedline and radiating patch

## 3.1.2 Effect of various parameters on antenna's performance

The performance of microstripline-fed antenna is quite sensitive to various parameters like patch length Lp, notch width Wn and notch length Ln of ground plane and feed gap (Lf-Ln-Lg). The various parameters affect the impedance matching at different frequencies. A parametric study was carried out by varying one parameter at a time, keeping other parameters constant.

## 3.1.2.1 Effect of variation in the length of the patch, Lp

Figure 3.4 illustrates the magnitude of S11 for different values of the length Lp. The other dimensions of the antenna were kept constant and are given in Table 3.1.

Table 3.1 Parameters of the antenna with Lp as a variable

| Parameters | Lf | L1 | Lg | Ln | Wp | Wg | Wn | Wf |
|---|---|---|---|---|---|---|---|---|
| Value(mm) | 8.075 | 6.75 | 2 | 5 | 11 | 11 | 7 | 3.463 |
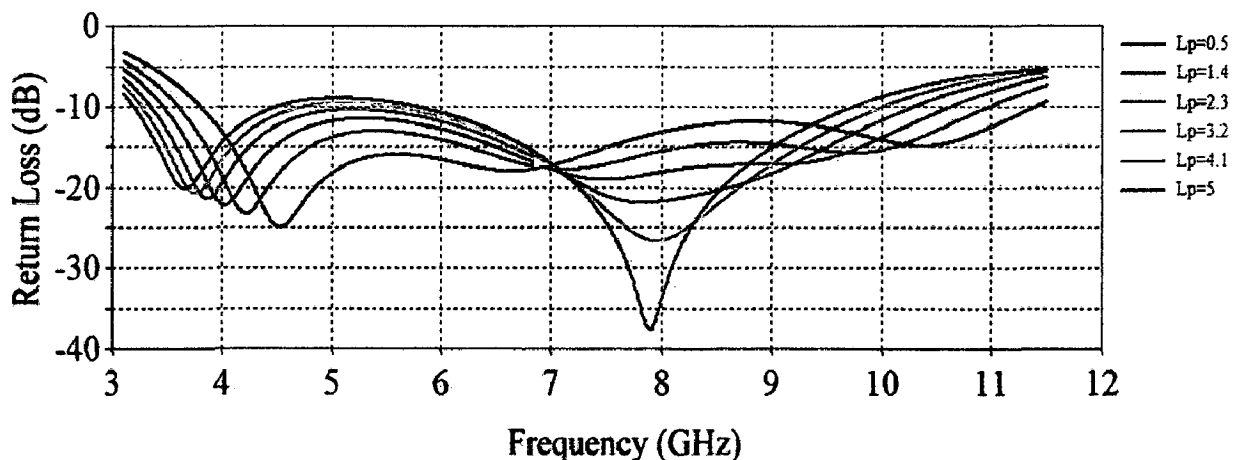


Figure 3.4 Variation of |S11| with Lp

Lp is an important parameter as it affects the overall length of the patch antenna. The overall length of the patch antenna decides the first resonant frequency. As Lp increases, the first resonant frequency shifts toward the left. Further increase causes impedance mismatch around 5GHz and 10.6GHz. The optimized value of Lp has been found to be 1.675mm.

### 3.1.2.2 Effect of variation in the notch width of the ground plane, Wn

Figure 3.5 illustrates the magnitude of S11 for different notch widths of the ground plane Wn. The other dimensions of the antenna were kept constant and are given in Table 3.2.

Table 3.2 Parameters of the antenna with Wn as a variable

| Parameters | Lf | Ll | Lp | Lg | Ln | Wp | Wg | Wf |
|---|---|---|---|---|---|---|---|---|
| Value(mm) | 8.075 | 6.75 | 1.675 | 2 | 5 | 11 | 11 | 3.463 |
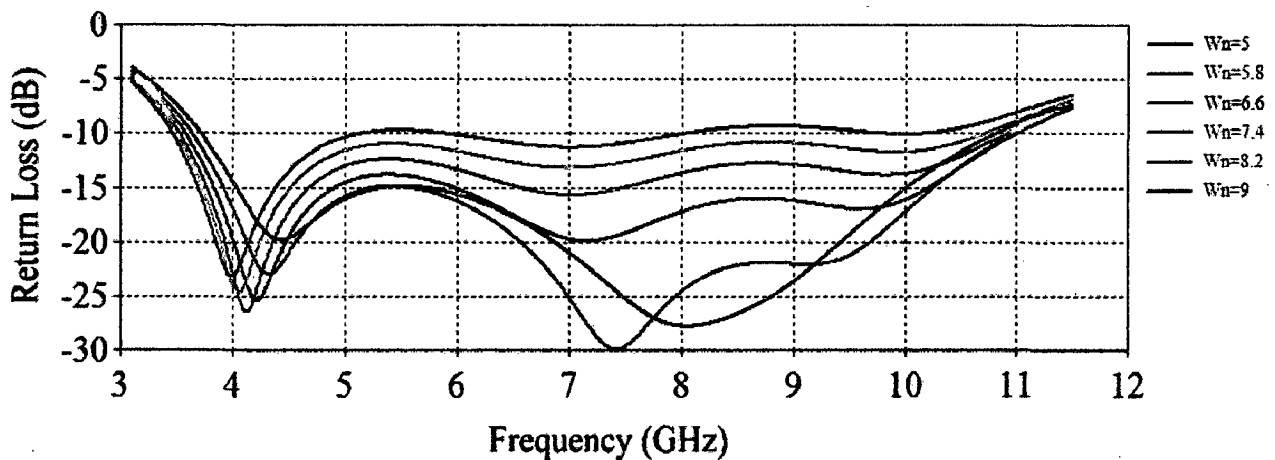


Figure 3.5 Variation of |S11| with Wn

The notch in the ground plane creates a capacitive load that neutralizes the inductive nature of the patch to produce an impedance match over a larger bandwidth [4]. As Wn increases, the first resonant frequency shifts toward the left. Further increase causes impedance mismatch in the frequency range of 5GHz-10.6GHz. The optimized value of Wn has been found to be 6.654mm.

### 3.1.2.3 Effect of variation in the notch length of the ground plane, Ln

Figure 3.6 illustrates the magnitude of S11 for different notch lengths of the ground plane Ln. The other dimensions of the antenna were kept constant and are given in Table 3.3.

Table 3.3 Parameters of the antenna with Ln as a variable

| Parameters | Lf | L1 | Lp | Lg | Wp | Wg | Wn | Wf |
|---|---|---|---|---|---|---|---|---|
| Value(mm) | 8.075 | 6.75 | 1.675 | 2 | 11 | 11 | 6.654 | 3.463 |
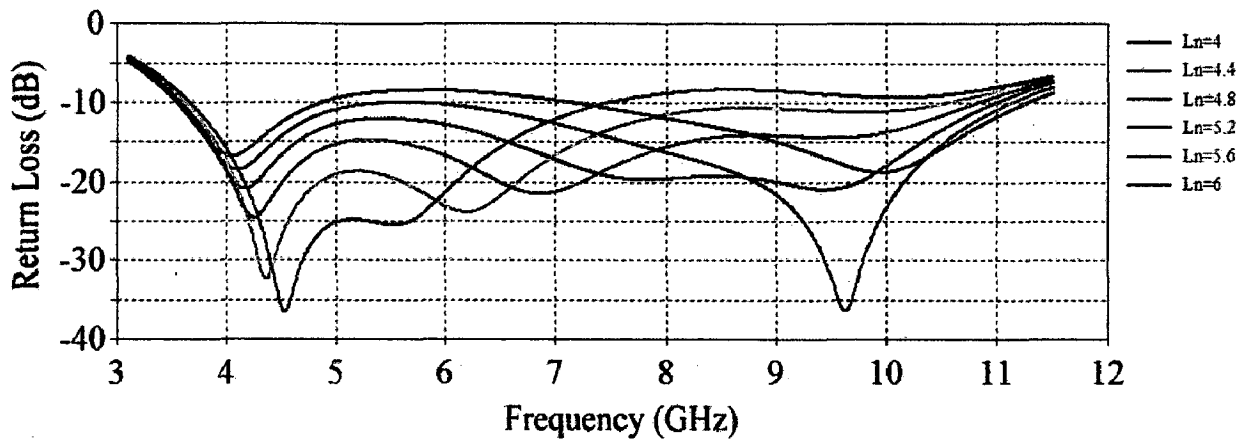


Figure 3.6 Variation of |S11| with Ln

As Ln increases, the first resonant frequency shifts toward the left. Further increase causes impedance mismatch in the frequency range of 7.2GHz-10.6GHz. The optimized value of Ln has been found to be 4.773mm.

### 3.1.2.4 Effect of variation in Lg

Figure 3.7 illustrates the magnitude of S11 for different lengths of Lg. The other dimensions of the antenna were kept constant and are given in Table 3.4.

Table 3.4 Parameters of the antenna with Lg as a variable

| Parameters | Lf | L1 | Lp | Ln | Wp | Wg | Wn | Wf |
|---|---|---|---|---|---|---|---|---|
| Value(mm) | 8.075 | 6.75 | 1.675 | 4.773 | 11 | 11 | 6.654 | 3.463 |
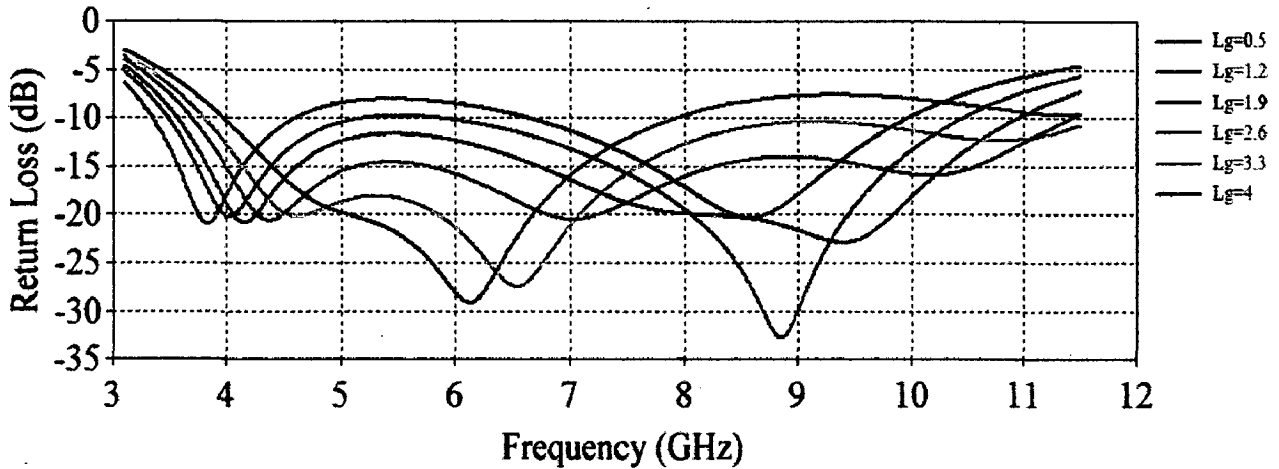
Figure 3.7 Variation of |S11| with Lg

When Lg varies, the gap between the upper side of the ground and the lower side of the patch is varied. Lg variation deeply influences the impedance matching of the antenna. As Lg decreases, the first resonant frequency shifts toward the right. Further decrease causes impedance mismatch in the frequency range of 4.5GHz-6.5GHz. From this, the importance of alignment of top and bottom side of the antenna during fabrication is clear. The optimized value of Lg has been found to be 2.5mm.

### 3.1.2.5 Magnitude of S11 for the antenna with and without the steps in the taper

The VSWR at the lower frequency end of the operating band is further improved by introducing steps in the taper [50] and shown in Figure 3.8. This happens as it gives additional parameters which affect the impedance profile of the UWB antenna. The size of the optimized steps is given in Table 3.5.

Table 3.5 Parameters of the steps in the taper

| Parameters | LS1 | LS2 | LS3 | WS1 | WS2 | WS3 |
|---|---|---|---|---|---|---|
| Value(mm) | 1 | 1 | 1 | 0.75 | 0.625 | 0.375 |
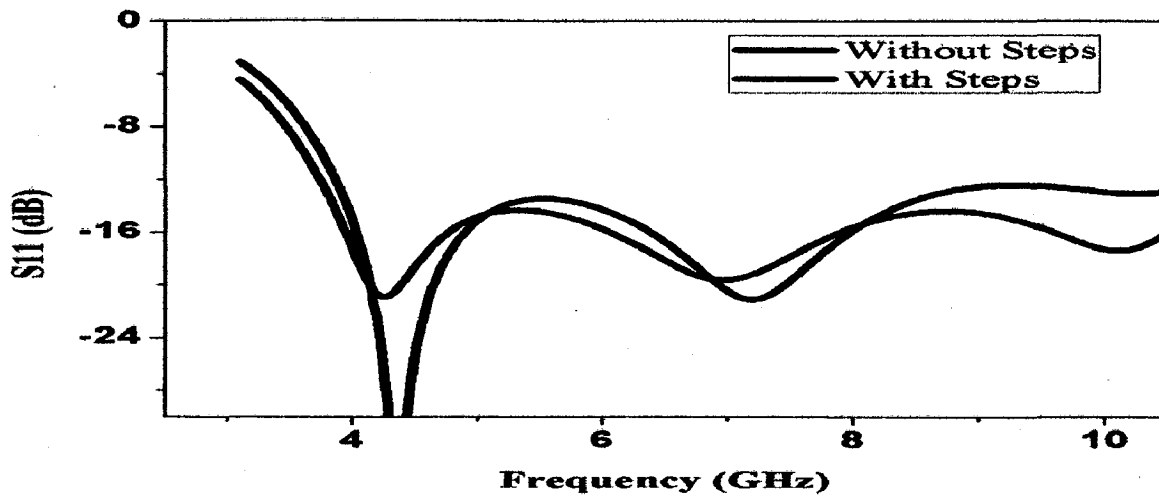
Figure 3.8 Magnitude of S11 with and without steps in taper

### 3.1.2.6 Optimized antenna parameters

The above mentioned parameters affect the impedance matching at different frequencies. The size of the optimized antenna is 11mm×16.5mm. The simulated VSWR of the optimized antenna is given in Figure 3.9.
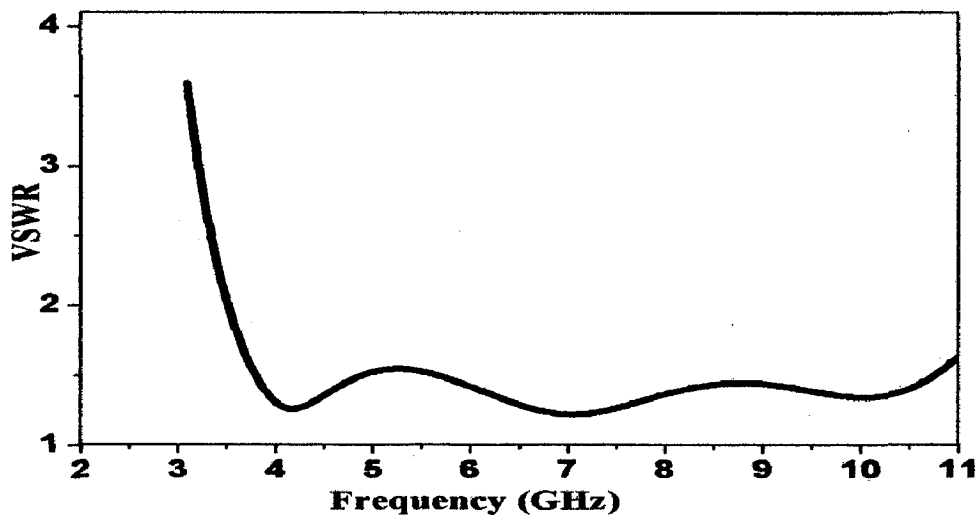


Figure 3.9 Simulated VSWR of the optimized antenna without band notch

### 3.1.3 Simulation and experimental results for the optimized antenna

The optimized microstripline-fed monopole antenna without bandnotch was fabricated. Simulation and experimental results have been obtained for the optimized antenna and comparison has been made.

31
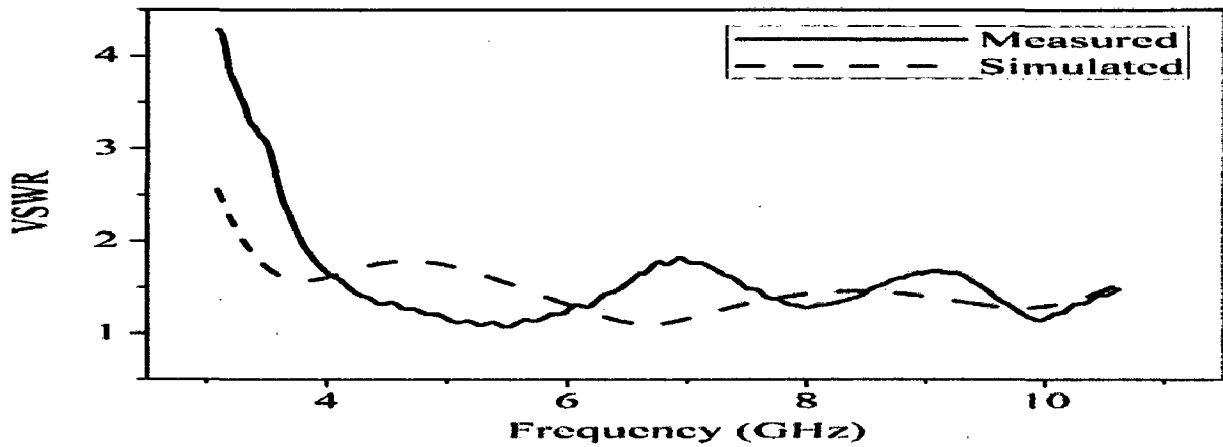
Figure 3.10 Measured and simulated VSWR of antenna without band notch

Figure 3.10 shows the simulated and measured VSWR of the proposed antenna without notch. The measured VSWR matches well with simulated VSWR except for the band of 3.6GHz to 3.9GHz.



(a)



(b)



(c)



(d)
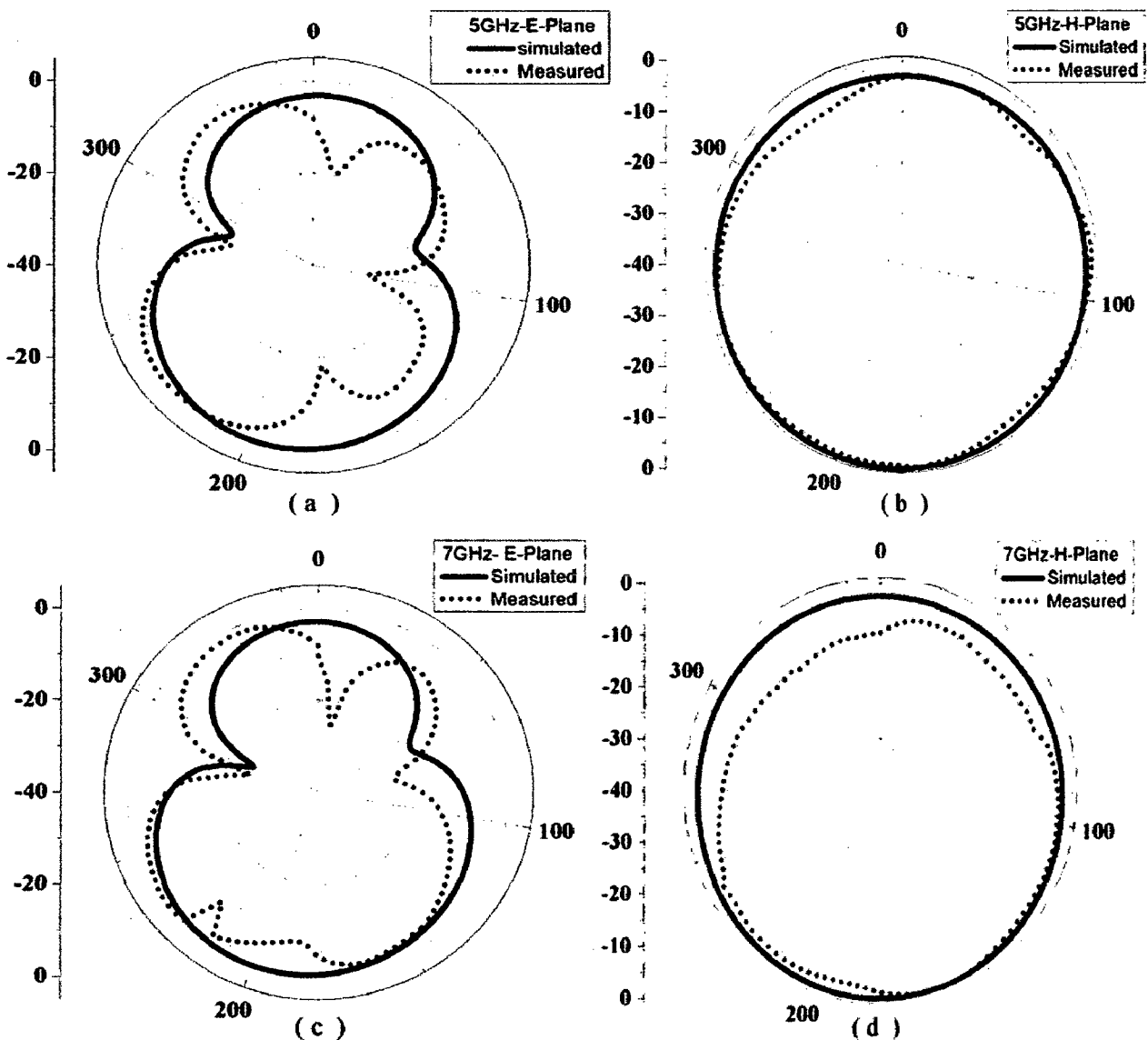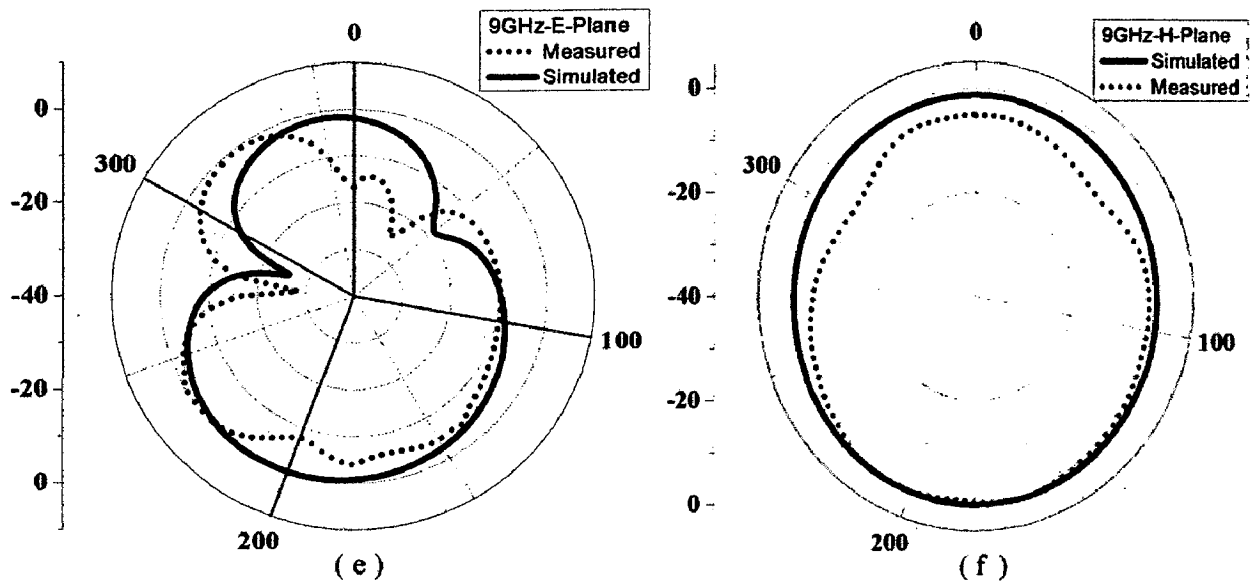
Figure 3.11 Simulated and measured radiation patterns (a) E-plane at 5GHz (b) H-plane at 5GHz (c) E-plane at 7GHz (d) H-plane at 7GHz (e) E-plane at 9GHz (f) H-plane at 9GHz

The measured and the simulated normalized E-plane and H-plane radiation patterns at 5GHz, 7GHz and 9GHz are shown in Figure 3.11. The $E$-plane patterns have large back lobes and look like a pinched donut at lower frequencies. Simulated and measured H-plane radiation patterns are reasonably Omni-directional over the operating bandwidth and have variations less than 10dB in most of the directions.
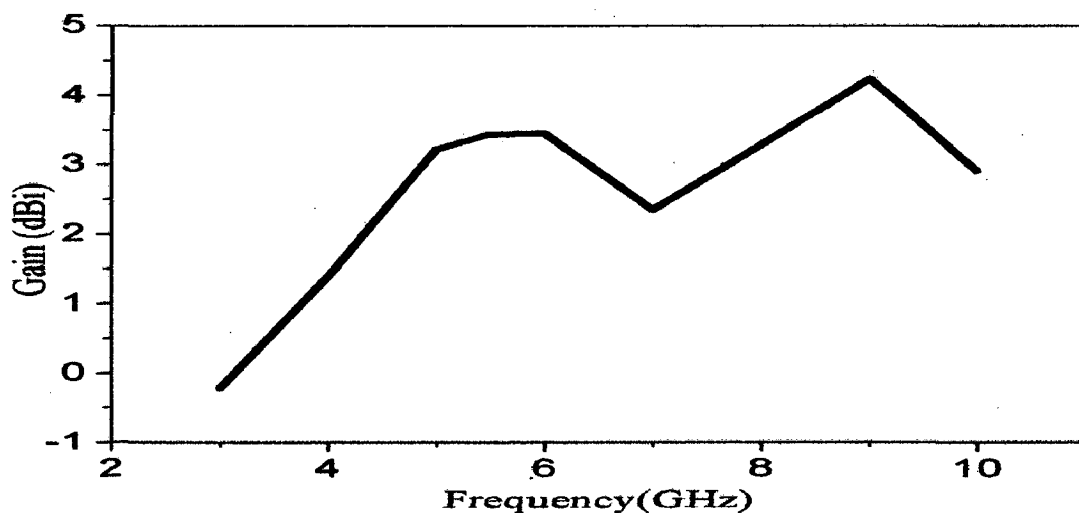


Figure 3.12 Measured gain of the proposed antenna

The measured peak gain of the proposed antenna is plotted in Figure 3.12. It can be seen that a gain of 2-4dB is obtained over most of the operating band.

Once the antenna receives a narrow pulse, it can oscillate and slowly dampen in time [53]. As a result, the pulse is spread in the time domain and it is no longer impulse like. The

time spreading of the signal due to reflections taking place in the antenna is called ringing effect. It gives an important measure about when the next pulse can be transmitted. Ringing effect reduces the channel capacity [50]. CST Microwave Studio has been used to simulate the ringing effect of the proposed antenna. The Gaussian modulated pulse is used in simulation and from Figure 3.13 it is clear that ringing effect is quite less. After 1ns another source pulse can be transmitted.
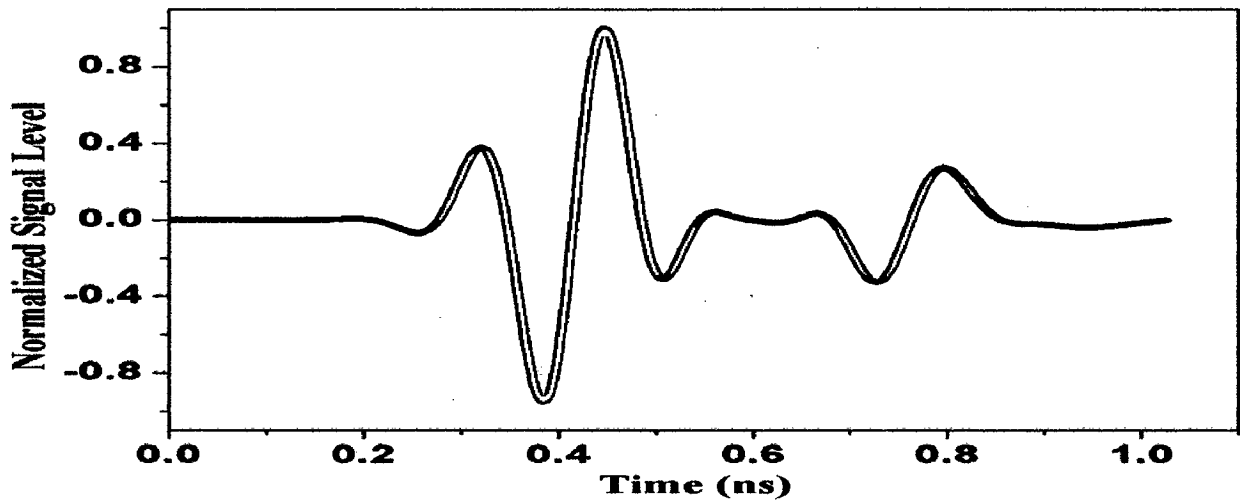


Figure 3.13 Ringing effect for antenna without band-notched function

## 3.1.4 Operating principle of microstripline-fed monopole antenna

The EM behaviour of the antenna can be understood by examining the field/current distribution. The working of the antenna either as a standing wave or as a travelling wave can be revealed by examining the field/current distributions [54].
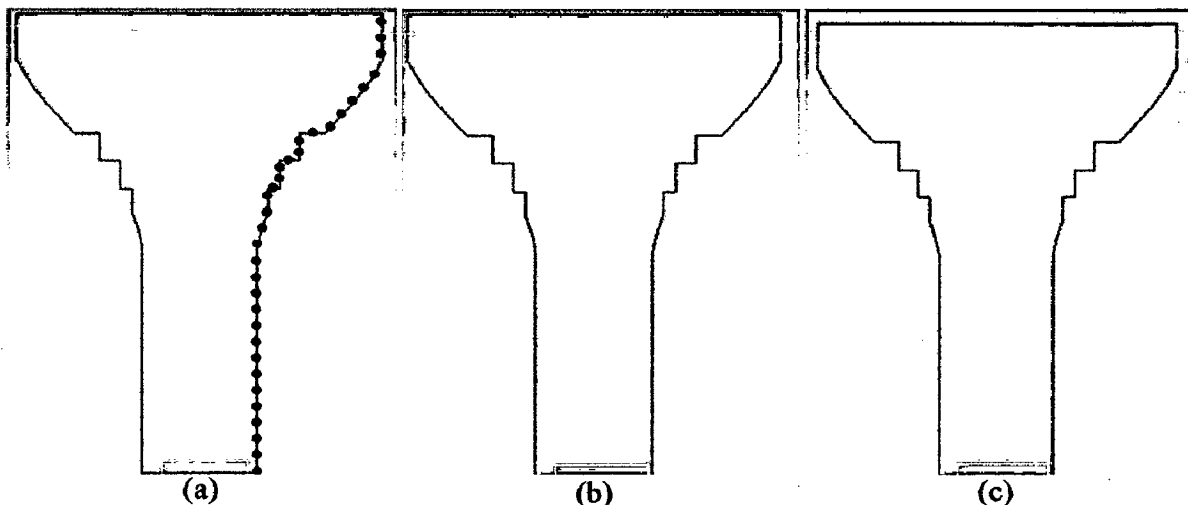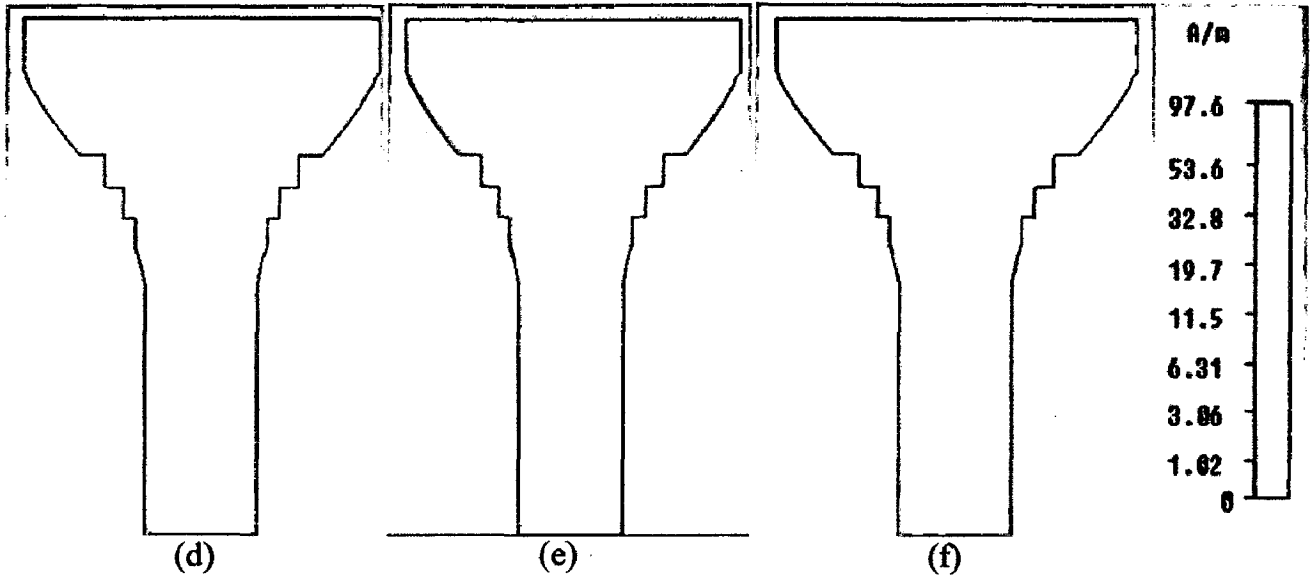
Figure 3.14 Snapshots of the magnetic field distribution at 4.2 GHz at different phases (a) phase=0 (b) phase=30 (c) phase=60 (d) phase=90 (e) phase=120 and (f) phase=150

The snapshots of the magnetic field distributions over the antenna at different phases have been shown in Figure 3.14 (a)–(e). The snapshots have been taken at 4.2GHz. The magnetic field distribution is observed along the edge which is highlighted by dots as shown in Figure 3.14 (a). If we closely observe along the edge at different phases, the amplitude seems to increase and decrease which confirms standing wave pattern. The antenna has a pure standing wave pattern along most parts of the edges. The antenna behaves like an oscillating monopole. So at low frequencies the antenna is dominated by standing wave.
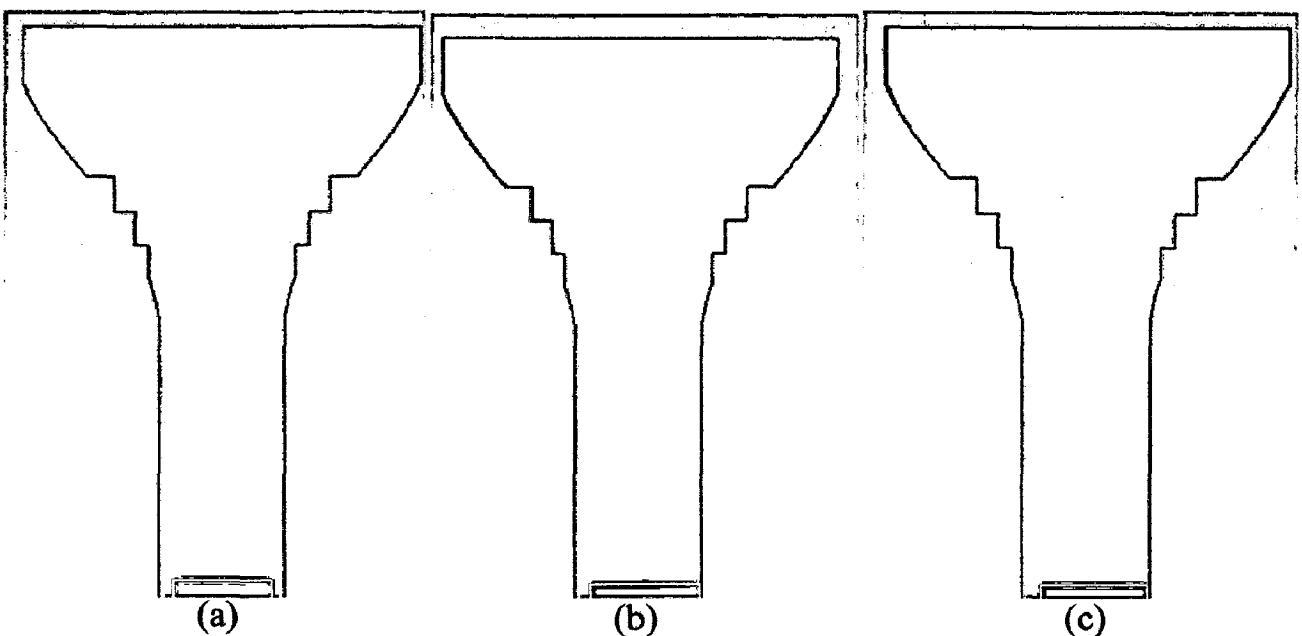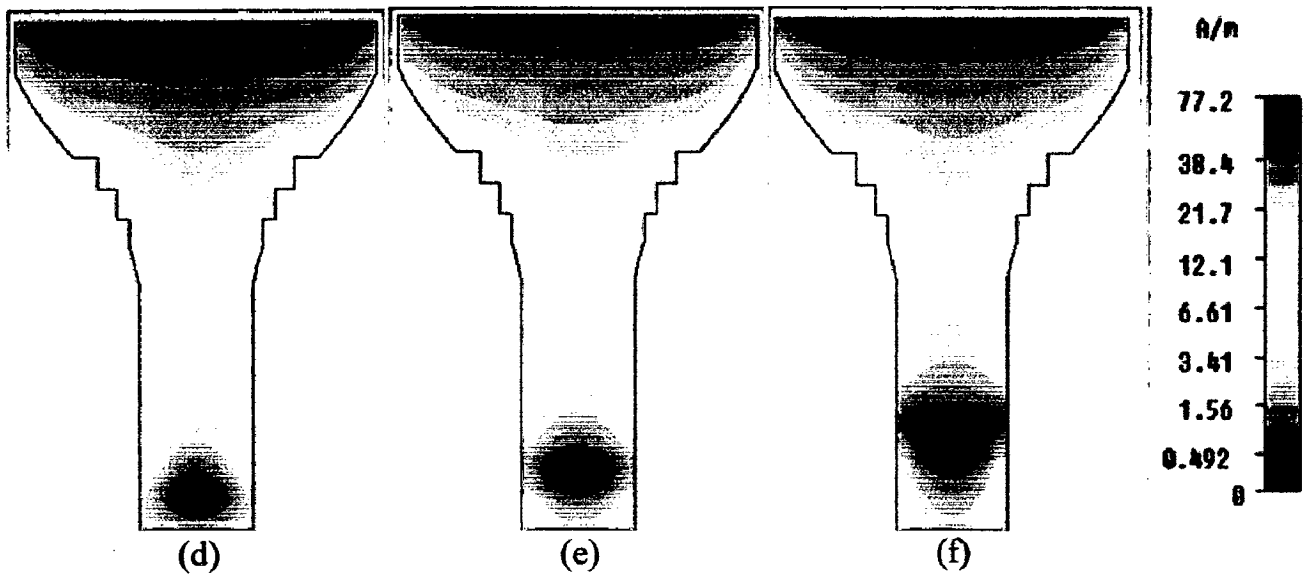
Figure 3.15 Snapshots of the magnetic field distribution at 7 GHz at different phases (a) phase=0 (b) phase=30 (c) phase=60 (d) phase=90 (e) phase=120 and (f) phase=150

Figure 3.15 (a)-(e) show the snapshots taken at 7 GHz. The nature of the antenna current distribution changes as the frequency is increased from 4.2GHz to 7GHz. The current travels along the edges of the feed line. But the current along the taper and top of the radiating patch is oscillating. Hence, the microstripline-fed monopole operates in a hybrid mode of standing wave and travelling wave as the frequency is increased.
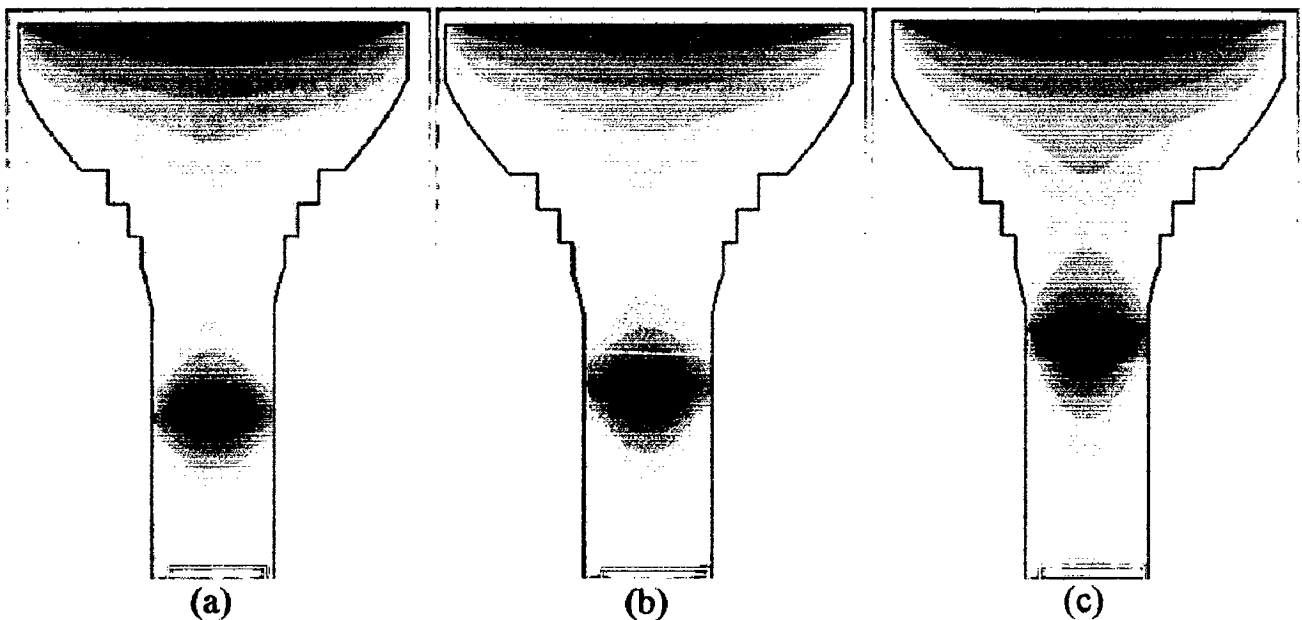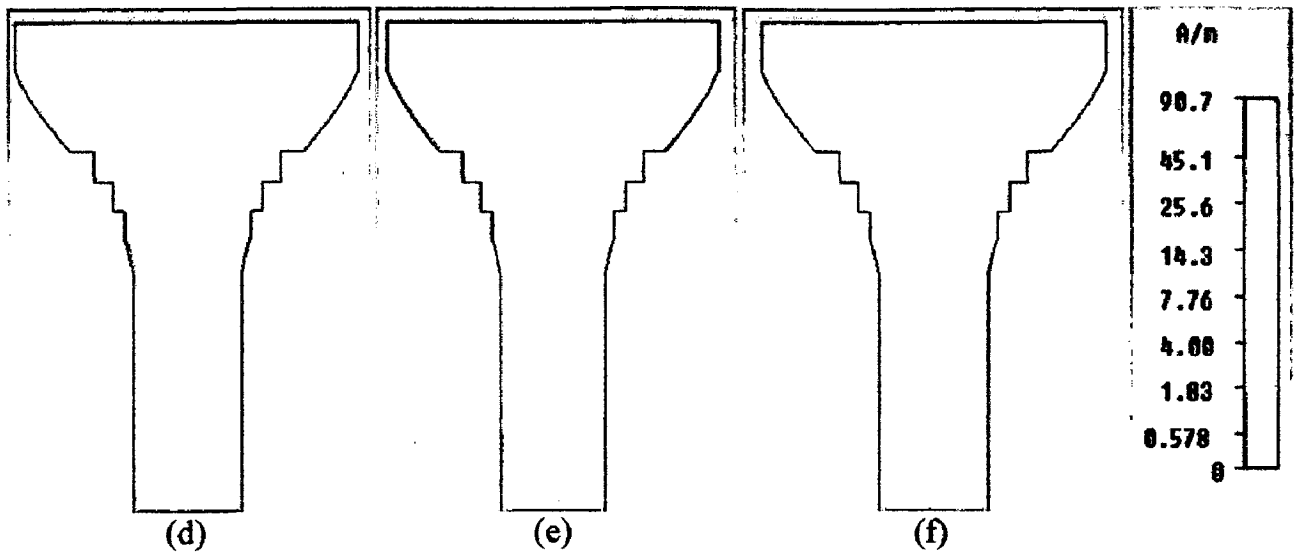
Figure 3.16 Snapshots of the magnetic field distribution at 10 GHz at different phases

(a) phase=0 (b) phase=30 (c) phase=60 (d) phase=90 (e) phase=120 and (f) phase=150

Figure 3.16 (a)-(e) corresponds to the snapshots taken at 10 GHz. At 10 GHz the travelling wave seems more prominent along the edges of the feed line and taper.

At 3.1GHz, the antenna dimension (16.5mm) is small compared to wavelength (65mm). So the EM wave gets reflected at the tip of the antenna structure. Due to this, the EM wave gets reflected from the end and the standing wave is formed. As the frequency is further increased, the antenna starts to operate in a hybrid mode consisting of a standing wave and a travelling wave. At the high frequency end, the antenna dimension (16.5mm) is comparable to wavelength (19.1mm). So, EM wave has to travel down the antenna structure before getting reflected. Therefore reflection takes place only at the tip of the antenna structure. Remaining portion of the antenna structure is dominated by the travelling wave at higher frequencies.
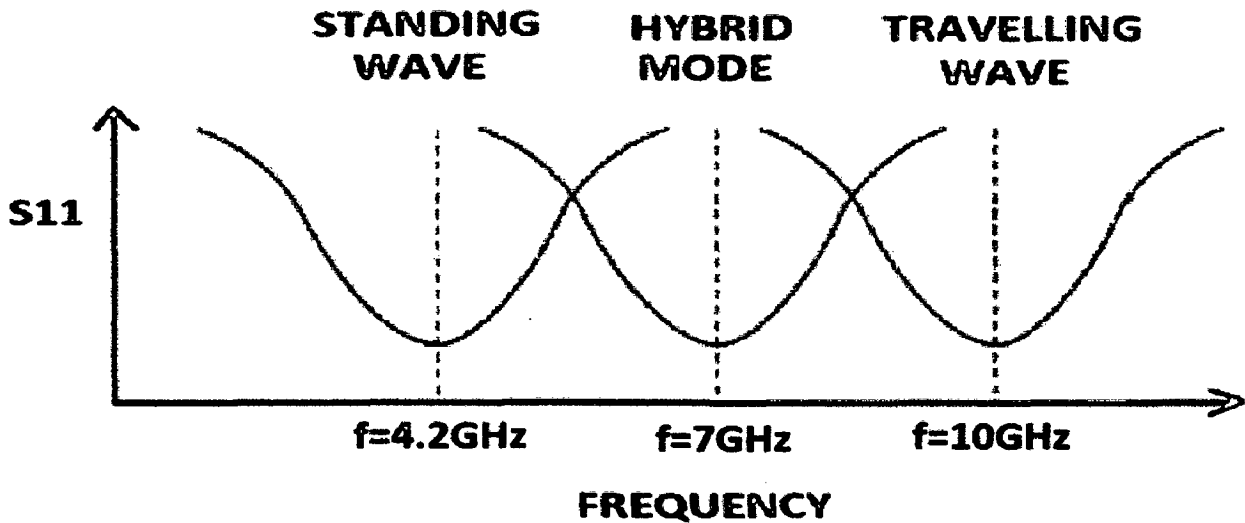
Figure 3.17 Operating principle of microstripline-fed monopole antenna

The overlapping of the closely spaced resonance modes in UWB antenna is responsible for the ultra-wide −10 dB bandwidth [54]. The resonance of the microstripline-fed monopole antenna occurs at the frequencies f=4.2 GHz, 7 GHz and 10 GHz. Figure 3.17 shows the change in nature of UWB antenna over the operating bandwidth.

## 3.2 Antenna with single band-notched function

One problem with UWB systems is that their operation may interfere with WLAN operating bands which exist at 5.2 GHz (5150-5350 MHz) and 5.8 GHz (5725-5825 MHz). To overcome this problem, a number of UWB Monopole antennas have been developed which reject the 5.1-5.8GHz frequency band. The common methods used to achieve band-notched characteristics include uses of slots such as, Inverted U-shaped [4] and complementary split ring resonator [5] in the patch and inserting a parasitic strip in the ground plane [6,7]. This method of band rejection has been explained in chapter 2.

The ringing depends on how much time the antenna takes to dissipate the stored reactive energy. As the energy is stored in the parasitic strip at the rejection frequency, the ringing effect is increased.

The ringing duration is inversely proportional to the notch bandwidth. When the notch bandwidth is more, the ringing is less. But increasing the notch bandwidth limits the bandwidth available for transmission. When the notch bandwidth is less, it causes more ringing.

## 3.2.1 UWB antenna with a wide notch bandwidth and reduced ringing

A T-shaped parasitic strip is placed at the bottom of the substrate above the ground plane as shown in Figure 3.18. The T-shaped parametric strip plays the role of a filter eliminating the limited band and leading to good impedance matching.
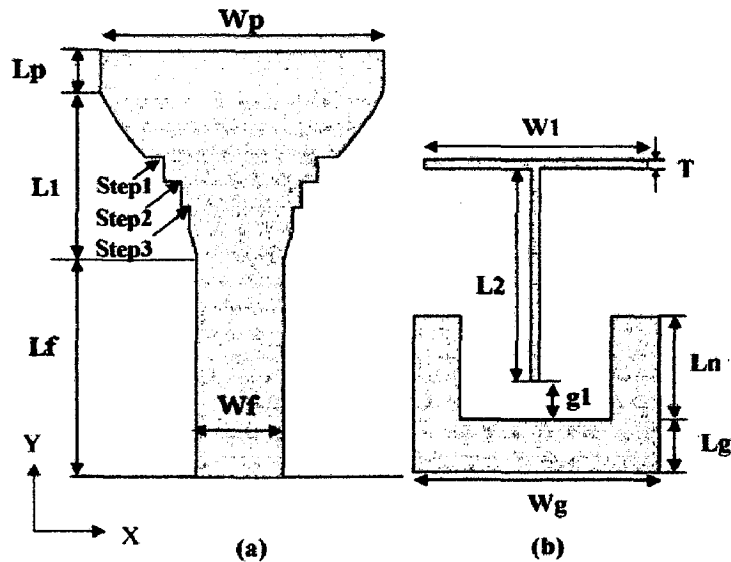


Figure 3.18 Geometry of the antenna with band-notched function (a) front side (b) back side

The initial length of the parasitic strip is half of the wavelength corresponding to the rejection frequency [4]. For The initial length L2+W1 is taken as 18.4mm for rejection of 5.5GHz. By using parametric sweep of CST the values of L2 and W1 are tuned to reject the frequency 5.5GHz.
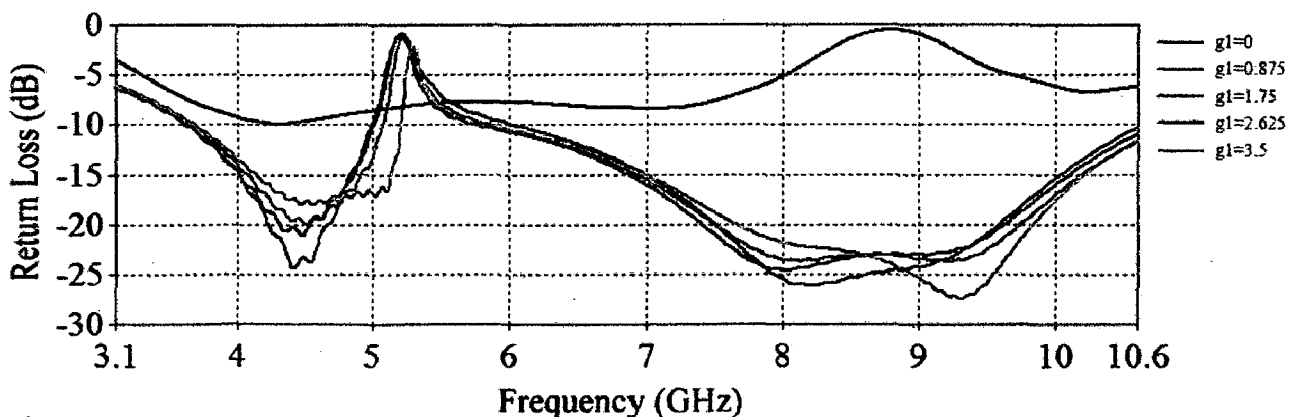


Figure 3.19 Variation of |S11| with g1

Figure 3.19 illustrates the magnitude of S11 for different values of g1. The length, g1 controls the notch bandwidth. When g1=0 the impedance matching is poor as the parasitic strip touches the ground plane. When g1 is increased the notch bandwidth reduces. Here g1 is

kept small in order to achieve a wide notch bandwidth. The parameters of parasitic strip are given in Table 3.6.

Table 3.6 Parameters of the parasitic strip

| Parameters | W1 | L2 | T | g1 |
|------------|-----|-----|-----|-----|
| Value(mm) | 9 | 11 | 0.4 | 1 |
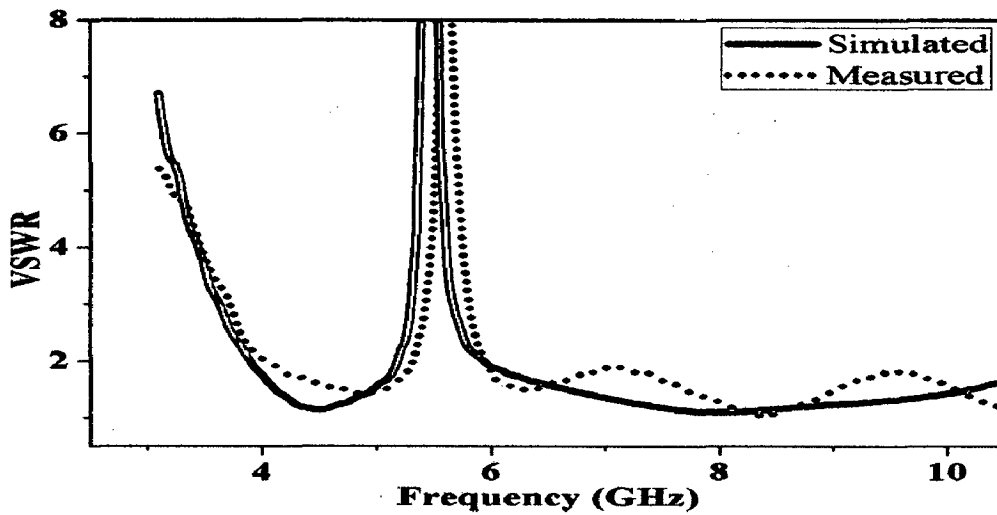


Figure 3.20 VSWR of the antenna with reduced ringing

The measured and simulated VSWR of the antenna with parasitic strip is shown in Figure 3.20 and they have good agreement. The measured notch bandwidth is from 5.3GHz to 5.95GHz.
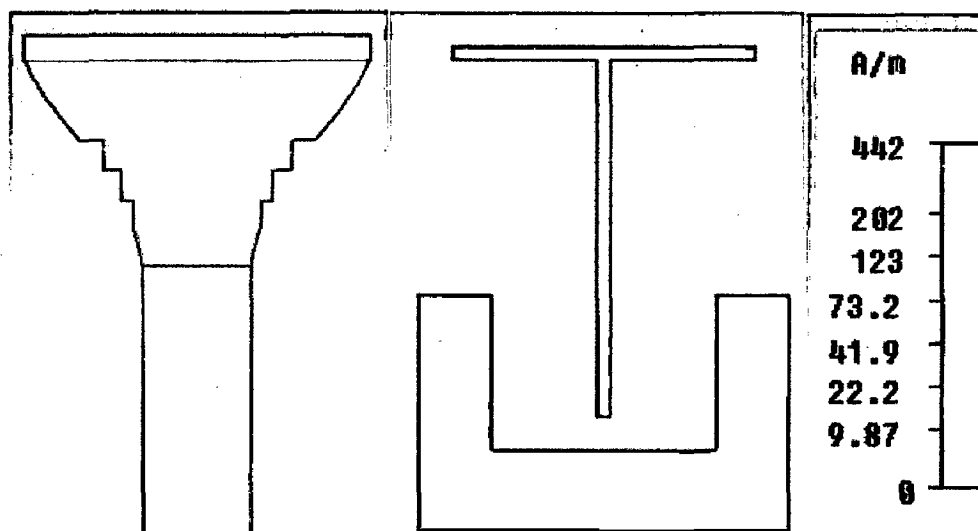


Figure 3.21 Surface current distribution at 5.5GHz

A/m

442
202
123
73.2
41.9
22.2
9.87
0
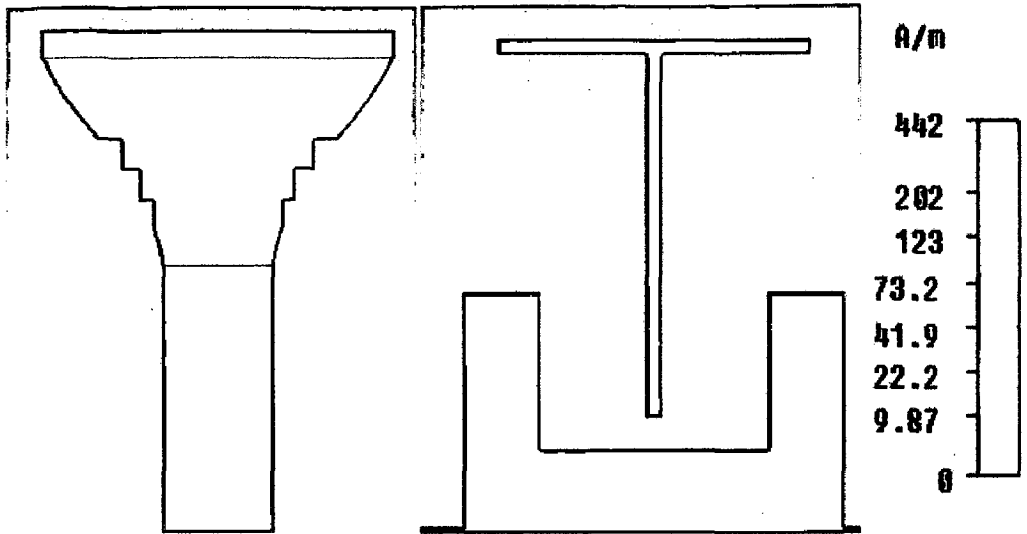
Figure 3.22 Surface current distribution at 8GHz

There is a strong electric coupling between the bottom of the patch and the parasitic strip at the rejection frequency. This strong coupling makes the surface current concentrate on the T-shaped parasitic strip as shown in Figure 3.21. So the area above the parasitic strip and the antenna does not radiate at this frequency. At 8 GHz the magnitude of surface current distribution is less over the antenna and evenly spread over the antenna as shown in Figure 3.22. So the antenna radiates at 8 GHz.



(a)

(b)
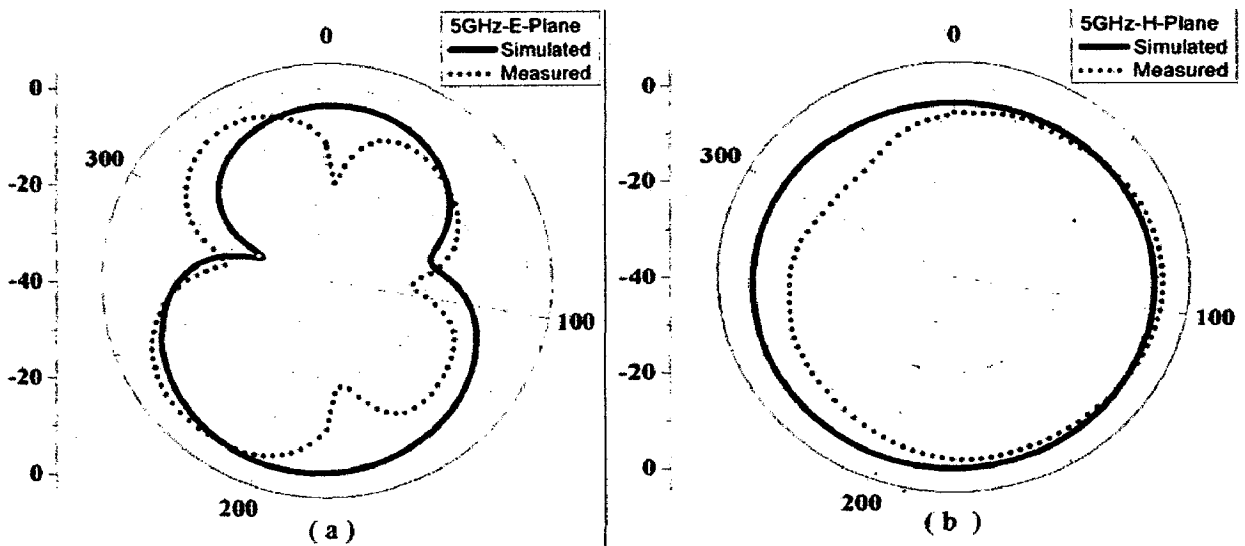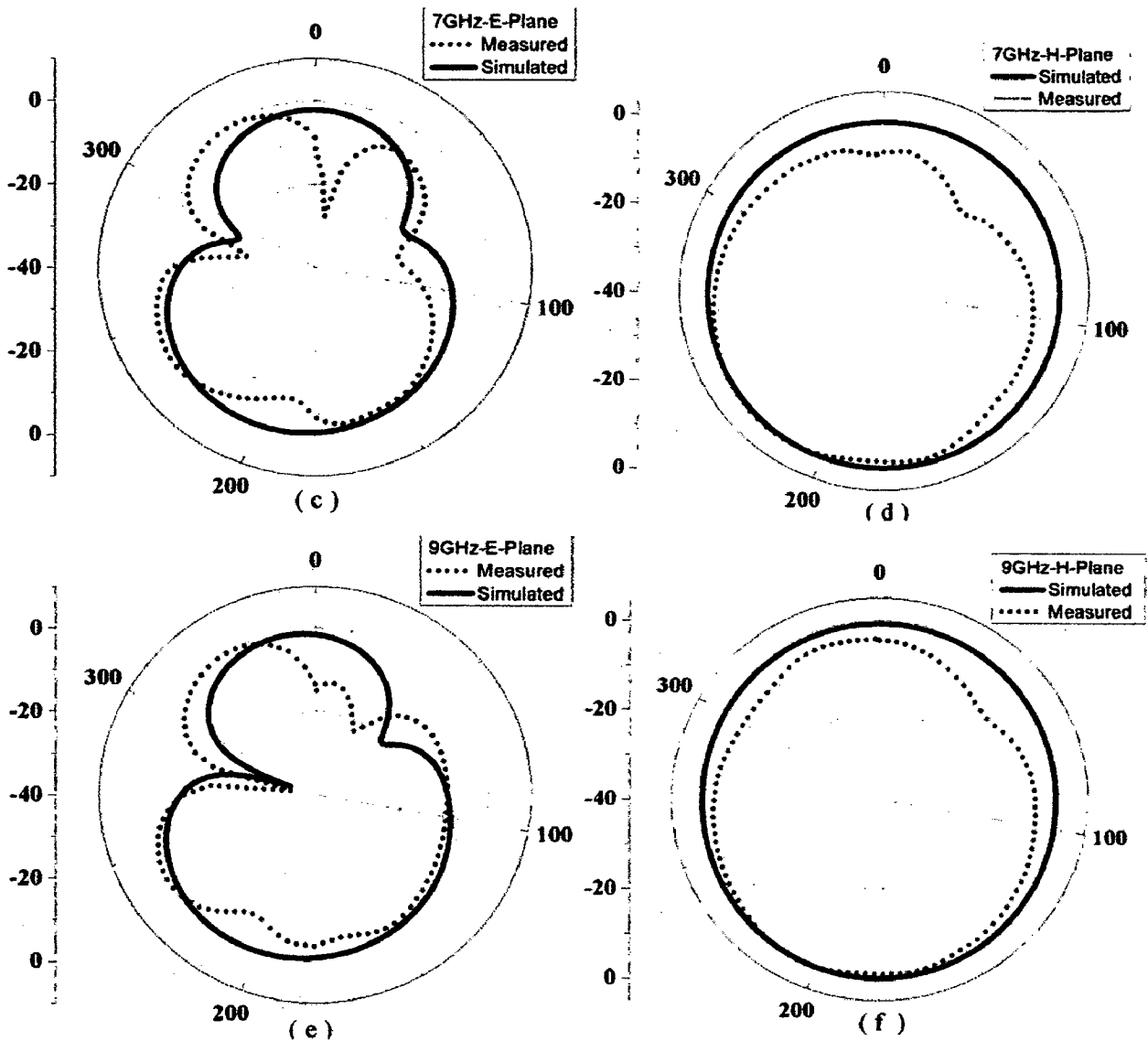
Figure 3.23 Simulated and measured radiation patterns (a) E-plane at 5GHz (b) H-plane at 5GHz (c) E-plane at 7GHz (d) H-plane at 7GHz (e) E-plane at 9GHz (f) H-plane at 9GHz

The measured and the simulated normalized E-plane and H-plane radiation patterns at 5GHz, 7GHz and 9GHz are shown in Figure 3.23. The E-plane patterns have a large back lobe. In the measured E-plane patterns, with the increase in the frequency, the front lobe starts splitting into minor ones. Measured H-plane radiation patterns are reasonably Omni-directional over the operating bandwidth and have variation less than 15dB in most of the directions.

Figure 3.24 Measured gain of the proposed antenna

The measured peak gain of the proposed antenna is plotted in Figure 3.24. It can be seen that a gain of 2-4dB is obtained over most of the operating band except at the notch frequency where a sharp dip is observed.
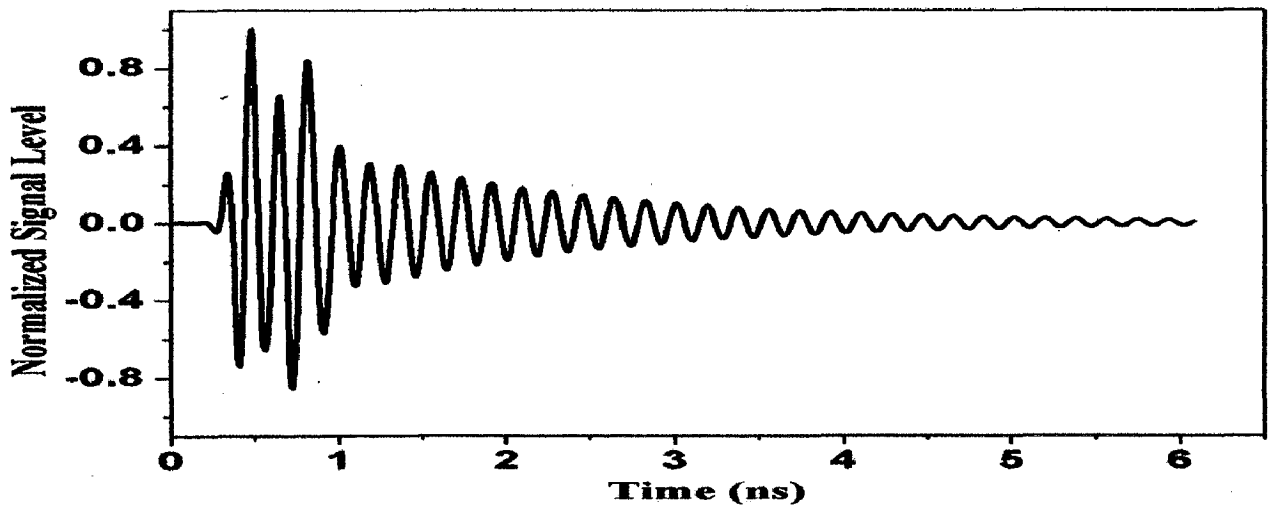


Figure 3.25 Ringing effect of the antenna

After the insertion of band notch, the duration of ringing is more compared to the antenna without band notch. For UWB antenna without band notch, the ringing occurs till 1ns and for antenna with wide band notch, the ringing occurs till 6ns.

## 3.2.2 UWB antenna with narrow notch bandwidth and increased ringing

In order to conserve bandwidth in some applications, small notch bandwidth is preferable. As mentioned earlier, the bandwidth at notch frequency is controlled by the parameter g1. An antenna with g1=3.5mm was also designed and fabricated.
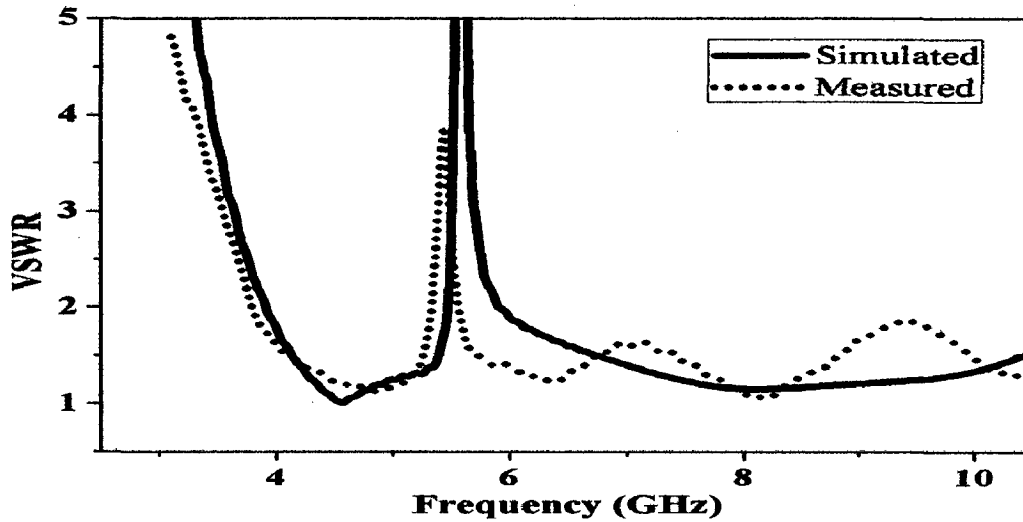


Figure 3.26 VSWR of antenna with increased ringing

The measured and simulated VSWR of the antenna with g=3.5mm is shown in Figure 3.26 and they have a good agreement. The measured notch bandwidth is from 5.335GHz to 5.56GHz.



( a )                                    ( b )
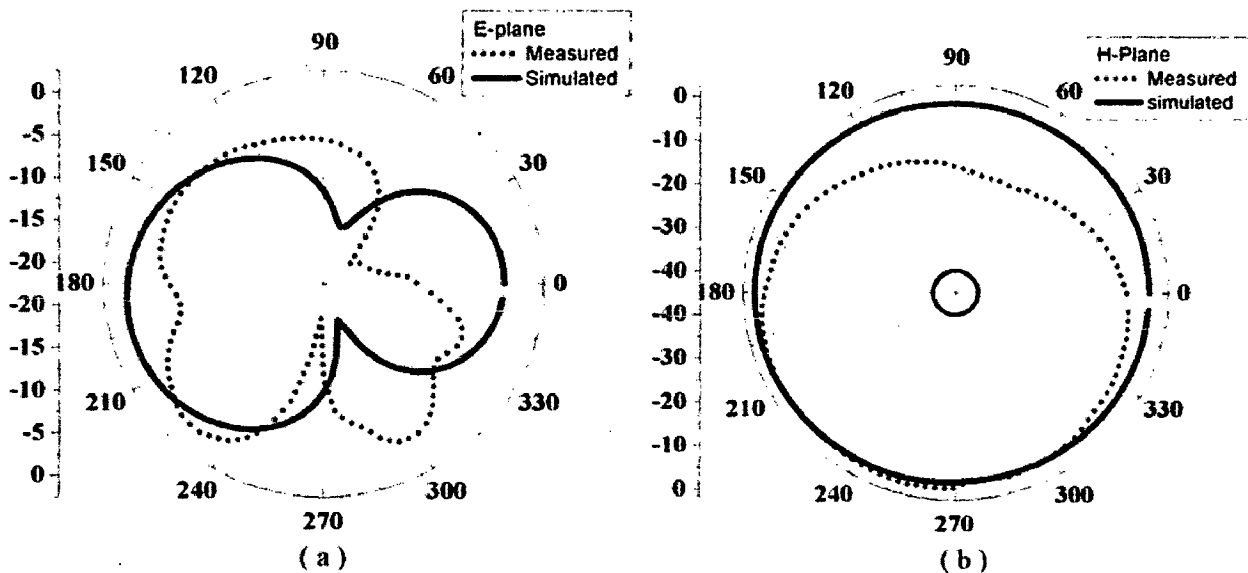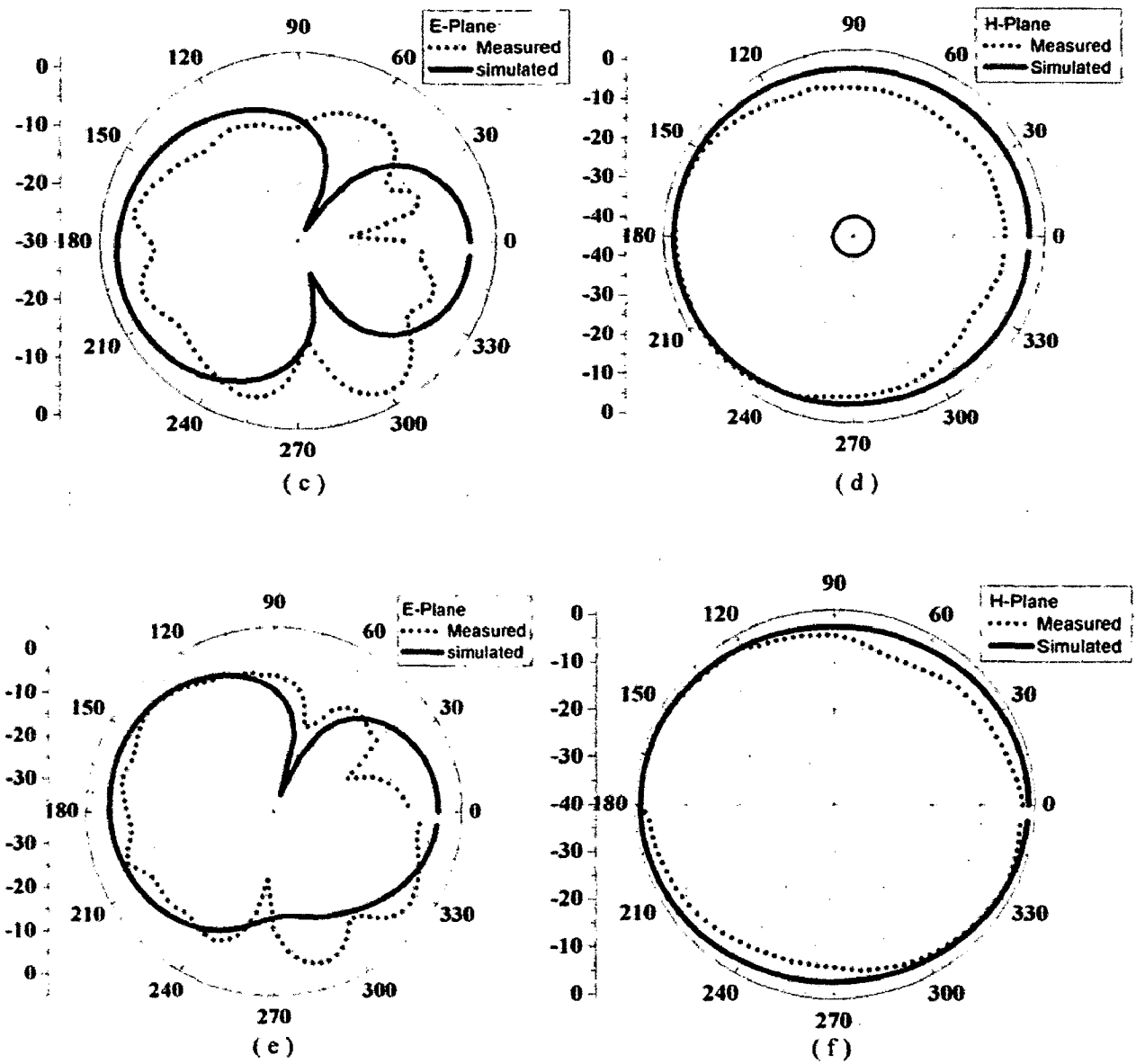
Figure 3.27 Simulated and measured radiation patterns (a) E-plane at 6.1GHz (b) H-plane at 6.1GHz (c) E-plane at 7.8GHz (d) H-plane at 7.8GHz (e) E-plane at 10GHz (f) H-plane at 10GHz

The measured and the simulated normalized E-plane and H-plane radiation patterns at 6.1GHz, 7.8GHz and 10GHz for this antenna are shown in Figure 3.27. The E-plane patterns have a large back lobe. The front lobe of the measured E-plane patterns is slightly tilted. The H-plane radiation pattern at 6.1GHz is slightly distorted. At other two frequencies, the H-plane radiation patterns are reasonably Omni-directional.
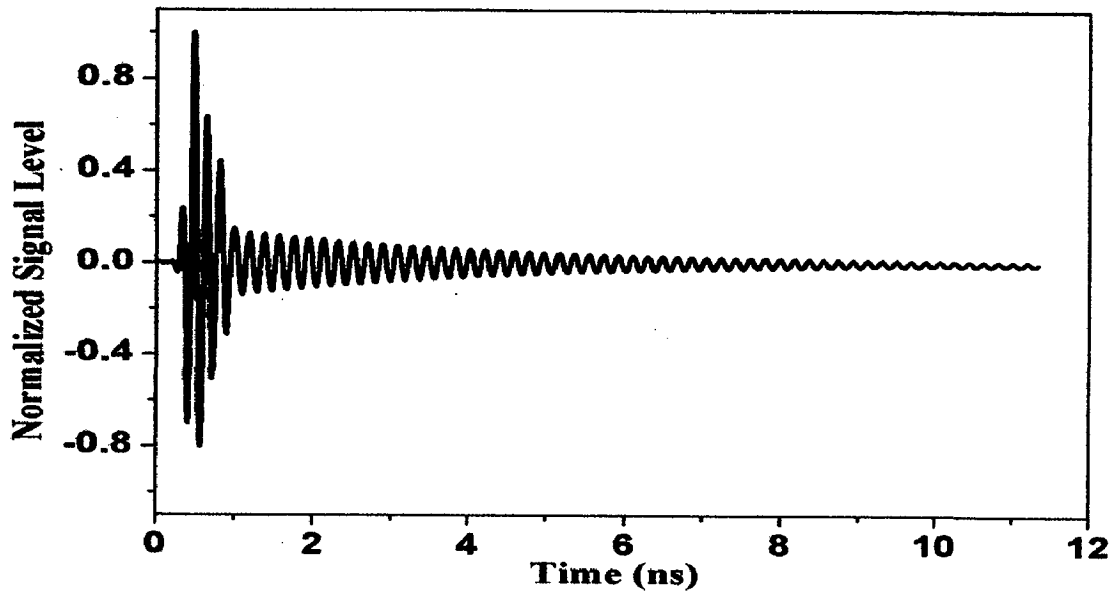
Figure 3.28 Ringing effect of the antenna

The ringing duration of the antenna with wide band notch was 6 ns. After inserting the narrow band notch the ringing duration is increased to 11.3ns. As the notch bandwidth is less, ringing effect is more pronounced which can be seen in Figure 3.28.

## 3.3 Antenna with double band-notched function

The double notch is obtained by combining two conventional methods of band notching. By combining a T-shaped parasitic strip in the ground plane and a Complementary Single Split Ring Resonator (CSSRR) in the patch, band-rejection notches have been introduced at 5.2 GHz and 5.8 GHz WLAN bands. The geometry of the proposed antenna with double notch is shown in Figure 3.29.
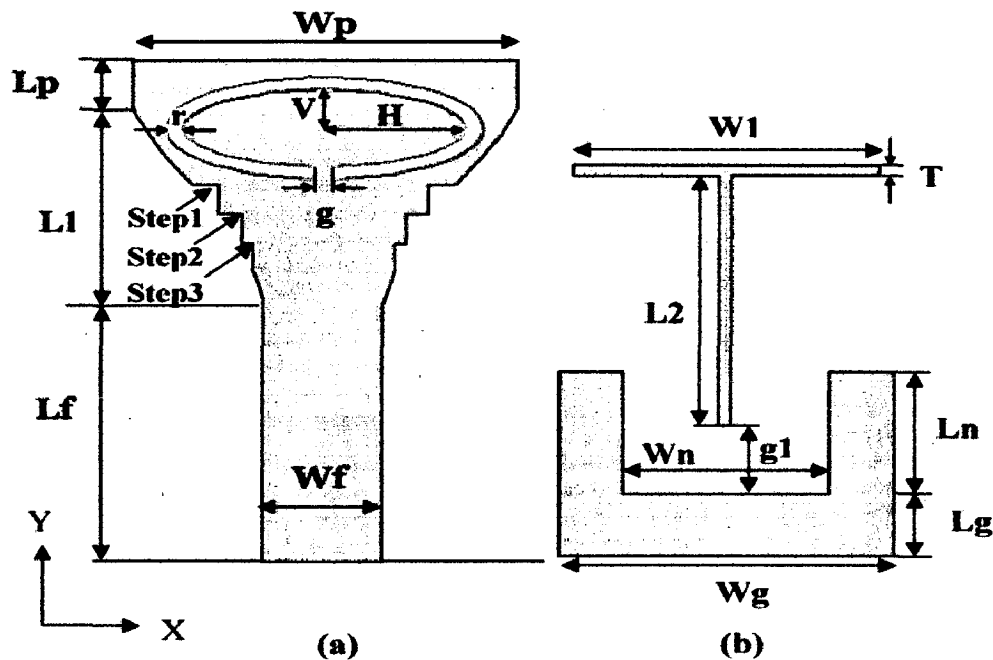


Fig. 3.29 Geometry of the proposed antenna with Double notch, (a) Front Side and (b) Back Side

Firstly, the two methods were implemented separately in the proposed antenna. In the first method, a T-shaped parasitic strip is placed in the ground plane to produce a notch at 5.8GHz. The T-shaped strip plays the role of a filter eliminating the 5.8GHz frequency band and enhancing the impedance match at lower frequencies. The strong electric coupling between the bottom of the patch and the parasitic strip at the rejected frequency makes the surface current to concentrate on the T-shaped parasitic strip as shown in Figure 3.30. From the surface current distribution on the patch at 5.8GHz we can conclude that the antenna ceases to radiate at this frequency.

To provide a notch at 5.2GHz, a CSSRR has been introduced on the patch. The initial value of the circumference of the CSSRR was taken to be half the rejection wavelength and can be found using the Equation 3.9 [50]. The impedance match is a strong function of the

parameters g and r which have to be optimized. At the rejected frequency, the surface current is observed to be concentrated at the spilt end of the slot as shown in Figure 3.30.

$$L_{slot} = \frac{0.45\,c}{f_{notch}\sqrt{\varepsilon_{eff\_slot}}}$$ (3.9)

where

$$\varepsilon_{eff_{slot}} = \frac{\varepsilon_r + 1}{2}$$ (3.10)

and c is the velocity of the light. $\varepsilon_r$ is the permittivity of the substrate and $\lambda_0$ is the free space wavelength corresponding to the rejection frequency.
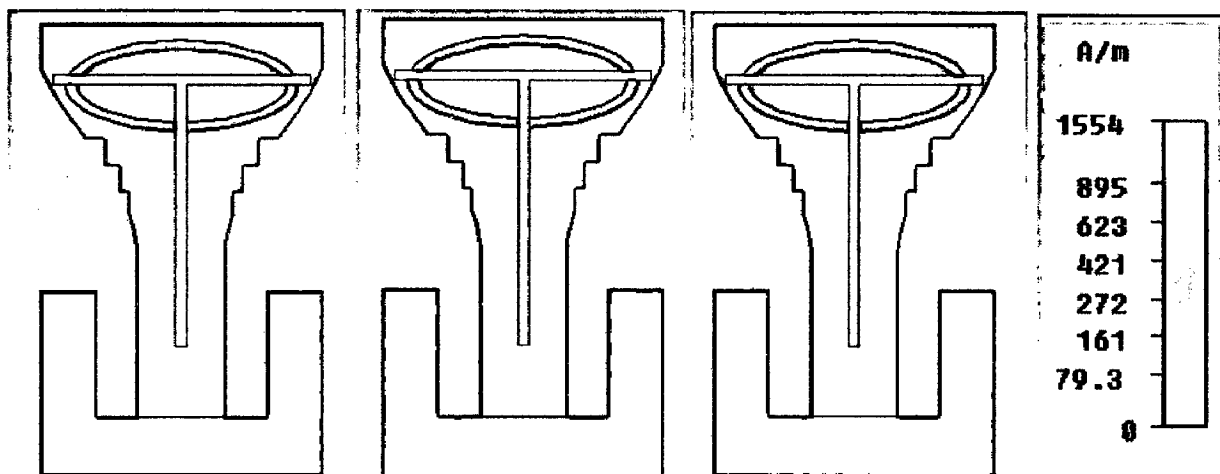


Figure 3.30 Surface current distribution (a) 5.2GHz (b) 5.8GHz (c) 8GHz

The above mentioned two methods were combined to produce notches at 5.2GHz and 5.8GHz. Upon combining them together, there is a shift in the notch frequencies and impedance matching becomes poor. Therefore, the position and size of T-shaped strip and CSSRR be properly adjusted for the desired impedance match and the location of notch frequencies. The Lp of the antenna is changed to 2.475mm. Optimized parameters of T-shaped strip and CSSRR are given in Table 3.7.

Table 3.7 Optimized parameters of CSSRR and T-shaped parasitic strip

| Parameters | V | H | g | r | W1 | T | g1 | L2 |
|---|---|---|---|---|---|---|---|---|
| Values(mm) | 1.4 | 4.1 | 0.5 | 0.3 | 10 | 0.4 | 2.67 | 9.83 |

## 3.3.1 Frequency domain characteristics

The optimized microstripline-fed monopole antenna with double notch has been fabricated and the experimental results are compared with simulation results.
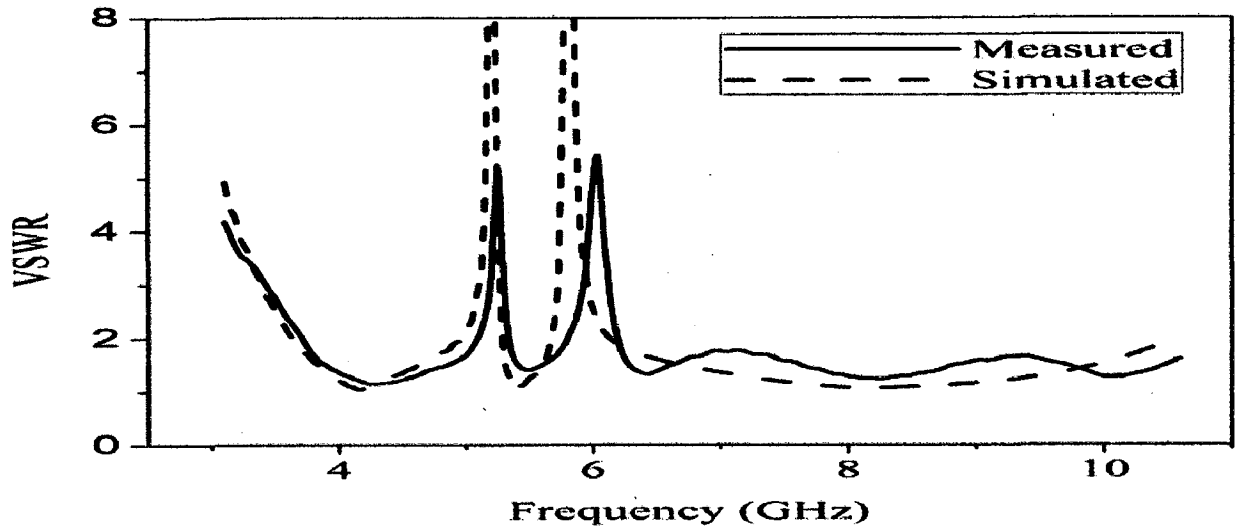


Figure 3.31 Measured and Simulated VSWR of the antenna with Double notch

Figure 3.31 shows the simulated and measured VSWR of the proposed antenna with double notch. The two notches of the fabricated antenna occur at 5.1-5.35GHz and 5.8-6.2GHz.



49
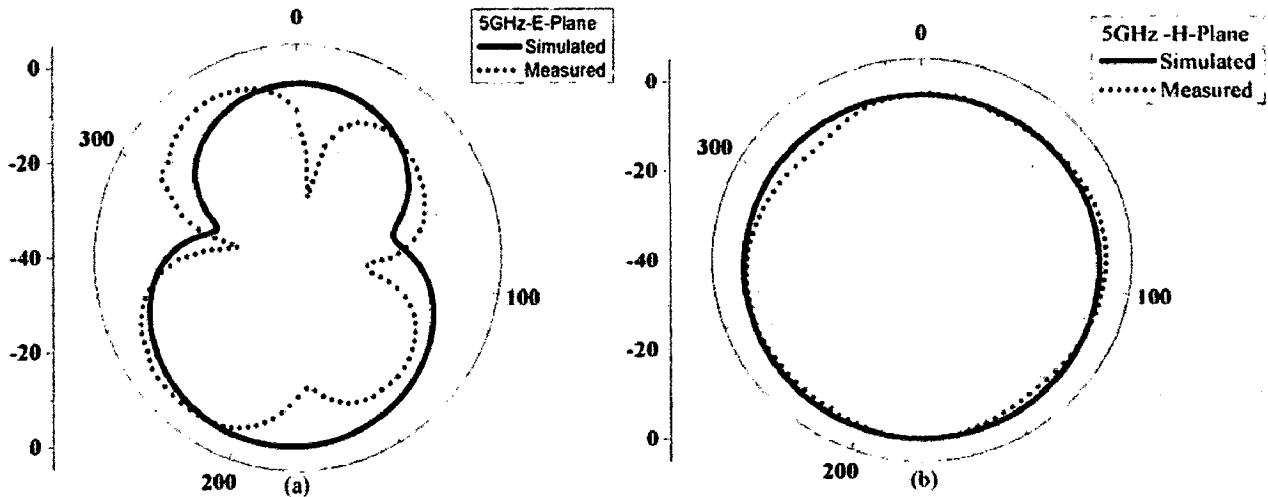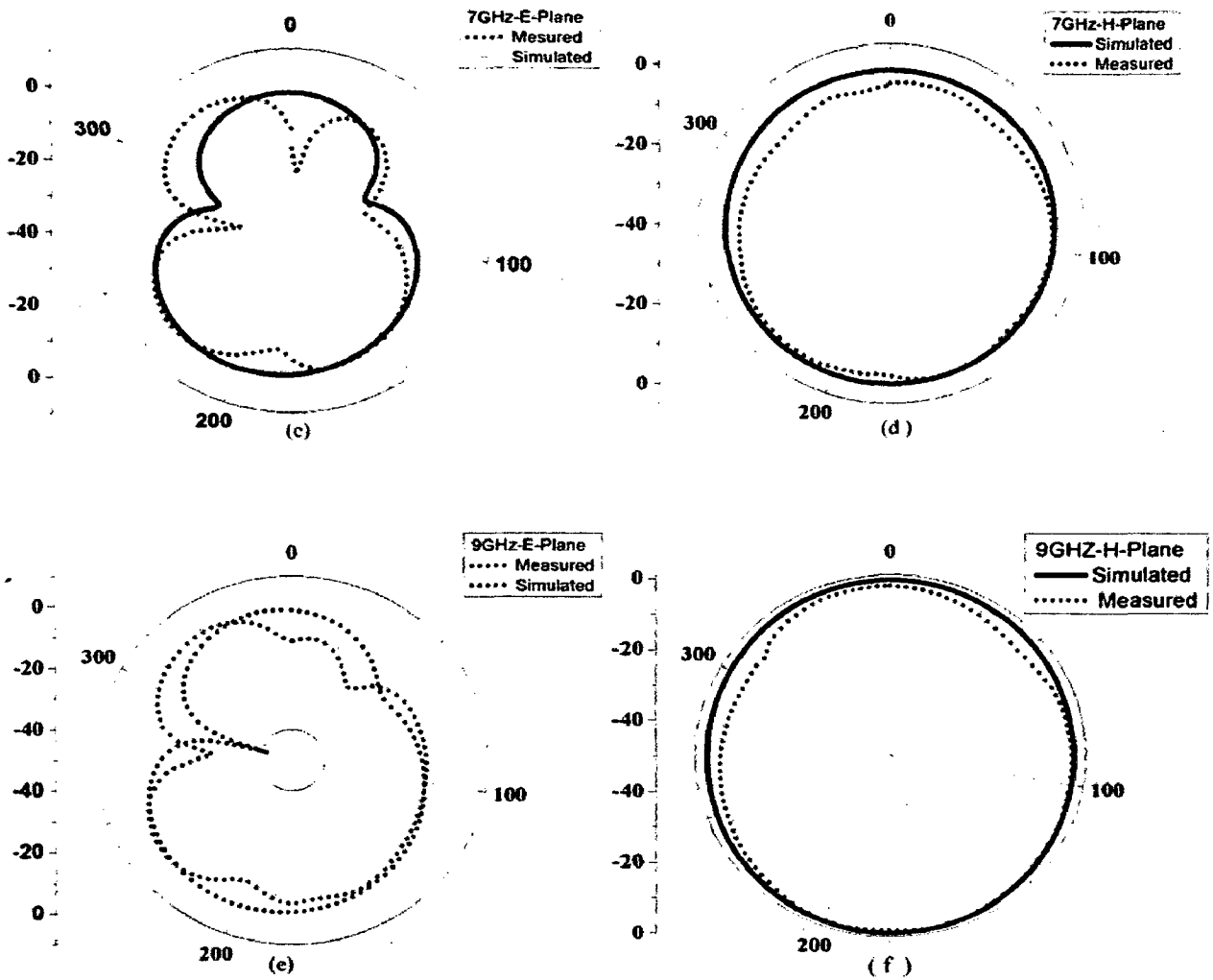
Figure 3.32 Simulated and measured radiation patterns of double notch antenna (a) E-plane at 5GHz (b) H-plane at 5GHz (c) E-plane at 7GHz (d) H-plane at 7GHz (e) E-plane at 9GHz (f) H-plane at 9GHz
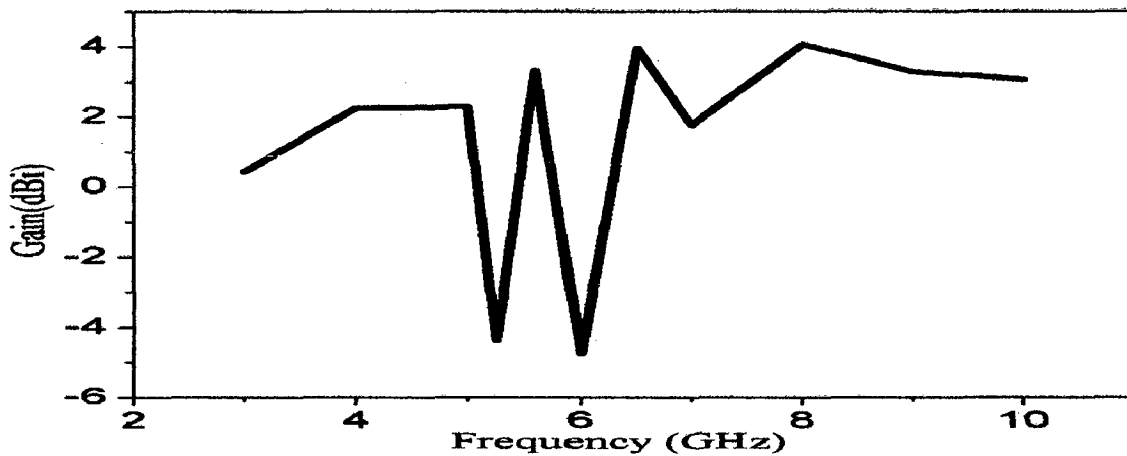


Figure 3.33 Measured gain of the proposed antenna with double notch

The measured and the simulated normalized E-plane and H-plane radiation patterns at 5GHz, 7GHz and 9GHz are shown in Figure 3.32. The front lobe of the E-plane patterns tilt at high frequencies. The H-plane radiation patterns are reasonably Omni-directional over the operating bandwidth and its variation is less than 5dB. The measured peak gain o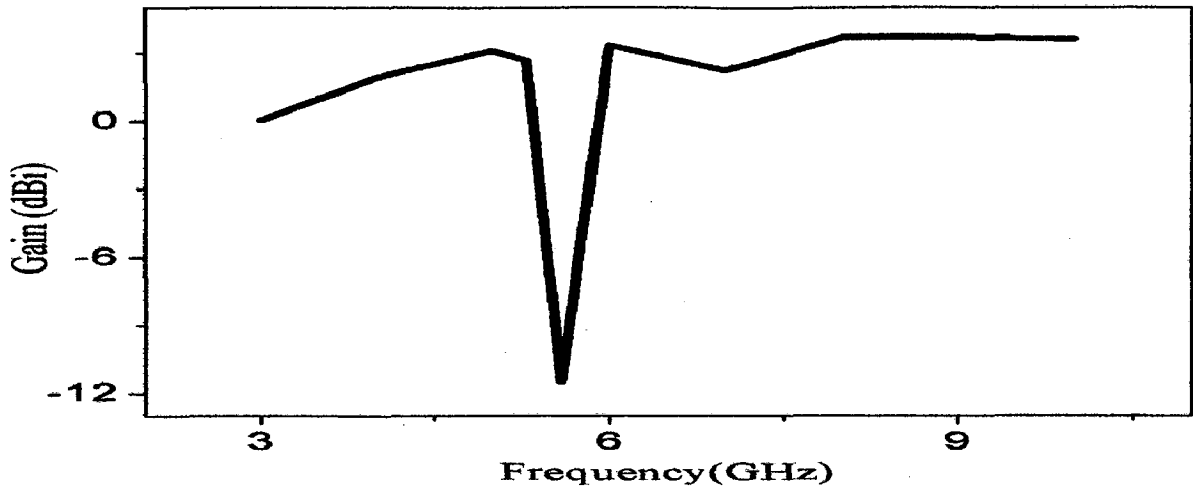f the proposed antenna is plotted in Figure 3.33. It can be seen that a gain of 2-3dB is obtained over most of the operating band except at the notch frequencies where there is sharp dip in the gain.

In UWB systems, linear phase response of the radiated field as well as stable group delay response is desired so that the shape of the transmitted electrical pulse is not distorted. The group delay is defined as the negative derivative of the phase $\psi$ of the transfer function S21 and is given by Equation 3.11. Only at the band notched frequency, group delay is more. Group delay is less at other frequencies, causing less distortion and it is shown in Figure 3.34.

$$Group\ delay = -\frac{d\psi}{df}$$ (3.11)
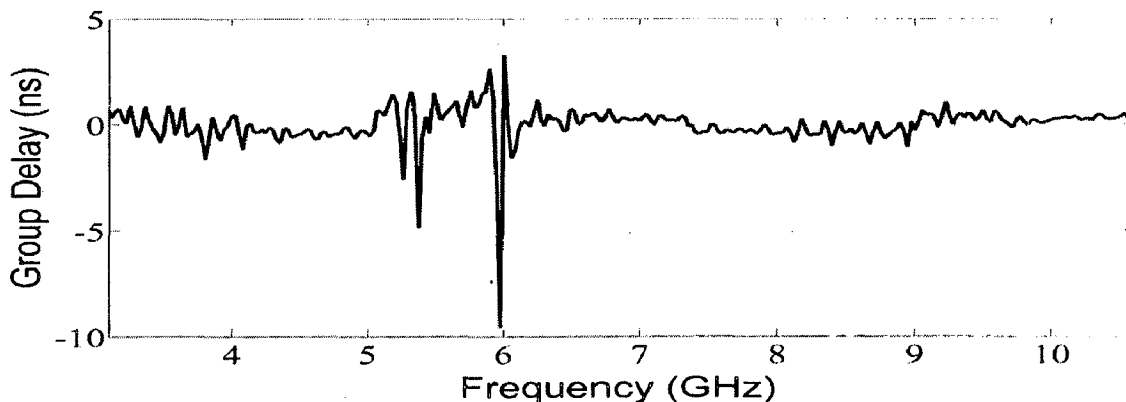


Figure 3.34 Group delay of UWB antenna with double notch

### 3.3.2. Time domain Characteristics

While only frequency domain behaviour of the antennas is important for narrow-band signal, the time domain behaviour becomes equally important for UWB antennas. Since UWB systems operate with very wide bandwidth, the antennas act as pulse shaping filters and have an important impact on system design which should take into account the characteristics of the source pulses. If the operating bandwidth of the UWB antenna is more and if source pulse does not satisfy the emission mask, it can cause interference to the other existing wireless systems.

51

### 3.3.2.1 Description of the UWB system

UWB antenna system can be modeled as a two port network as shown in Figure 3.35[55]. The UWB antenna system consists of a transmitting antenna, channel and the receiving antenna as shown in Figure 3.36.
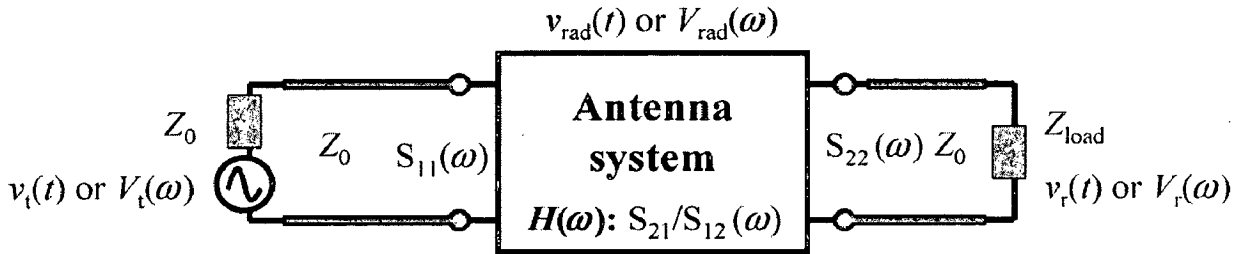


Figure 3.35 UWB Antenna System as a Two Port Network [56]
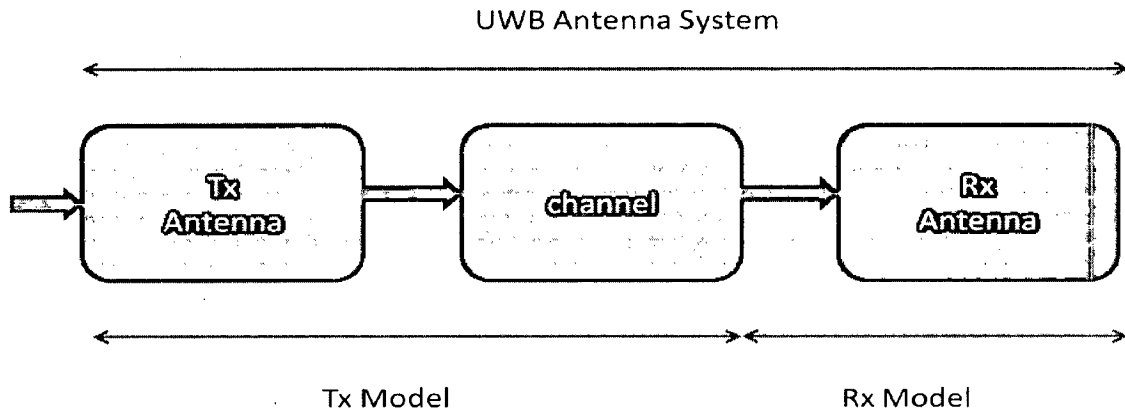


Figure 3.36 UWB Antenna System

As the UWB system operates over a wide bandwidth, the traditional Friis transmission Equation has to be modified as gain, reflection coefficient, polarization matching and power depends on the frequency of operation. The frequency dependent Friss transmission Equation is given by Equation 3.12[56].

$$\frac{P_r(\omega)}{P_t(\omega)} = (1 - |\Gamma_t(\omega)|^2)(1 - |\Gamma_r(\omega)|^2)G_r(\omega)G_t(\omega)|\hat{\rho}_t(\omega)\,\hat{\rho}_r(\omega)|^2(\frac{\lambda}{4\pi d})^2 \quad (3.12)$$

where $P_r(\omega)$ and $P_t(\omega)$ are the frequency dependent time average input power of the transmitting antenna and time average output power of the receiving antenna, respectively. $\Gamma_t(\omega)$ and $\Gamma_r(\omega)$ are the frequency dependent voltage reflection coefficient at the input terminals of the transmitting and receiving antenna respectively. $G_t(\omega)$ and $G_r(\omega$ are the frequency dependent gain of transmitting and receiving antenna respectively. $\hat{\rho}_t(\omega)$ is the frequency dependent polarization unit vector of the scattered waves. $\hat{\rho}_r(\omega)$ is the frequency

dependent polarization unit vector of the receiving antenna. d is the distance between the UWB antennas.

For UWB antenna with reflection and polarization matched and one which is oriented for maximum reception at both the transmitter and receiver side, Equation 3.12 is reduced to Equation 3.13 [56].

$$\frac{P_r(\omega)}{P_t(\omega)} = G_r(\omega)G_t(\omega)(\frac{\lambda}{4\pi d})^2 \tag{3.13}$$

$$P_t(\omega) = \frac{1}{2Z_0}\left(\frac{V_t(\omega)}{2}\right)^2 \tag{3.14}$$

$$P_r(\omega) = \frac{V_r(\omega)^2}{2Z_{Load}} \tag{3.15}$$

where $Z_0$ is the characteristic impedance of the transmission line and $Z_{load}$ is the load at the receiver side. The transfer function, S21 is defined as the ratio of the output signal to source signal. $V_t(\omega)$ and $V_r(\omega)$ are the RMS voltages at the transmitter and receiver sides and can be written from Equation 3.14 and Equation 3.15 respectively.

$$S_{21} = \frac{V_r(\omega)}{V_t(\omega)} = \left|\sqrt{\frac{P_r(\omega)}{P_t(\omega)}\frac{Z_l}{4Z_0}}\right| e^{-j\phi(\omega)} \tag{3.16}$$

$$\phi(\omega) = \phi_t(\omega)+\phi_r(\omega) + \frac{\omega d}{c} \tag{3.17}$$

where c denotes the velocity of light. $\phi_t(\omega)$ and $\phi_r(\omega)$ are the phase variations due to the transmitting and receiving antennas respectively. From Equation 3.16 it is clear that the transfer function integrates all the important system performance of transmitting and receiving antennas, such as impedance matching, gain and polarization matching. The S21 of the UWB antenna can be used to find out the group delay and impulse response of the system. It can be written in terms of $A(\omega)$ which is the transmitting response and $H(\omega)$- the receiving response and a scalar green's function[57].

$$S_{21}(\omega) = A(\omega)H(\omega)\frac{e^{jkd}}{d} \tag{3.18}$$

By the principle of reciprocity given in Equation 3.19, the transmitting response is proportional to the temporal derivative of the receiving response. This relation plays an important role in understanding the UWB radio channel model. The received signal is differentiated to obtain the original transmitted signal.

$$h_{TX}(t) = \frac{1}{2\pi c}\frac{dh_{RX}(t)}{dt} \tag{3.19}$$

$$S_{21}(\omega) = A(\omega)H(\omega)\frac{e^{-jkd}}{d} \propto \frac{1}{j\omega}A(\omega)A(\omega)\frac{e^{-jkd}}{d} \propto j\omega H(\omega)H(\omega)\frac{e^{-jkd}}{d} \tag{3.20}$$

Hence, the transmitting characteristics $A(\omega)$ $(a(t))$ and the receiving characteristics $H(\omega)$ $(h(t))$ can be calculated when the measured system transfer function $S21(\omega)$ is available.

### 3.3.2.2 Design of source pulses

Different type of source pulses can be studied based on their PSD. A narrow pulse occupies large bandwidth. If the operating bandwidth of the antenna is less than the bandwidth of the signal, received signal is distorted. Due to the wide bandwidth occupied by the signal, ringing occurs and it causes spreading in time domain. Source signal can be designed not to transmit at the notch frequency. MATLAB codes for the generation of source pulses and computation of their PSD are given in Appendix.

### 3.3.2.2.1 Gaussian pulse

The Gaussian pulse is given by the Equation 3.21 [58] and is shown in Figure 3.37.

$$F(t) = e^{-(\frac{t-1}{a})^2} \qquad (3.21)$$
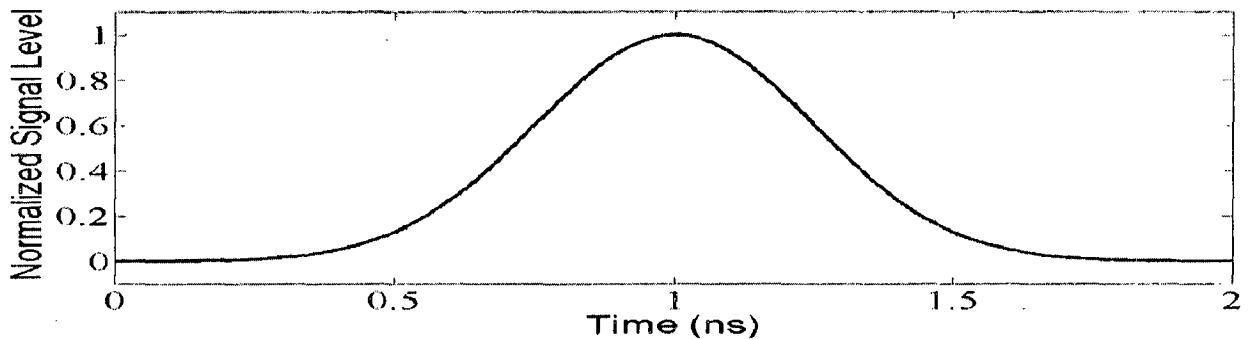


Figure 3.37 Gaussian pulse with a=350Ps
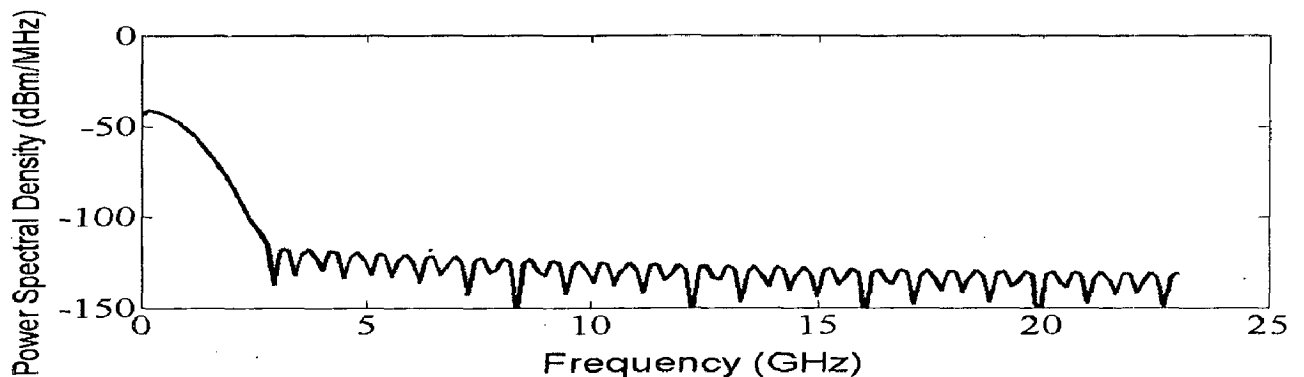


Figure 3.38 PSD of Gaussian pulse with a=350Ps

54

The PSD of Gaussian pulse is shown in Figure 3.38 where it can be seen that it is out of the FCC's emission mask (3.1-10.6GHz). So, this pulse is not suitable for transmission. However, center frequency of Gaussian pulse can be shifted by modulating it with a sine carrier which is explained in next section.

### 3.3.2.2.2 Modulated Gaussian pulse

The modulated Gaussian pulse is given by Equation 3.22 [58]. The Gaussian pulse can be modulated with a sine wave carrier of different frequencies. The carrier frequency is denoted by fc. The modulated Gaussian pulse with fc=4GHz, 6GHz and 8GHz are shown in Figs. 3.39-3.41, respectively.

$$F(t) = sin[2\pi f_c(t-1)] \, e^{-(\frac{t-1}{a})^2} \qquad (3.22)$$
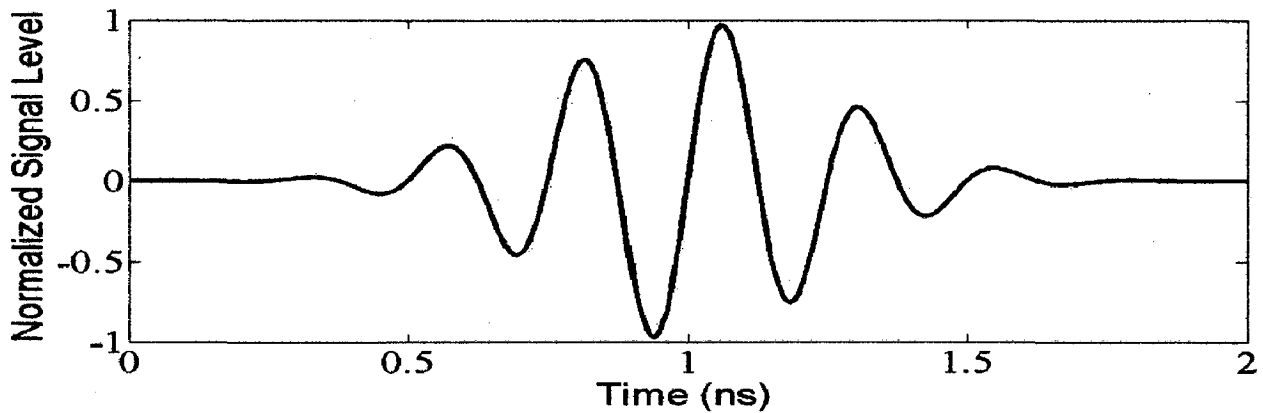


Figure 3.39 Modulated Gaussian pulse with fc=4GHz
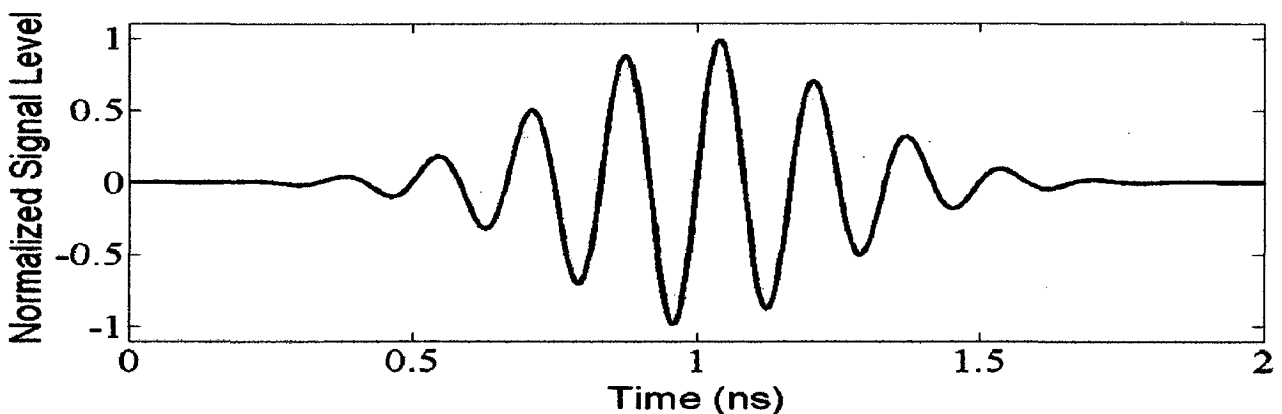


Figure 3.40 Modulated Gaussian pulse with fc=6GHz
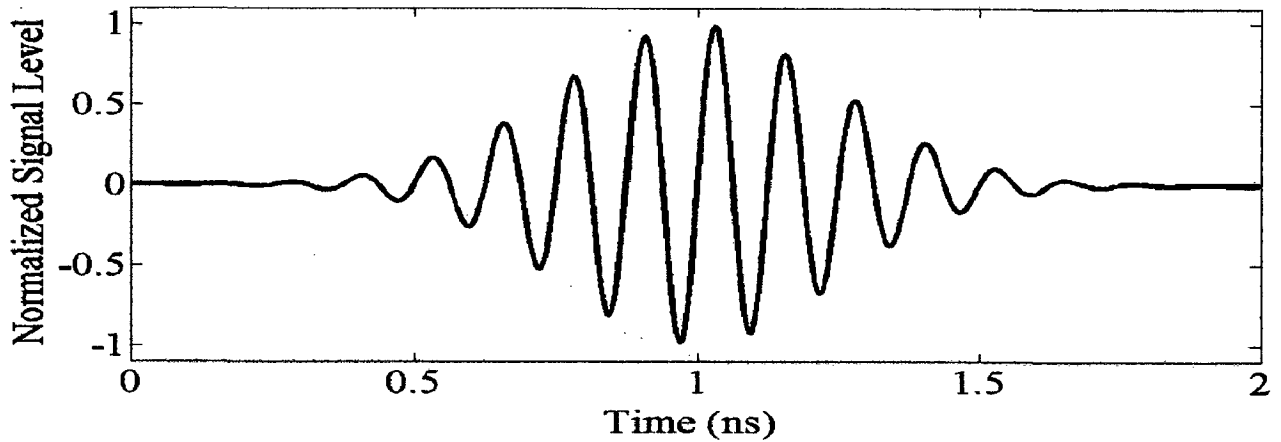
Figure 3.41 Modulated Gaussian pulse with fc=8GHz
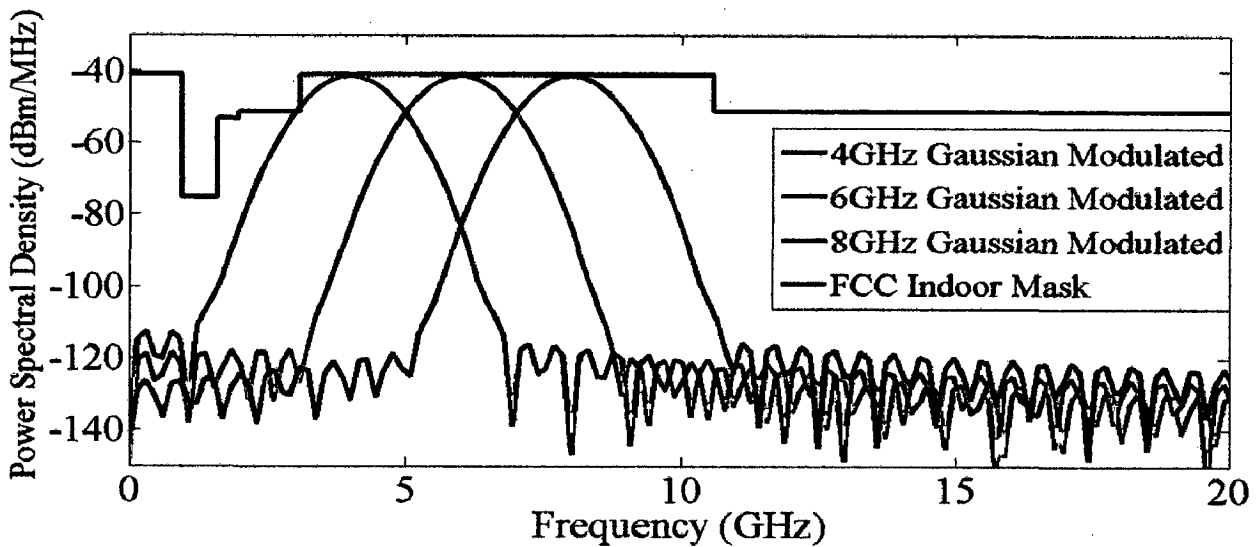


Figure 3.42 PSD of FCC's indoor mask and modulated Gaussian pulse with fc=4GHz, 6GHz and 8GHz

The PSD of modulated Gaussian pulses and FCC's emission mask are shown in Figure 3.42. The modulated Gaussian type of pulses give very high fidelity as it occupies less bandwidth.

### 3.3.2.2.3 First order Rayleigh pulse

The first order Rayleigh pulse is given by the Equation 3.23 [58].

$$F(t) = \frac{-2(t-1)}{a^2} e^{-(\frac{t-1}{a})^2} \tag{3.23}$$
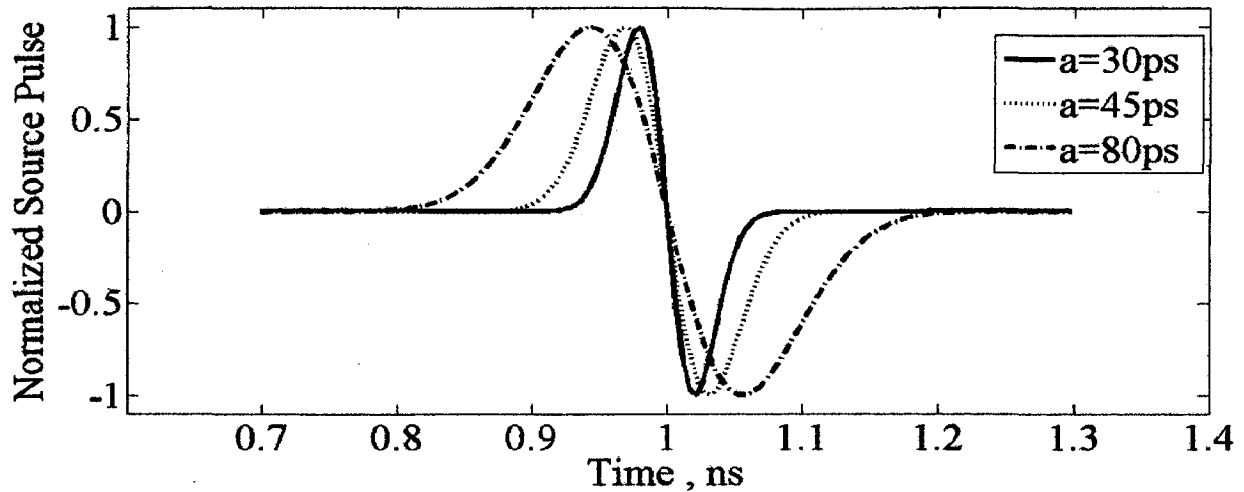
Figure 3.43 First order Rayleigh pulse with a=30Ps, a=45Ps and a=80Ps
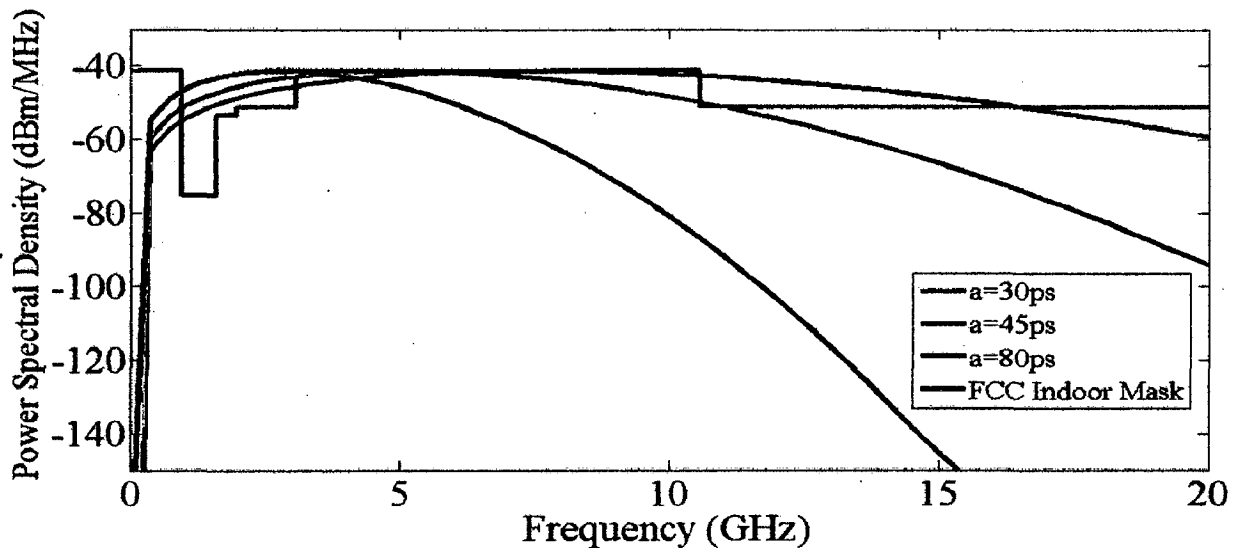


Figure 3.44 PSD of First order Rayleigh pulse with a=30Ps, a=45Ps and a=80Ps

where $a$ stands for the characteristic time. By increasing $a$, the signal is spread in time domain and limited in frequency domain. Figure 3.43 shows the waveform for the normalized source pulses with three different values of $a$. For $a$=30ps, the 10dB bandwidth ranges from 1.5GHz to 16.6GHz and so it is not suitable for transmission. When $a$ = 45ps, the 10dB bandwidth is reduced to 10.1GHz, from 1GHz to 11.1GHz. Still, the PSD at lower end of UWB band does not fit the FCC's emission mask. When a=80ps its 10dB bandwidth is only from 0.55GHz to 6.2GHz. Although first order Rayleigh pulse does not satisfy the FCC's emission mask, it has been used as its simple monocycle waveform can be easily generated by RF circuits [58].

### 3.3.2.2.4 Fourth order Rayleigh pulse

The fourth order Rayleigh pulse is given by the Equation 3.24 [58] and is shown in Figure 3.45.

$$F(t) = \left(\frac{12}{a^4} - \frac{48(t-1)^2}{a^6} + \frac{16(t-1)^4}{a^8}\right) e^{-\left(\frac{t-1}{a}\right)^2} \qquad (3.24)$$
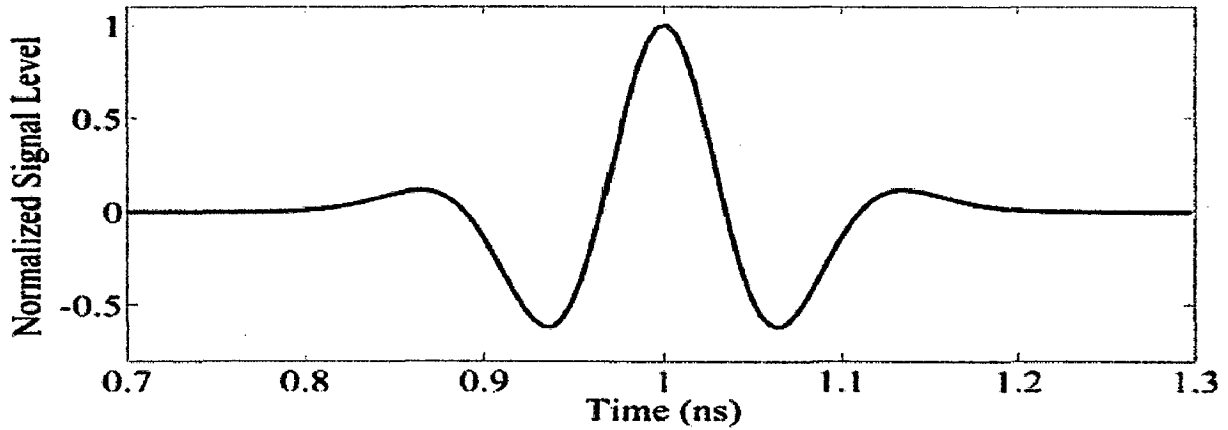


Figure 3.45 Rayleigh Fourth order pulse with a=67Ps
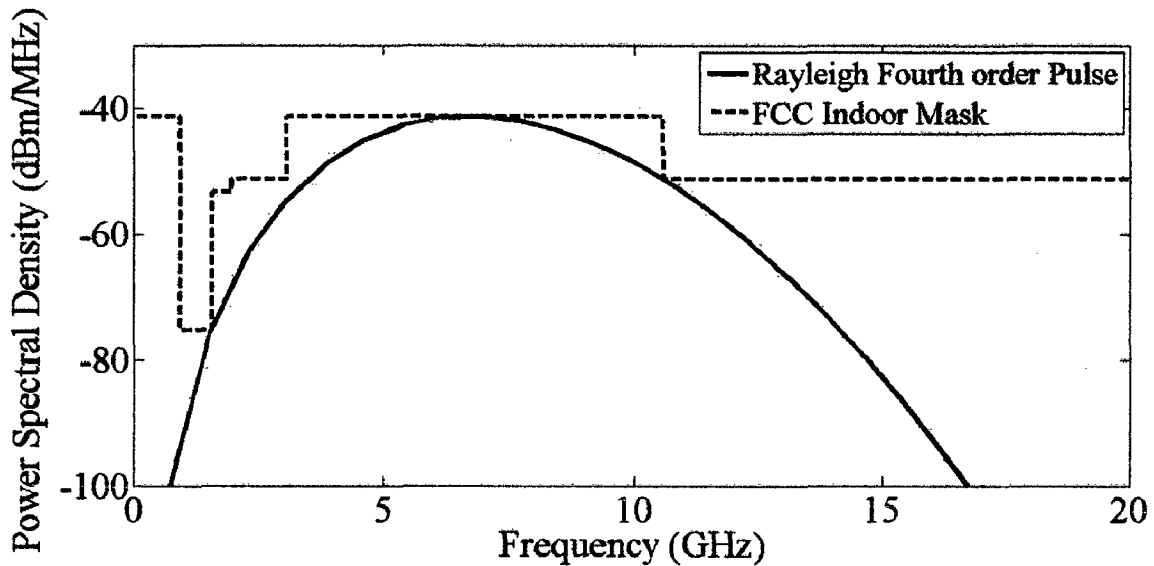


Figure 3.46 PSD of Rayleigh Fourth order Rayleigh pulse with a=67Ps

For, $a$ =64 ps, the 10dB bandwidth of Rayleigh pulse has been shown to match well with the FCC's emission mask as shown in Figure 3.46. So this source pulse is suitable for transmission as it will not cause any potential interference to the existing systems.

## 3.3.2.3 Simulated time domain response
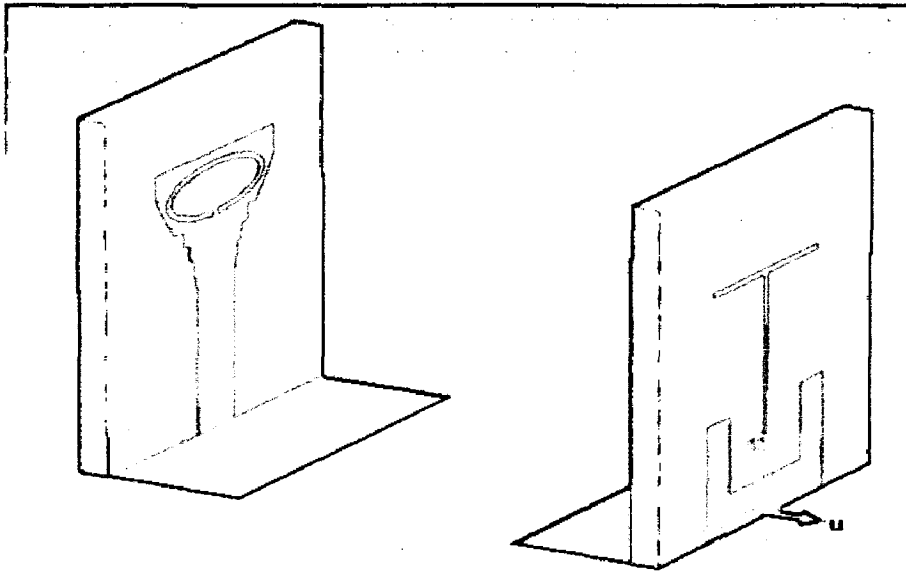


Figure 3.47 UWB antennas with face to face orientation

The time domain characteristics have been analyzed using CST microwave studio. Two identical UWB antennas are placed in the solver domain. The UWB antenna with face to face orientation is shown in Figure 3.47. The distance between the antennas is taken to be 30mm. S21 obtained using CST is shown in Figure 3.48 and the two dips at notch frequencies can be observed. As a default signal, only Gaussian pulse is present in CST corresponding to the frequency of operation. The Rayleigh fourth order pulse is of interest as it satisfies the FCC's emission mask. First, the Rayleigh function is written in MATLAB and it is sampled. Later these value are imported to CST.
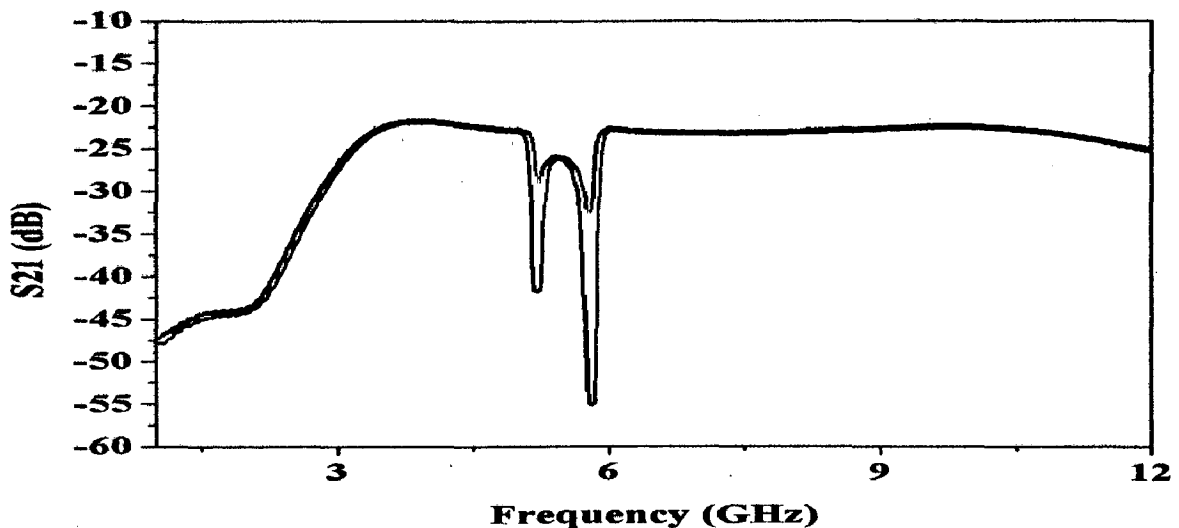


Figure 3.48 Magnitude of simulated S21 with face to face orientation

The Received Rayleigh signal is shown in Figure 3.49. The fidelity factor is used to find how far the output signal has been recovered without getting distorted by the system. The fidelity factor for Rayleigh fourth order pulse is found to be 0.93 and 0.99 for modulated Gaussian pulse.
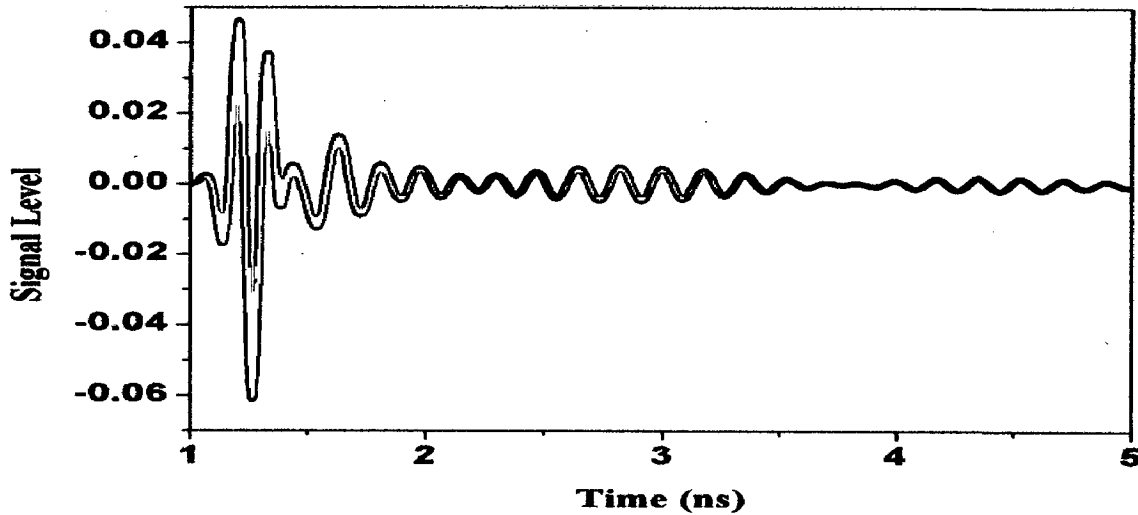


Figure 3.49 Received Rayleigh fourth order pulse

The UWB antenna with side to side orientation is shown in Figure 3.50. The distance between the antennas is taken to be 30mm. The S21 obtained using CST is shown in Figure 3.51 and the two notches at 5.2GHz and 5.8GHz can be observed. The received Rayleigh pulse is shown in Figure 3.52.
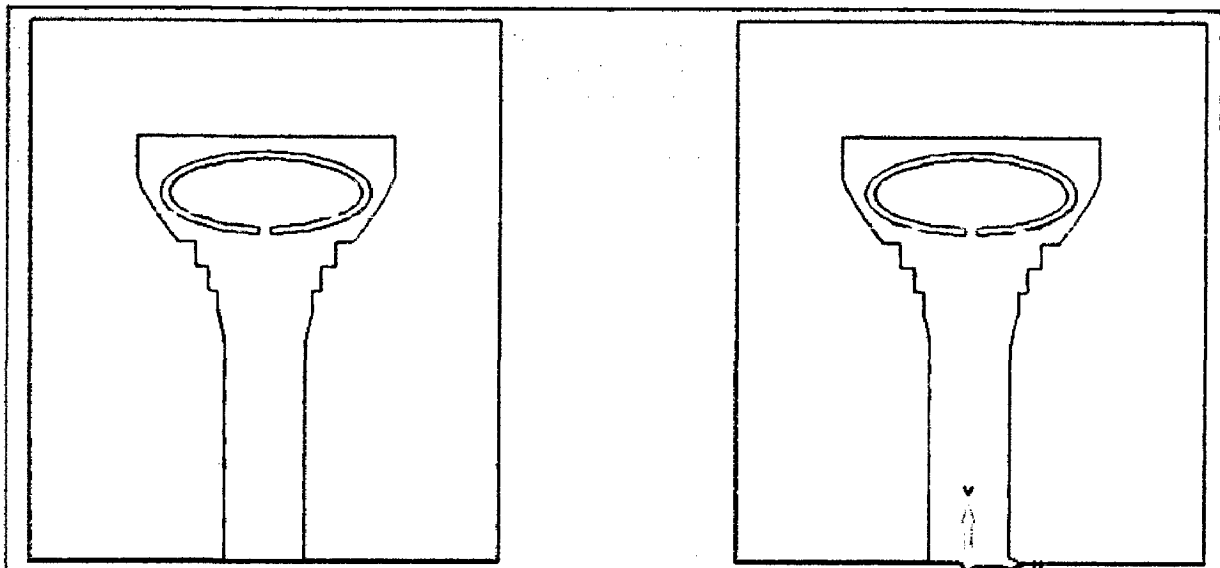


Figure 3.50 UWB antennas with side to side orientation
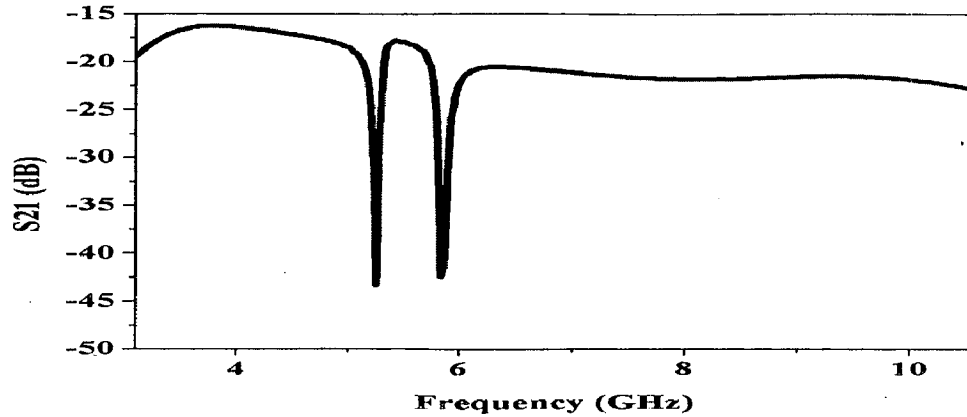
Figure 3.51 Magnitude of simulated S21 with face to face orientation
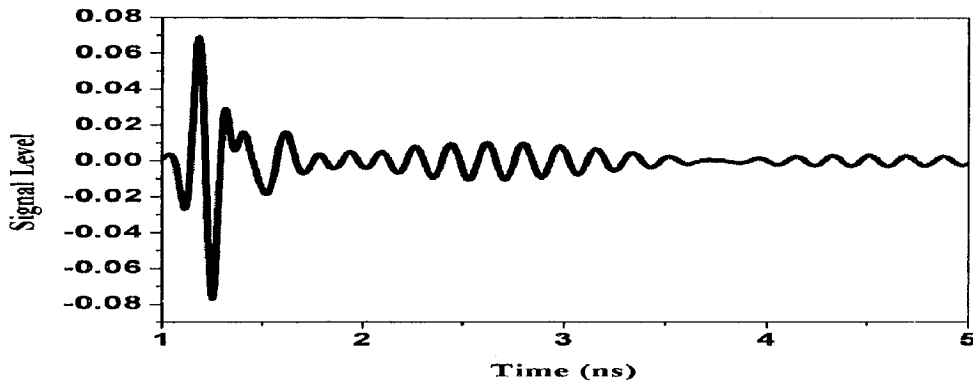


Figure 3.52 Received Rayleigh fourth order pulse

### 3.3.2.4 Measurement setup

The UWB communication link can be modelled as the transmitting antenna, the channel and receiving antenna [55]. Two identical antennas were fabricated for studying the time-domain performance of the proposed double band-notched antenna. Measurement of complex S21 was carried out in real indoor scenario by using Rohde & Schwarz ZVM Vector Network Analyzer (VNA). The measurement setup is shown in Figure 3.53. The Transmitter antenna is connected to the port 1 and the receiver antenna connected to the port 2 of the network analyzer.
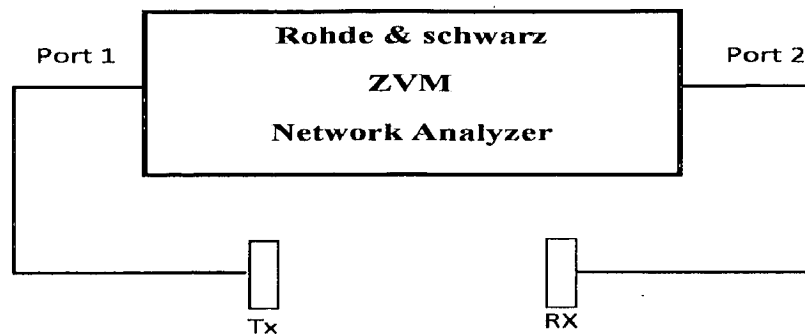


Figure 3.53 The basic network analyzer diagram for the antenna measurement

Considering the free space propagation, the transfer function S21 is proportional to the transmitting and receiving characteristics of the antenna. The magnitude of S21 is shown in Figure 3.54 where the two dips at notch frequency can be clearly observed. The phase of S21 varies linearly with frequency except at notch frequencies and is shown in Figure 3.55.
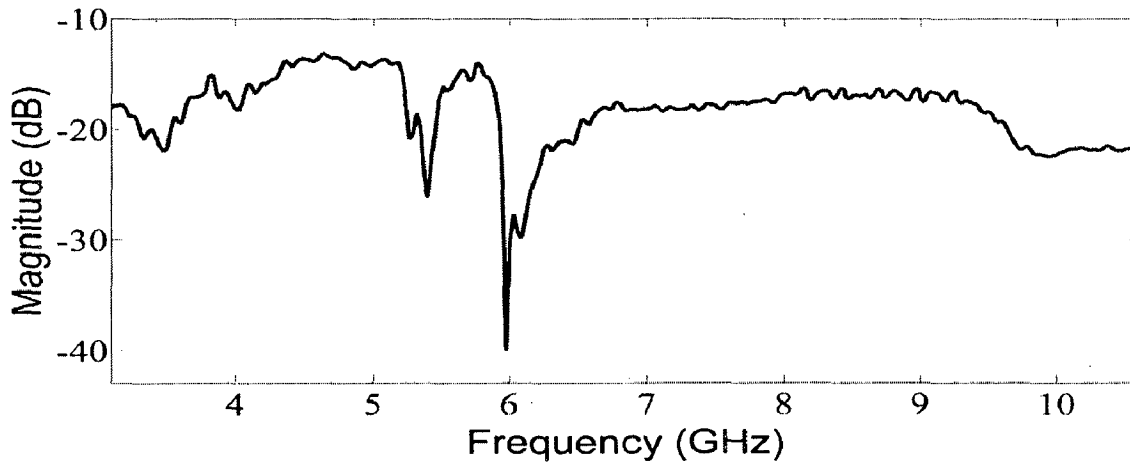


Figure 3.54 Magnitude of the measured transfer function
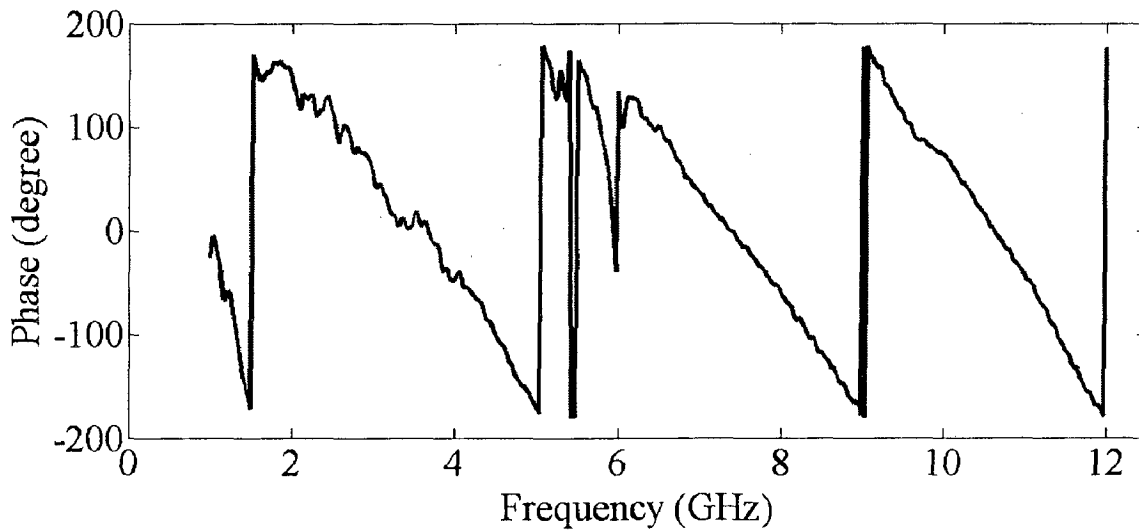


Figure 3.55 Phase of the measured transfer function

### 3.3.2.5 Impulse response of UWB antenna

The transfer function measured by vector network analyzer is the frequency response of the system. This frequency domain data can be transformed to the time domain by taking inverse fast Fourier transform (IFFT). Here, Hermitian processing is used for the data conversion [59], as illustrated in Figure 3.56.
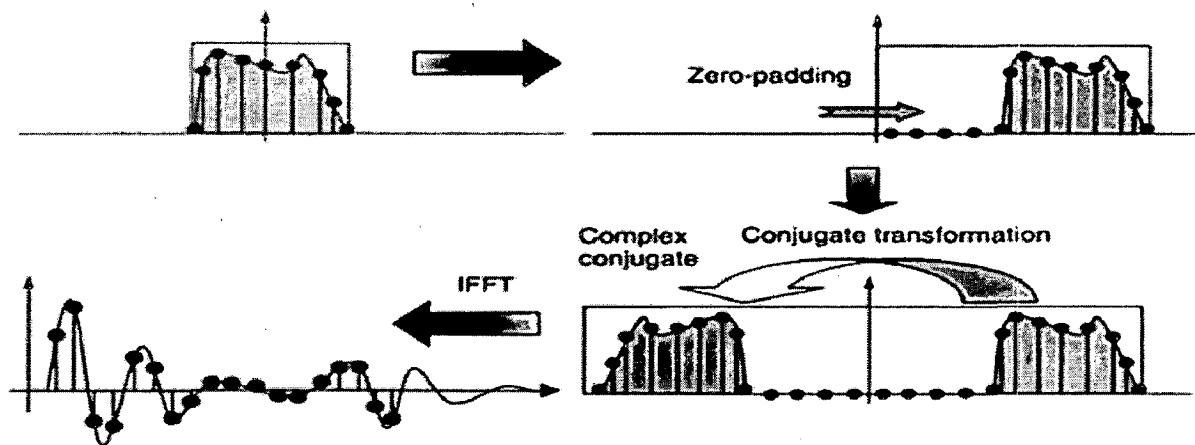


Figure 3.56 Zero padding, conjugate reflection and resulting impulse response [59]

The pass-band signal was obtained with zero padding from the lowest frequency measured in VNA to Direct Current (DC). Successively, the conjugate of the signal was taken and reflected in the negative frequency. The inverse fast Fourier transform (IFFT) of the resulting double-sided spectrum gives real impulse response [60]. Finally, the system impulse response is convolved with the input pulse to obtain the received signal.

The S21 measured using Network analyzer is discrete and has 401 Points. The IFFT has to be performed on S21 to obtain the impulse response. In the network analyzer the frequency response S21 has been displayed by performing Fast Fourier transform of the impulse response. As the S21 obtained from network analyzer is discrete it is clear that sampling has been performed. The time spacing between the time domain data of the impulse response can be found only with the knowledge of the sampling frequency. The sampling frequency of the convolution inputs must match in order to perform discrete convolution. The sampling frequency is taken twice the stop frequency of the network analyzer. The stop frequency of network analyzer was taken as 12GHz. The Hermitian processing has been explained in detail with Figures 3.57-3.60. A MATLAB program has been written to find impulse response, received signal and fidelity and is given in Appendix. S21 is obtained from the network analyzer in the frequency range of 1 to 12GHz and is shown in Figure 3.57.
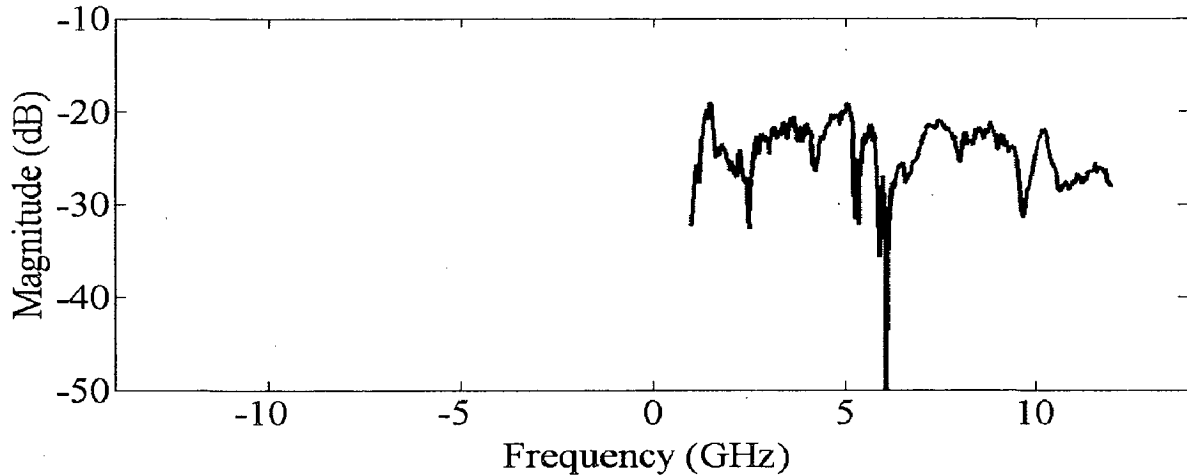
Figure 3.57 Magnitude of S21 in the 1-12GHz frequency range

The pass band signal is obtained by zero padding from 0GHz to the start frequency of network analyzer. The start frequency of network analyzer has been taken as 1GHz. Figure 3.58 shows S21 with zero padding in the 0 to 1 GHz frequency range.
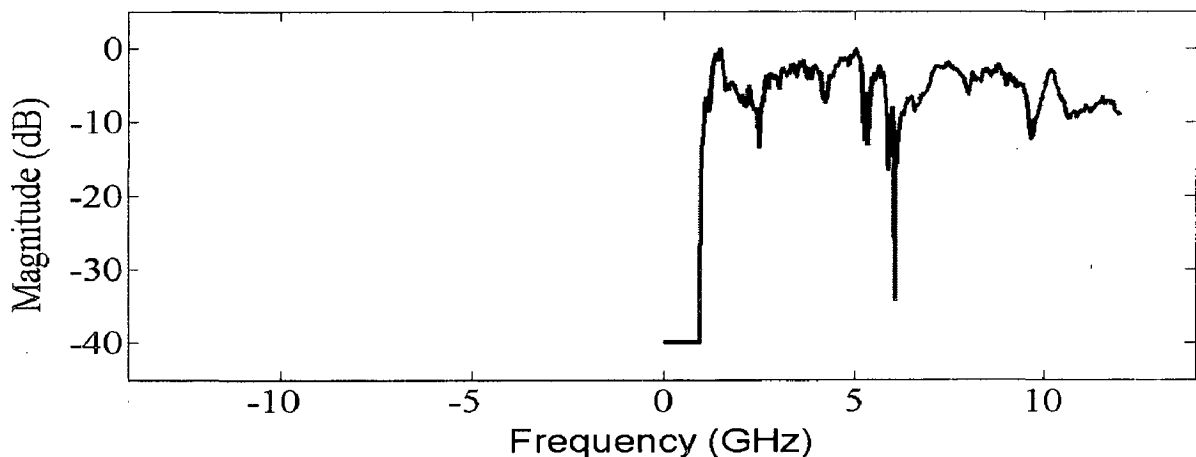


Figure 3.58 Magnitude of S21with zero padding in 0-1GHz frequency range

If X[n] is the real valued function, its FFT $X(e^{-j\omega})$ is conjugate symmetric. Likewise the IFFT of complex conjugate signal gives real valued function. Hence, conjugate of the zero padded signal is taken and reflected in the negative frequency to make the conjugate symmetric. The condition for the conjugate symmetry is given by Equation 3.25. So in order to get the real valued impulse response, S21 is made to satisfy the conjugate symmetry condition and shown in Figure 3.59.

$$X(e^{j\omega}) = X^*(e^{-j\omega})$$
(3.25)
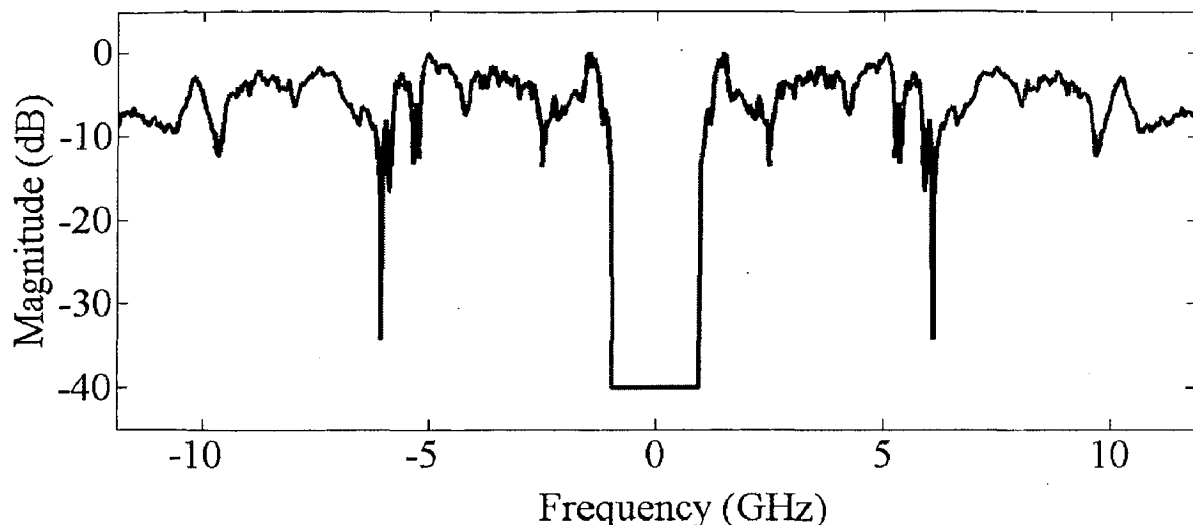
Figure 3.59 Magnitude of S21 with conjugate reflection in the negative frequency

The sampling frequency of 24GHz is enough for modulated Gaussian pulse with carrier frequency less than 9GHz. But for Rayleigh first order signal and Rayleigh fourth order signal PSD lies outside the 12GHz and so the sampling frequency of 24GHz is not enough for source pulse. Thus, zero padding is done on the high frequency side of S21 to increase the maximum frequency as shown in Figure 3.60.
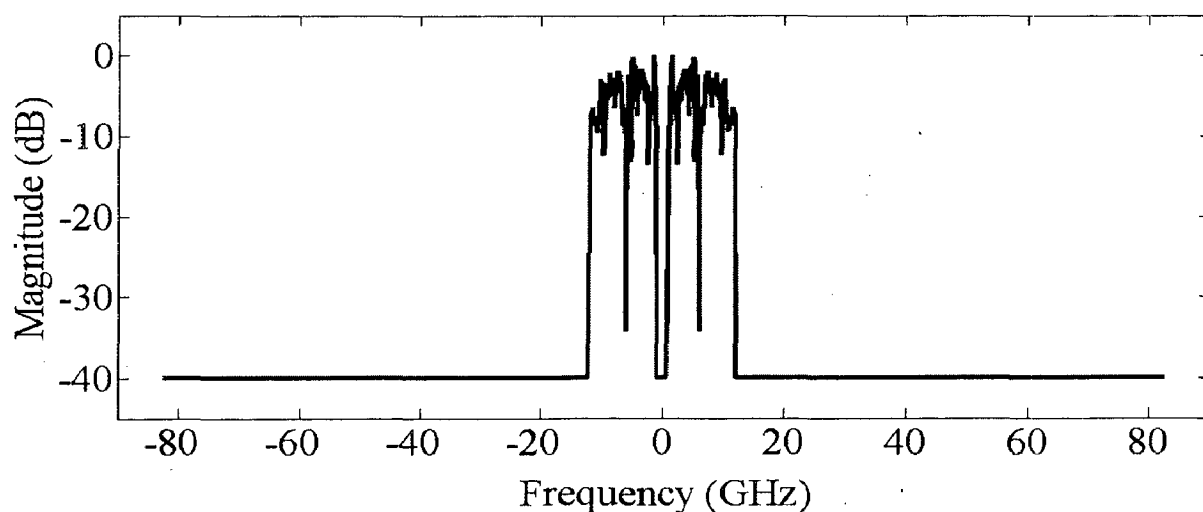


Figure 3.60 Magnitude of S21 with zero padding in 12GHz-83GHz

The IFFT of the above S21 which has complex conjugate gives the real valued impulse response of the fabricated antenna as shown in Figure 3.61. The impulse response can be used to perform convolution with the desired source pulse.
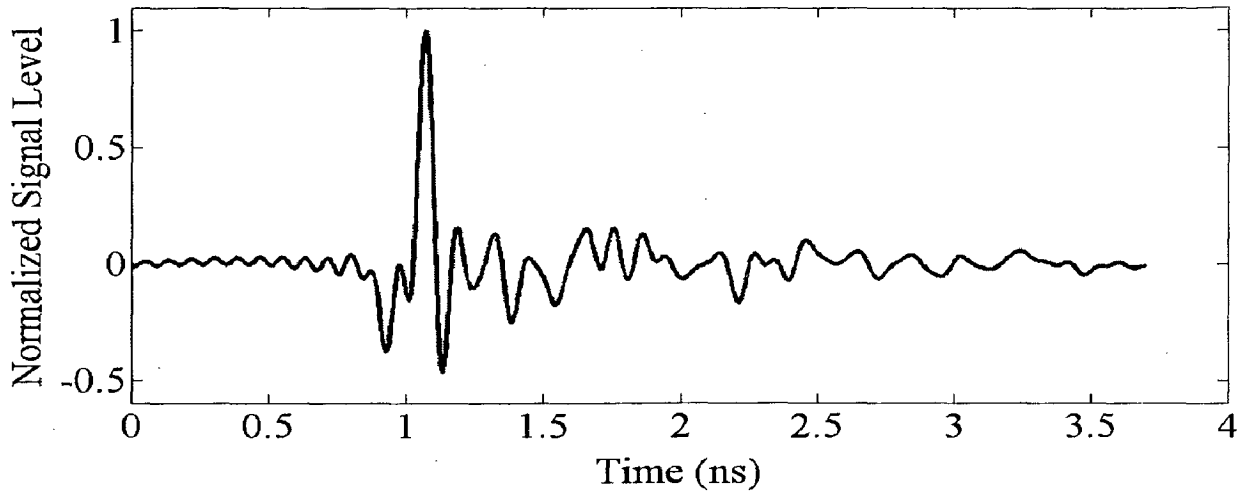
Figure 3.61 Impulse response of UWB antenna with double notch

### 3.3.2.6 Received signal waveform

Fidelity can be used to find the quality of the received signal waveform and is given by equation 3.26 [58]

$$F = \frac{max}{\tau} \left[ \frac{\int_{-\infty}^{\infty} f(t) s_R(t+\tau) dt}{\sqrt{\int_{-\infty}^{\infty} f^2(t) dt \int_{-\infty}^{\infty} s_R^2(t) dt}} \right] \qquad (3.26)$$

First the source pulse $f(t)$ and the received signal $S_R(t)$ are normalized by their energy. The fidelity $F$ is used to find the maximum correlation coefficient of the two signals by varying the time delay $\tau$. When the transmitted signal and received signal waveforms are identical to each other, the fidelity reaches its maximum. This implies that the antenna system and channel do not distort the input signal. When the two pulses are totally different in shape, fidelity decreases to a minimum value.
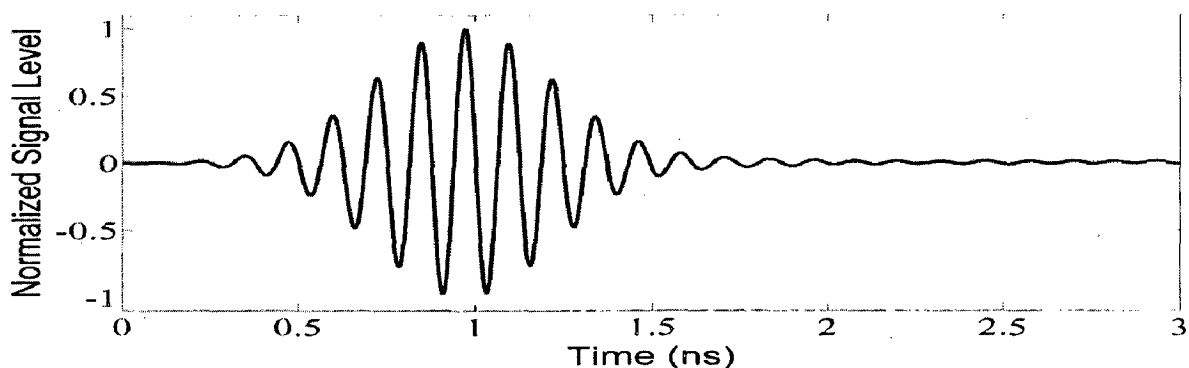


Figure 3.62 Received Pulse for Modulated Gaussian pulse

66
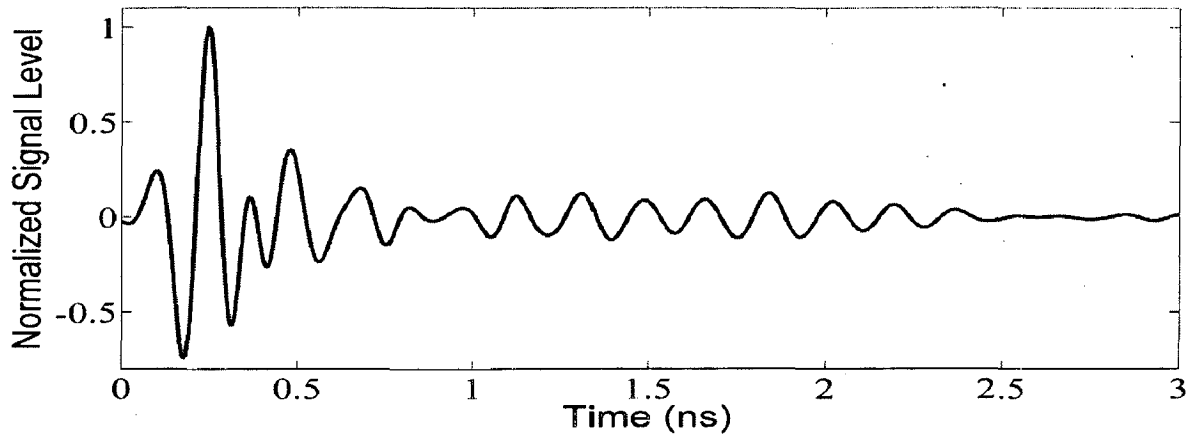
Figure 3.63 Received Pulse for Rayleigh Fourth order pulse

The received signal can be obtained by convolving the input pulse and the impulse response of the antenna. Figure 3.62 and Figure 3.63 illustrate the received pulses for Gaussian and Rayleigh transmitted pulses. The main energy of modulated Gaussian input signal lies from 7GHz to 9GHz which is not affected by the double notch. So fidelity factor is near to 0.9873 and the received signal is almost distortionless. For Rayleigh pulse, the fidelity factor has slightly come down to 0.8543 as its PSD includes notch bandwidth. Thus UWB antenna just acts as a band-pass filter and does not reshape the signal.

# 4 Coplanar waveguide fed UWB monopole antennas

In this chapter, we present two designs for a coplanar waveguide fed monopole antenna. CPW structure has advantages such as wide operating bandwidth, single metallic layer, and easy integration with monolithic microwave integrated circuits (MMICs). As it consists of single metallic layer, fabrication error due to the alignment of the top and bottom structure can be avoided.

First a monopole antenna to cover the entire UWB band of 3.1-10.6GHz has been designed. Different types of tapers are investigated to achieve the impedance match over the desired band. A parametric study of various dimensional parameters is carried out on CST Microwave Studio with the aim of understanding their effect on antenna characteristics.

The operating principle of the antenna is studied based upon the H-field distribution over the antenna. It is observed that at the low frequency end of UWB spectrum, standing wave dominates. When the frequency is increased, a hybrid mode of travelling wave and standing wave appears over the antenna. As the frequency is increased towards the high-frequency end of UWB spectrum, travelling wave dominates except at the top of the antenna structure.

Next, two band-rejection notches at 5.2GHz and 5.8GHz are introduced by combining two traditional band-notching techniques. By combining a slot in the patch and a CSSRR in the ground plane, band-rejection notches have been introduced at 5.2 GHz and 5.8 GHz WLAN bands. Performance of the proposed antenna has been investigated in both frequency and time domain.

The antenna parameters have been optimized with CST MICROWAVE STUDIO and an NH9338 substrate of thickness 1.524mm and relative permittivity of 3.38 has been used in simulation as well as for the fabrication of the antenna.

## 4.1 Antenna without band-notched function

Figure 4.1 (a) shows the basic CPW fed monopole antenna. The impedance matching is affected by coupling between the ground and patch. The impedance match in basic CPW fed monopole is poor as there is sudden increase in the distance between the ground plane and patch beyond L1. This sudden change affects the impedance matching. Figure 4.1 (b) shows the proposed antenna without band notches. The increase in the distance between patch and ground plane is reduced by introducing a taper of length L2 in the ground plane.
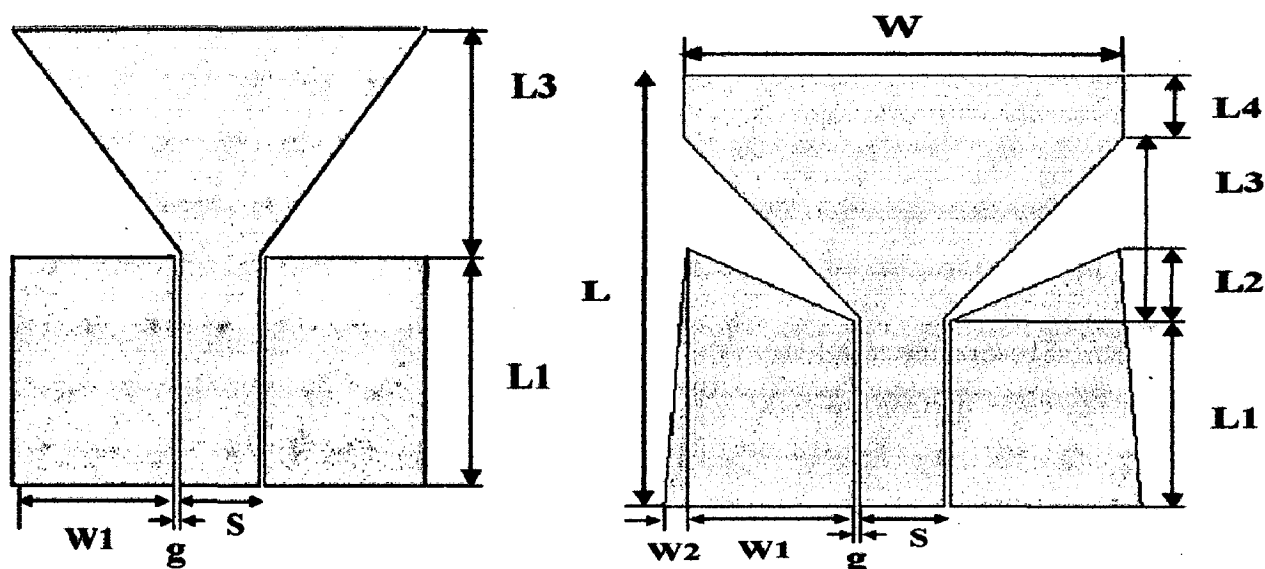


Figure 4.1 Geometry of the antenna without double notch (a) Basic CPW fed monopole antenna (b) Proposed CPW fed monopole antenna

The overall length L affects the first resonant frequency. The length of the basic CPW fed monopole antenna is equal to L1+L3 where L1 is equal to the length of the feed line and L3 is equal to the length of the taper. In order to shift the first resonant frequency downwards, the overall length should be increased. When L3 is increased, it affects the impedance matching as it affects the coupling between the patch and the ground plane. In the proposed antenna an additional length L4 is introduced to increase the overall length.

W2 is found to affect the performance of the antenna on the lower frequency side. By increasing W2, better impedance match is achieved around 3.1GHz. Parameters S and g are selected to obtain a 50 Ω CPW line.

## 4.1.1 Effect of various parameters on antenna's performance

The performance of coplanar waveguide fed antenna is quite sensitive to various parameters like length of the patch L4, L2, W2 and taper length L3. These parameters affect the impedance matching at different frequencies. A parametric study was carried out by varying one parameter at a time, keeping other parameters constant.

## 4.1.1.1 Effect of variation in patch length, L4

Figure 4.2 illustrates the magnitude of S11 for different values of the length L4. The other dimensions of the antenna were kept constant and are given in Table 4.1.

Table 4.1 Parameters of the antenna with L4 as a variable

| Parameter | L | L1 | L2 | L3 | S | g | W | W1 | W2 |
|-----------|-----|------|-----|------|-----|------|------|-----|-----|
| Value(mm) | 28.1 | 12.1 | 5.3 | 12.5 | 3.8 | 0.25 | 19.6 | 7.4 | 0.5 |

The first resonance frequency is affected by the overall length of the antenna. When L4 is small, there is impedance mismatch around 3.1GHz and 7.8GHz. As L4 is increased, the first resonant frequency shifts toward the left as shown in figure 4.2. Further increase in L4 causes impedance mismatch around 4.8GHz. The optimized value of L4 has been found to be 4mm.
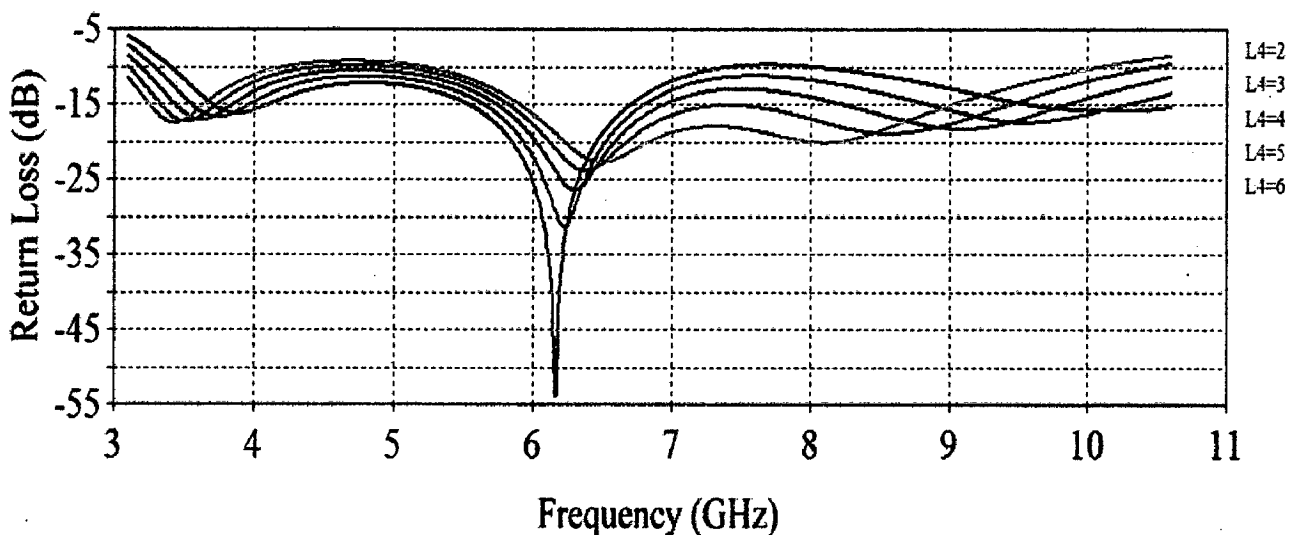


Figure 4.2 Variation of |S11| with L4

## 4.1.1.2 Effect of variation in W2

Figure 4.3 illustrates the magnitude of S11 for different values of the width W2. The other dimensions of the antenna were kept constant and are given in Table 4.2.

Table 4.2 Parameters of the antenna with W2 as a variable

| Parameter | L | L1 | L2 | L3 | L4 | S | g | W | W1 |
|-----------|-----|------|-----|------|----|-----|------|------|-----|
| Value(mm) | 28.1 | 12.1 | 5.3 | 12.5 | 4 | 3.8 | 0.25 | 19.6 | 7.4 |

When width W2 is increased the impedance matching gets better in the 3.1-10.6GHz frequency range and the first resonant frequency shifts towards the left as shown in figure 4.3. W2=1mm is chosen to keep the size of the antenna small.
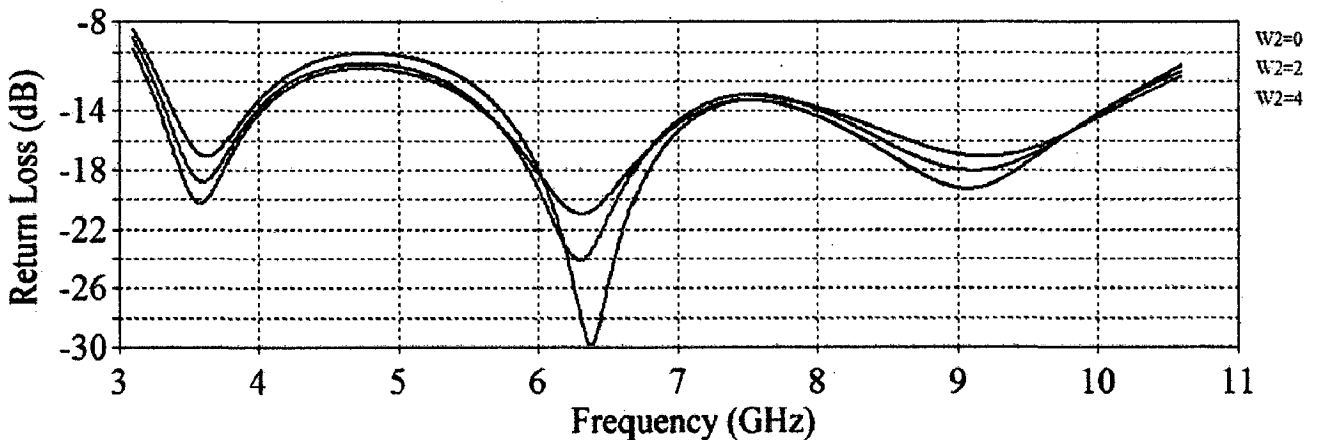


Figure 4.3 Variation of |S11| with W2

## 4.1.1.3 Effect of variation in L2

Figure 4.4 illustrates the magnitude of S11 for different values of the length L2. The other dimensions of the antenna were kept constant and are given in Table 4.3.

Table 4.3 Parameters of the antenna with L2 as a variable

| Parameter | L | L1 | L3 | L4 | S | g | W | W1 | W2 |
|-----------|-----|------|------|-----|-----|------|------|-----|----|
| Value(mm) | 28.1 | 12.1 | 12.5 | 4.0 | 3.8 | 0.25 | 19.6 | 7.4 | 1 |

The impedance matching is highly affected by coupling between the ground and the patch. When L2 is small the impedance matching around 5.5GHz is getting worst. As L2 is

increased, first resonant frequency shifts towards right as shown in figure 4.4. The optimized value of L2 has been found to be 4.7mm.
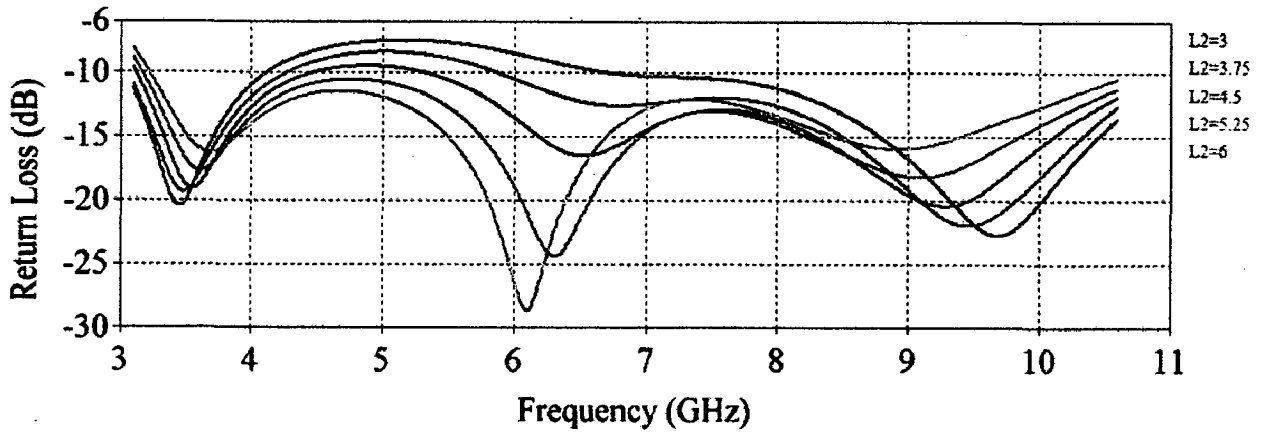


Figure 4.4 Variation of |S11| with L2

## 4.1.1.4 Effect of variation in the taper length, L3

Figure 4.5 illustrates the magnitude of S11 for different values of the taper length L3. The other dimensions of the antenna were kept constant and are given in Table 4.4.

Table 4.4 Parameters of the antenna with L3 as a variable

| Parameter | L | L1 | L2 | L4 | S | g | W | W1 | W2 |
|-----------|------|------|-----|----|-----|------|------|-----|----|
| Value(mm) | 28.1 | 12.1 | 4.7 | 4  | 3.8 | 0.25 | 19.6 | 7.4 | 1  |

When the taper length L3 is increased the first resonant frequency shifts toward the left as shown in figure 4.5. Further increase in the length affects the coupling between the taper and ground plane and thus affects the impedance matching around 5GHz. The optimized value of L3 has been found to be 11.9mm.
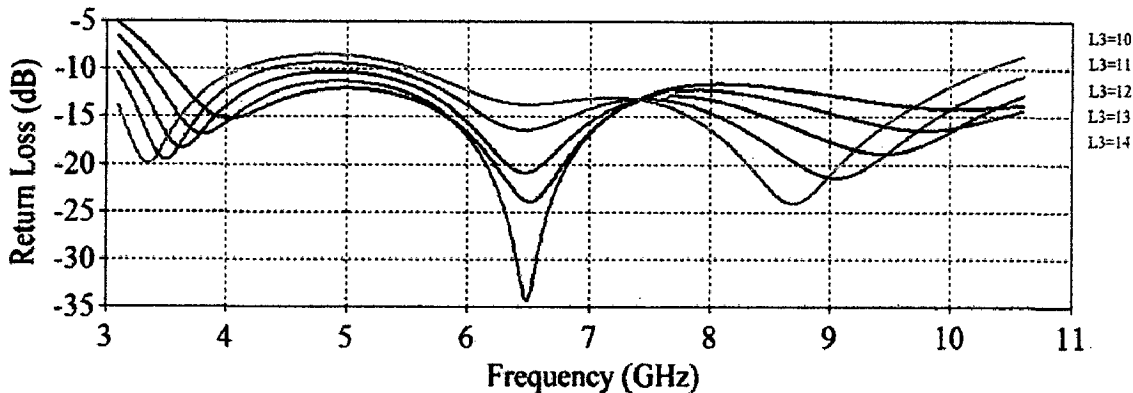


Figure 4.5 Variation of |S11| with L3

## 4.1.1.5 Optimized antenna parameters

The above mentioned parameters affect the impedance matching at different frequencies. The size of the optimized antenna is 21.2 mm × 28.1 mm. The parameters of optimized antenna are given in Table 4.5. The simulated VSWR of the optimized antenna is given in Figure 4.6.

Table 4.5 Parameters of the optimized antenna without bandnotch

| Parameter | L | L1 | L2 | L3 | L4 | S | g | W | W1 | W2 |
|-----------|------|------|-----|------|----|-----|------|------|-----|----|
| Value(mm) | 28.1 | 12.1 | 4.7 | 11.9 | 4 | 3.8 | 0.25 | 19.6 | 7.4 | 1 |
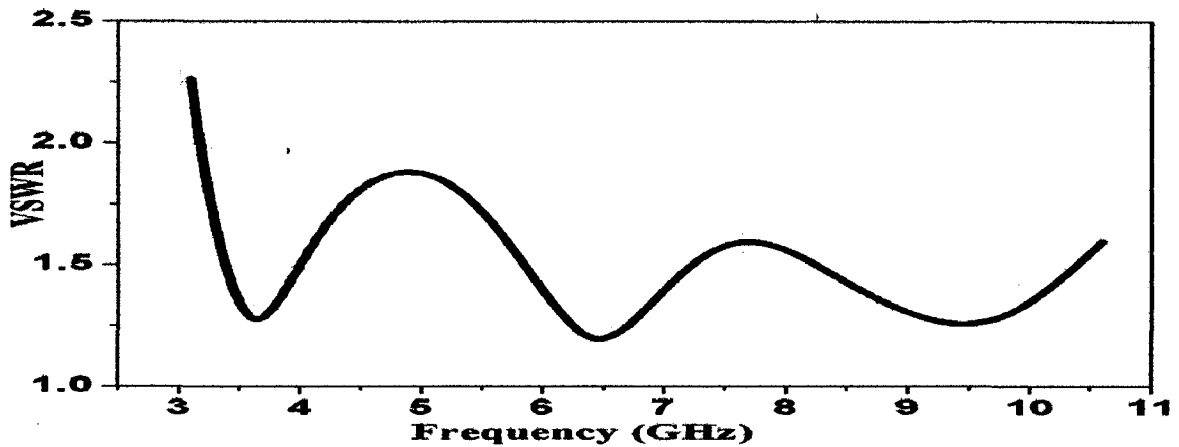


Figure 4.6 Simulated VSWR of the optimized antenna without band notch

## 4.1.2 Simulation and experimental results for the optimized antenna

The optimized CPW-fed monopole antenna without bandnotch was fabricated. Simulation and experimental results have been obtained for the optimized antenna and a comparison has been made.
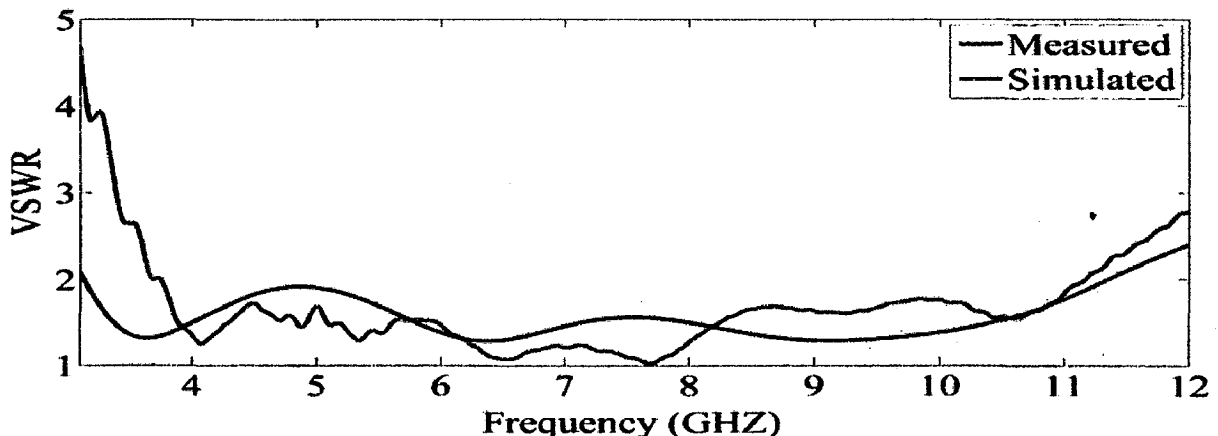


Figure 4.7 Measured and simulated VSWR of the proposed antenna without band notch

Figure 4.7 shows the Simulated and measured VSWR of the proposed antenna. The measured VSWR matches with the simulated VSWR except in the band of 3.1GHz- 3.8GHz.
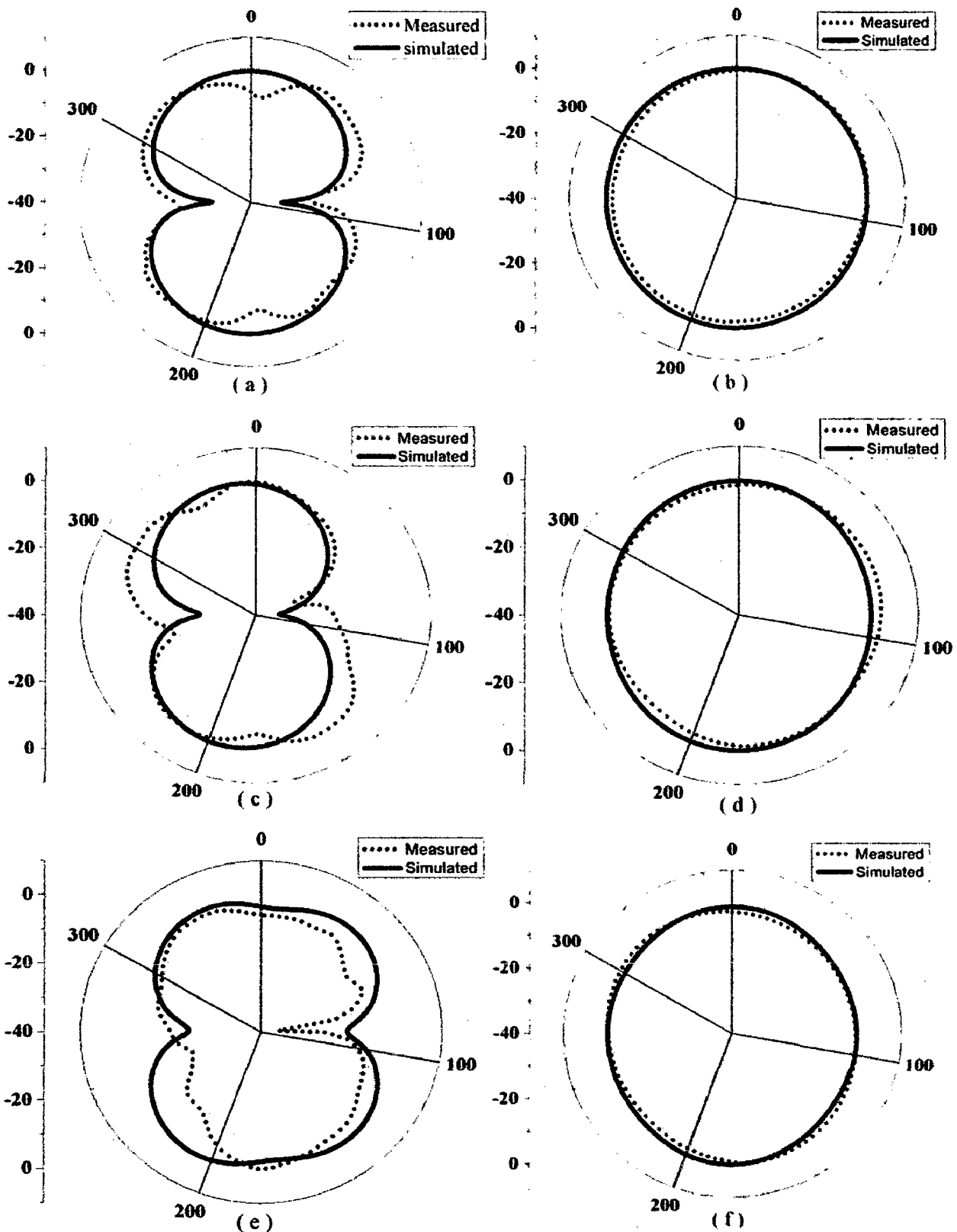


Figure 4.8    Simulated and measured radiation patterns of double notch antenna (a) E-plane at 4GHz (b) H-plane at 4GHz (c) E-plane at 6GHz (d) H-plane at 6GHz (e) E-plane at 9GHz (f) H-plane at 9GHz

The measured and the simulated normalized E-plane and H-plane radiation patterns at 4GHz, 6GHz and 9GHz are shown in Figure 4.8. The front lobe and back lobe of E-plane does not spilt into minor ones over the operating bandwidth. The H-plane radiation patterns are Omni-directional over the operating bandwidth and have variation less than 5dB in most of the direction.
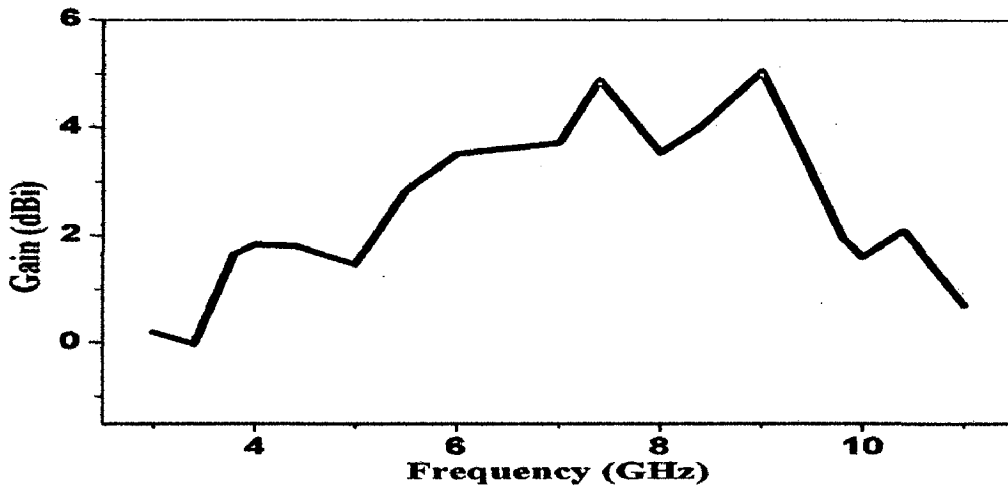


Figure 4.9 Measured gain of the CPW fed monopole antenna without band notch function

The measured peak gain of the proposed antenna is plotted in Figure 4.9. It can be seen that a gain of 2-5dB is obtained over most of the operating band.

### 4.1.3 Operating Principle of CPW fed UWB monopole antenna

The working of the CPW fed monopole antenna can be revealed by examining the magnetic field distributions over the antenna.



(a)  (b)  (c)

A/m

80.1
44.0
26.9
16.2
9.42
5.18
2.51
0.834
0

(d)  (e)  (f)
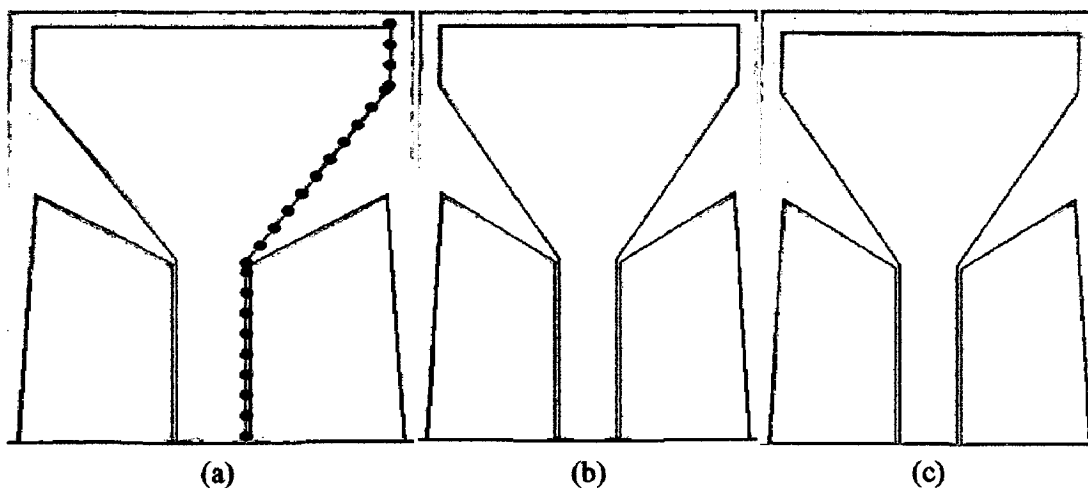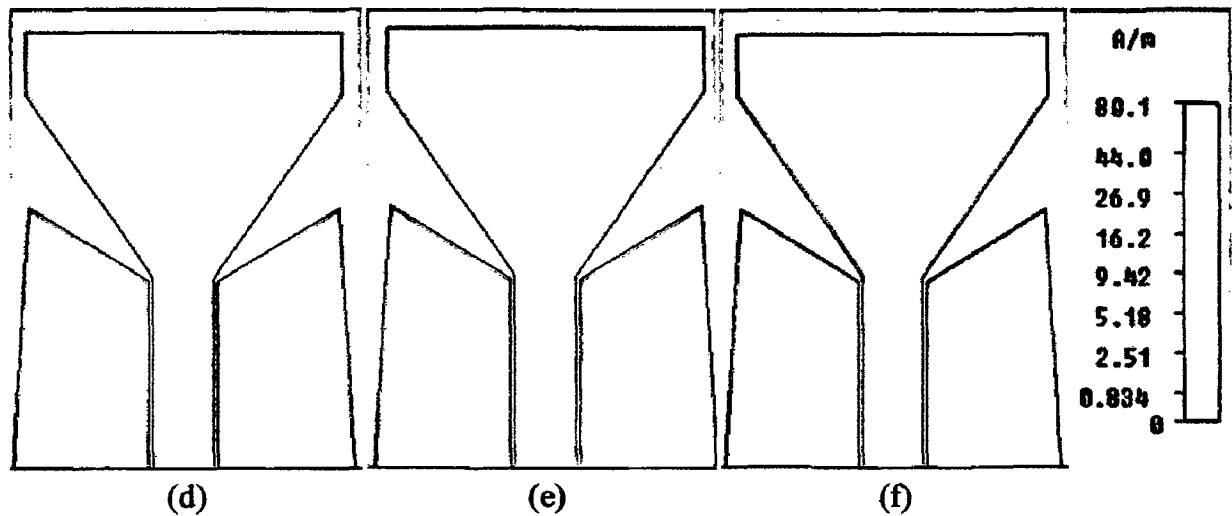
Figure 4.10 Snapshots of the magnetic field distribution at 3.3 GHz at different phases (a) phase=0 (b) phase=30 (c) phase=60 (d) phase=90 (e) phase=120 and (f) phase=150

The snapshots of the magnetic field distributions over the antenna at different phases have been shown in Figure 4.10 (a)–(e). The snapshots have been taken at 3.3 GHz. The field distribution is observed along the edges of the center conductor of CPW feed which is highlighted by dots as shown in figure 4.10 (a). If we closely observe along the edge at different phases, the amplitude seems to increase and decrease which confirms standing wave pattern. The antenna has a pure standing wave pattern along most part of the edges. So at low frequencies the antenna is dominated by standing wave.



(a)  (b)  (c)

76
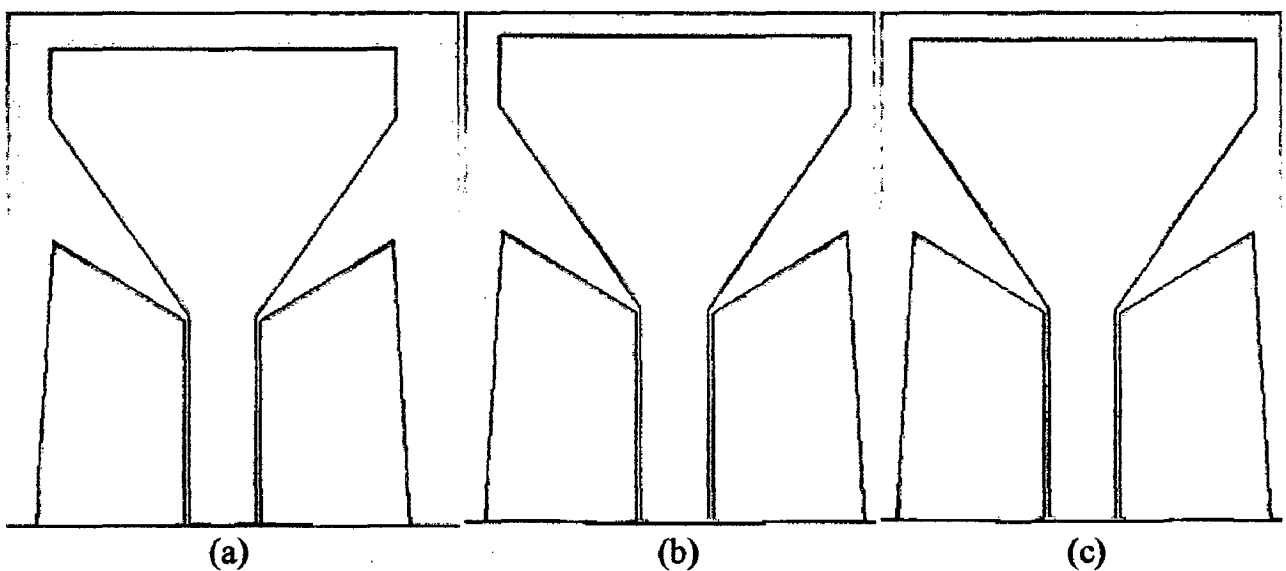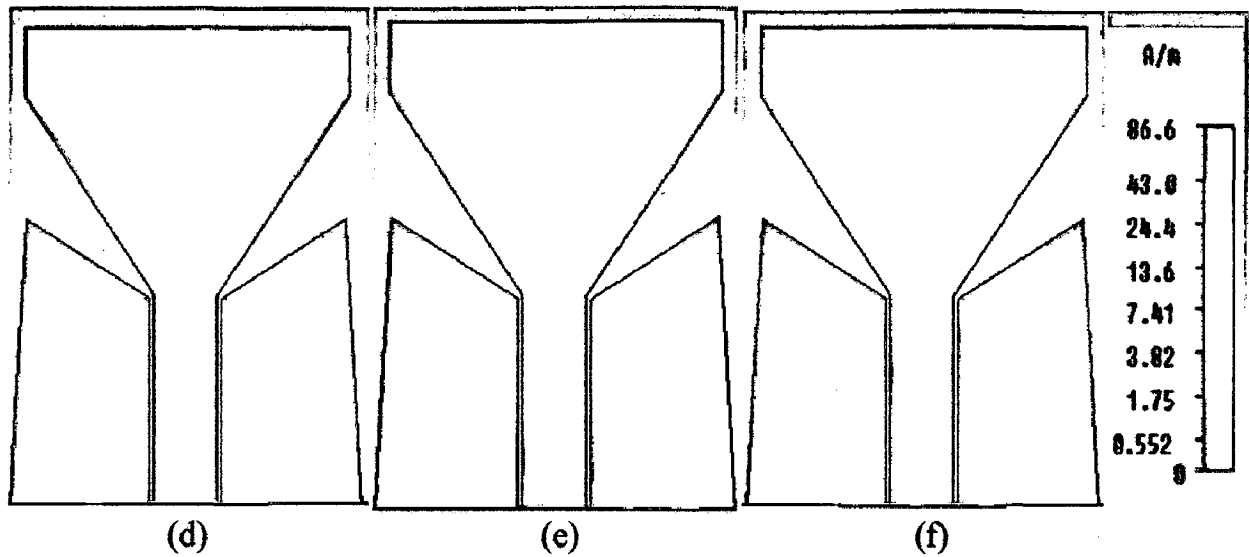
Figure 4.11 Snapshots of the magnetic field distribution at 5 GHz at different phases (a) phase=0 (b) phase=30 (c) phase=60 (d) phase=90 (e) phase=120 and (f) phase=150

Figure 4.11 (a)-(e) show the snapshots taken at 5 GHz. The nature of the antenna current distribution changes as the frequency is increased from 3.3GHz to 5GHz. The current travels along the edges of the feed line. But the current along the edges of the taper is oscillating. Hence, the CPW-fed monopole operates in a hybrid mode of standing wave and travelling wave as the frequency is increased.

|       |
|-------|
| a/m   |
| 82.9  |
| 41.2  |
| 23.3  |
| 13.8  |
| 7.89  |
| 3.66  |
| 1.67  |
| 0.528 |
| 0     |

(d)                    (e)                    (f)
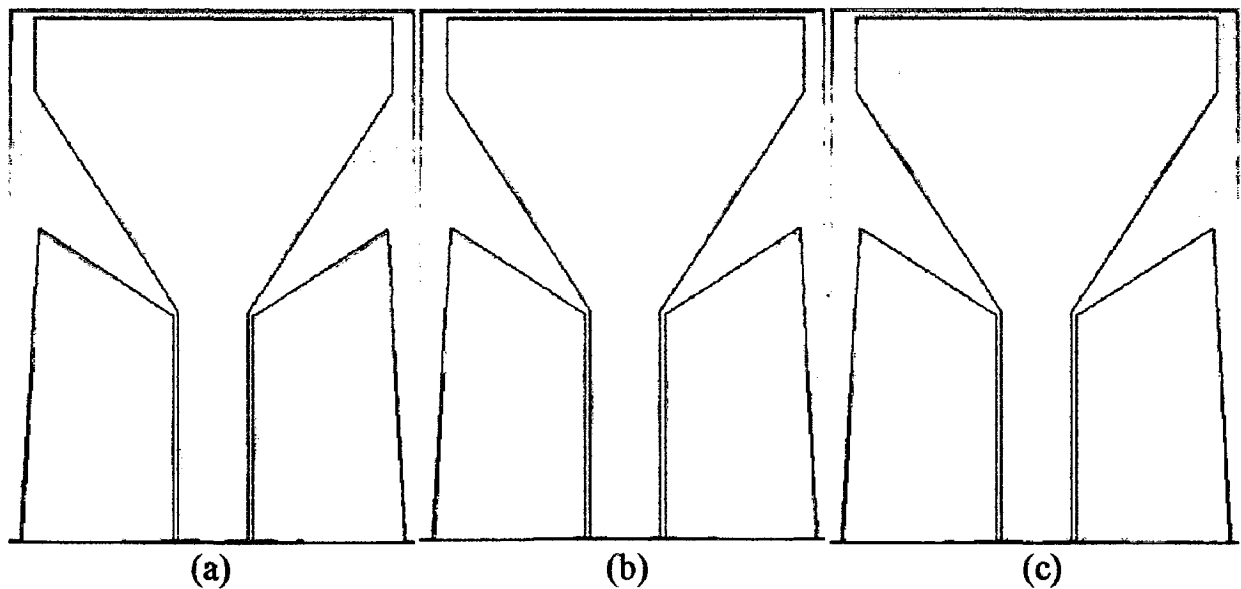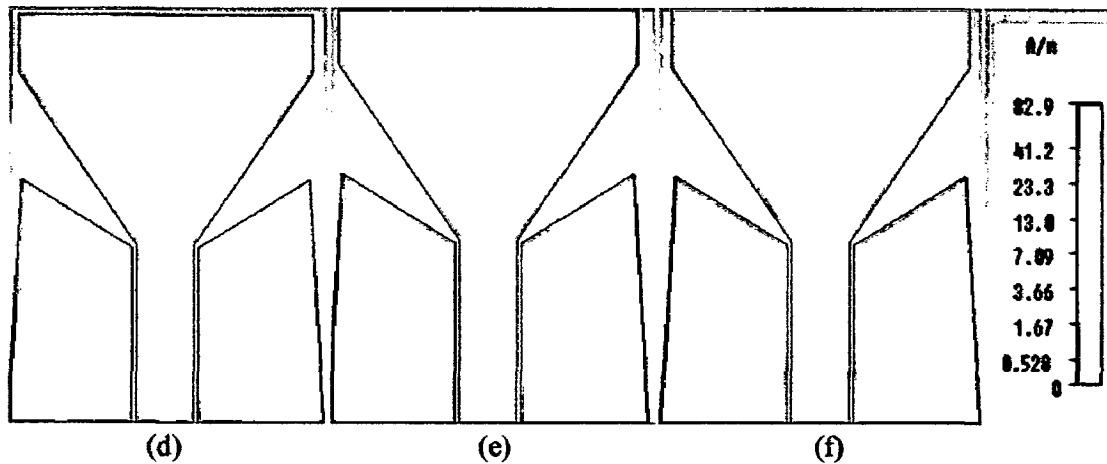
Figure 4.12 Snapshots of the magnetic field distribution at 9.3 GHz frequency at different phases (a) phase=0 (b) phase=30 (c) phase=60 (d) phase=90 (e) phase=120 and (f) phase=150

The Figure 4.12 (a)-(e) corresponds to the snapshots taken at 9.3GHz. At 9.3 GHz the travelling wave seems more prominent along the edges of the feed line and the taper.

At 3.1GHz, compared to wavelength (65mm) the antenna dimension (28.13mm) is small. So the EM wave gets reflected at the tip of the antenna structure. Due to this, the EM wave gets reflected from the end and standing wave is formed. As the frequency is further increased, the antenna starts to operate in a hybrid mode consisting of a standing wave and travelling wave. At the high frequency end, the antenna dimension (28.13 mm) is large compared to wavelength (19.1mm). So, EM wave has to travel down the antenna structure before getting reflected. Therefore, reflection takes place only at the tip of the antenna structure. Remaining portion of the antenna structure is dominated by the travelling wave at higher frequencies.
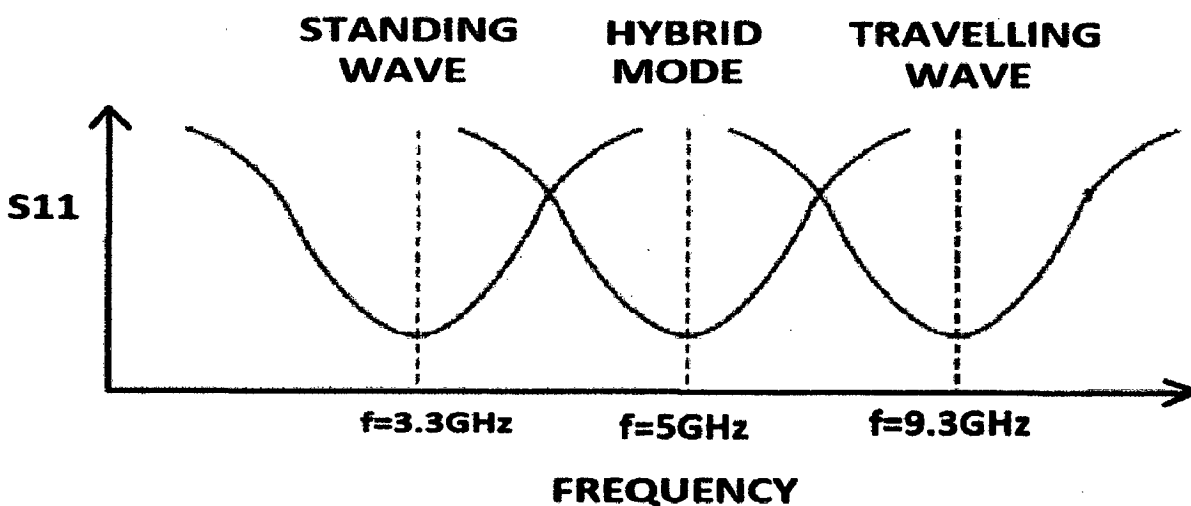


Figure 4.13 Operating principle of microstrip line fed monopole antenna

78

The operation of the CPW-fed monopole antenna across the whole spectrum is illustrated in Figure 4.13. The overlapping of the closely spaced resonance modes in CPW-fed monopole antenna is responsible for the ultra-wide −10 dB bandwidth. The resonance of the CPW-fed monopole antenna occurs at the frequencies f=3.3 GHz, 5 GHz and 9.3 GHz.

## 4.2 Antenna with double band-notched function

The double notch is obtained by combining two conventional methods of band notching. By combining a slot in the patch and a Complementary Single Split Ring Resonator (CSSRR) in the ground plane, band-rejection notches have been introduced at 5.2 GHz and 5.8 GHz WLAN bands. The geometry of the proposed antenna is shown in figure 4.14.
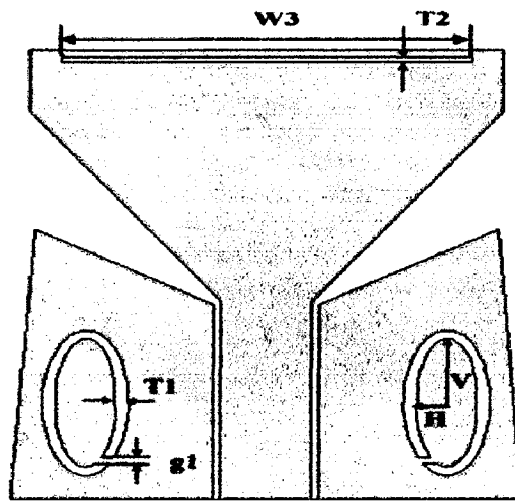


Figure 4.14 Geometry of the proposed antenna with double notch

First, the two methods were implemented separately in the proposed CPW-fed monopole antenna. A slot was introduced in the patch to produce a notch at 5.8GHz. The initial length of the slot was taken to be half of the wavelength (17.5mm) corresponding to the rejection frequency [50].

To provide a notch at 5.2GHz, a CSSRR has been introduced in the ground plane. The starting value of the circumference of the CSSRR (19.5mm) was taken to be half of the rejection wavelength [50].
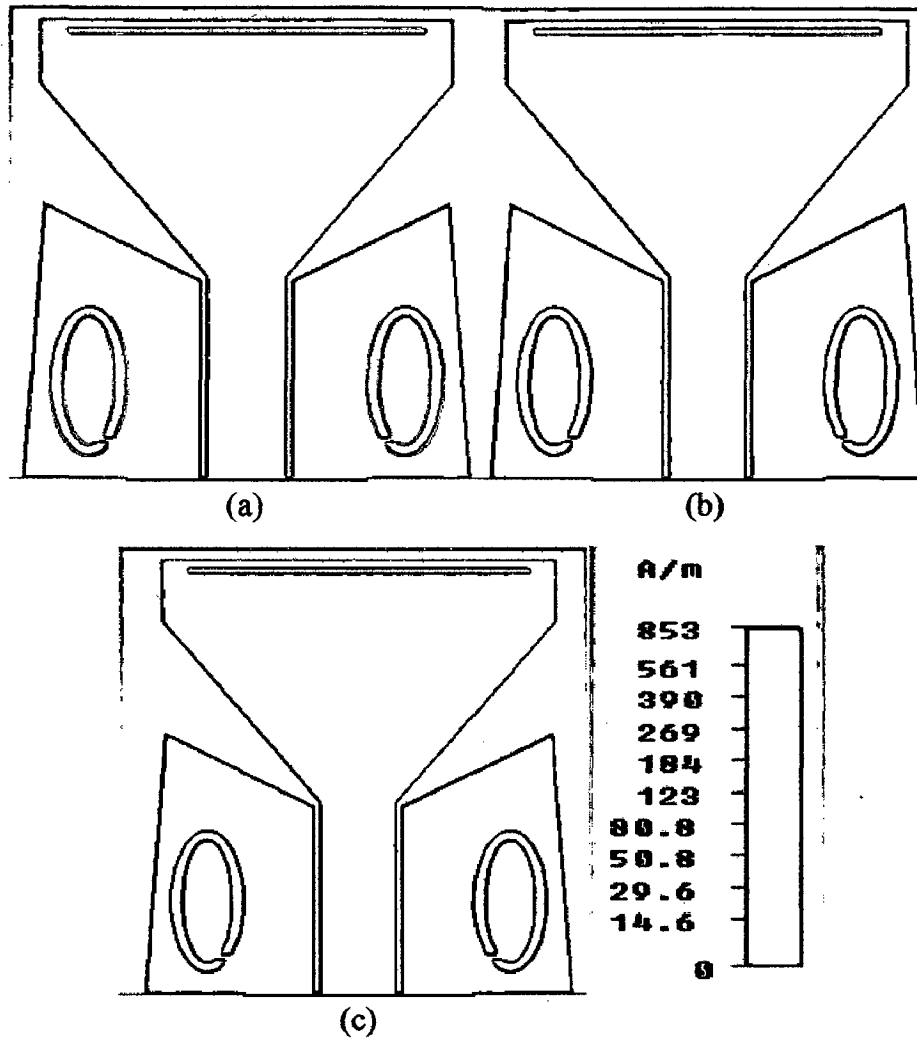
Figure 4.15 Surface current distribution (a) 5.2GHz (b) 5.8GHz (c) 8GHz

The above mentioned two methods were combined to produce notches at 5.2GHz and 5.8GHz. Upon combining them together the mutual coupling between the slot in the patch and CSSRR makes them a single notch covering 5.2GHz-5.8GHz. This happens as the notch frequencies are closely placed. From the surface current distribution of CSSRR at 5.2GHz it is clear that surface current is concentrated at the spilt end. So, in order to reduce the mutual coupling the spilt end in CSSRR is varied from center to bottom as shown in figure 4.14 as opposed to the conventional CSSRR. From the surface current distribution over the antenna at 5.8GHz as shown in figure 4.15 (b) we can conclude that the antenna ceases to radiate at this frequency. The optimized parameters of slot and CSSRR are given in Table 4.6.

Table 4.6 Optimized parameters of CSSRR and slot in patch

| Parameters | W3 | T1 | T2 | g1 | V | H |
|------------|-----|-----|-----|-----|----|-----|
| Values(mm) | 17 | 0.5 | 0.3 | 0.4 | 4 | 1.3 |

## 4.2.1 Frequency domain characteristics

The optimized CPW-fed monopole antenna with double notch has been fabricated and the experimental results are compared with simulation results.
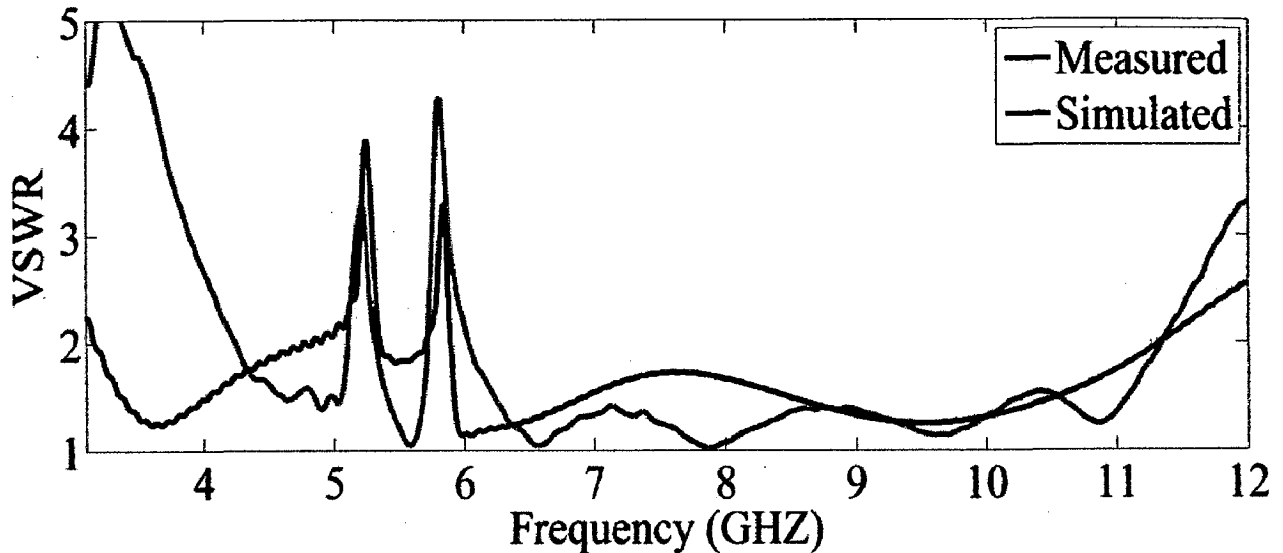


Figure 4.16 Measured and simulated VSWR of the CPW fed monopole antenna with double notch

Figure 4.16 shows the simulated and measured VSWR of the proposed antenna with double notch. The two notches of the fabricated antenna occur at 5.1-5.3GHz and 5.7-6.05GHz. As is evident from the figure, the results of experimental antenna are in good agreement with the simulation results.
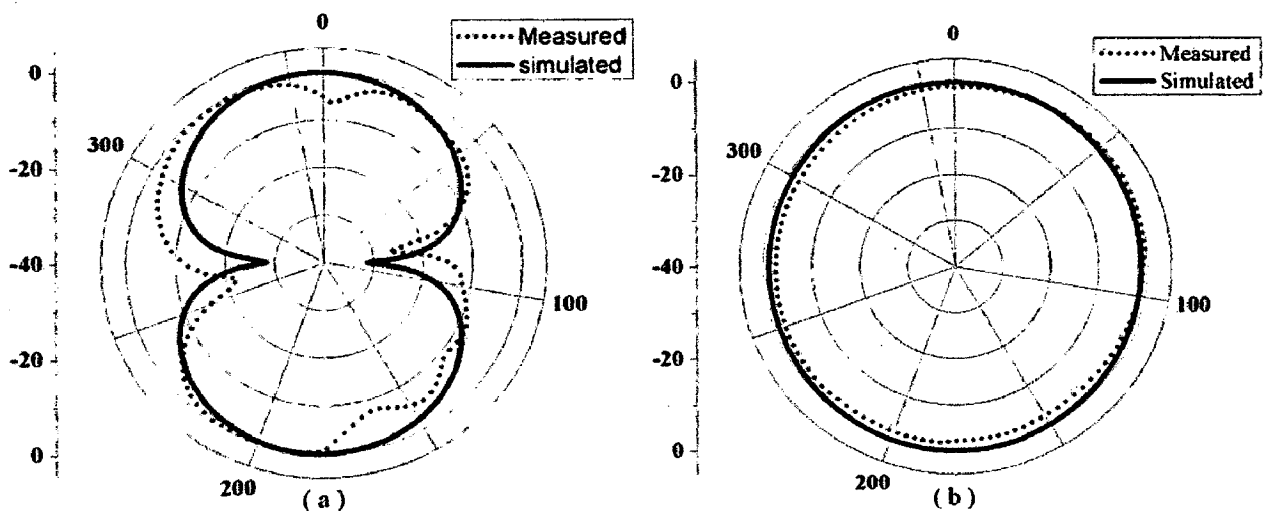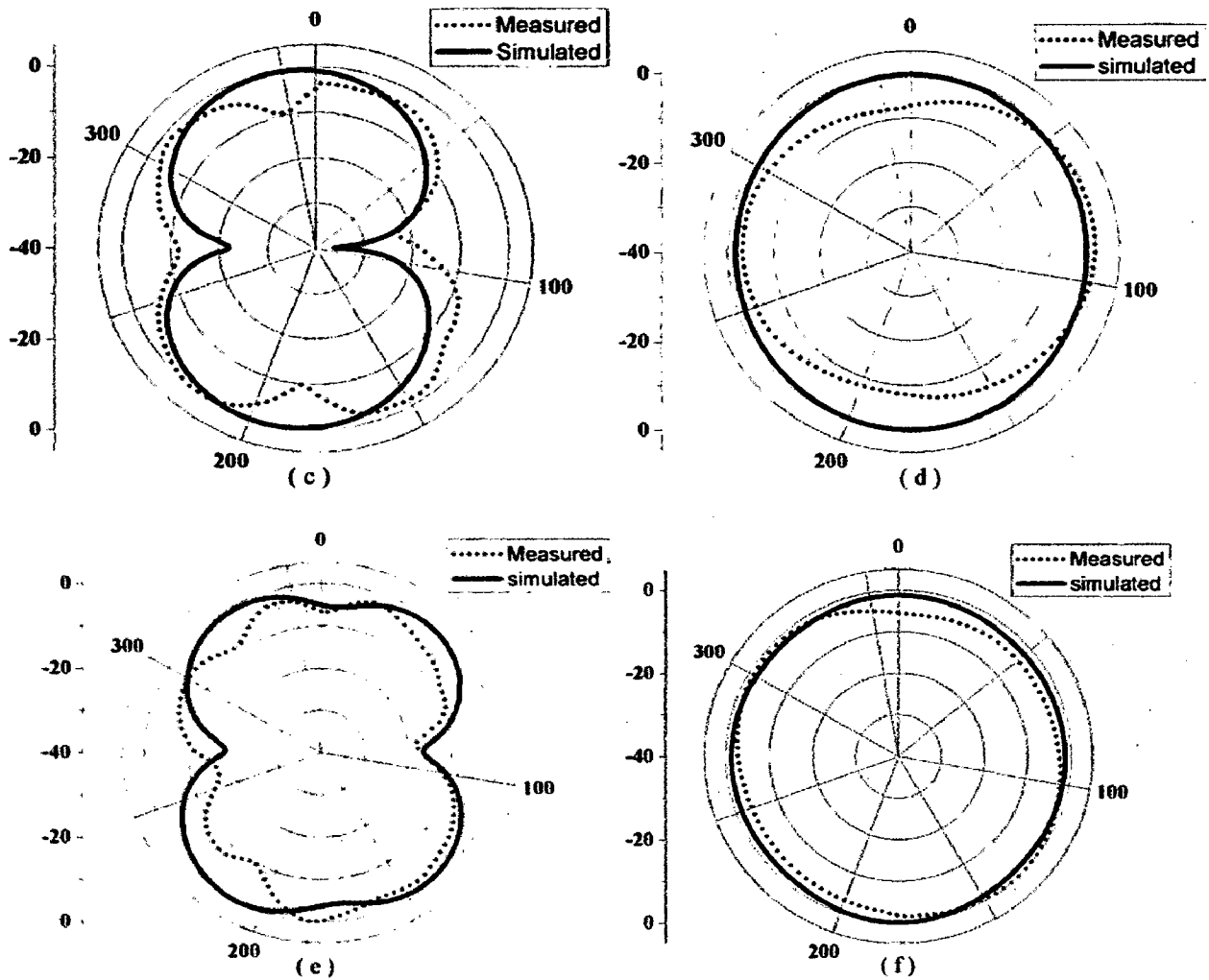
Figure 4.17    Simulated and measured radiation patterns of double notch antenna (a) E-plane at 4GHz (b) H-plane at 4GHz (c) E-plane at 6GHz (d) H-plane at 6GHz (e) E-plane at 9GHz (f) H-plane at 9GHz

The measured and the simulated normalized E-plane and H-plane radiation patterns at 4GHz, 6GHz and 9GHz are shown in figure 4.17. Again a good agreement between the two can be seen. In the case of CPW-fed antenna, it is found that the E-plane radiation patterns do not tilt like they do in microstripline-fed monopole antenna (Figure 3.28). The H-plane radiation patterns are reasonably Omni-directional over the operating bandwidth.
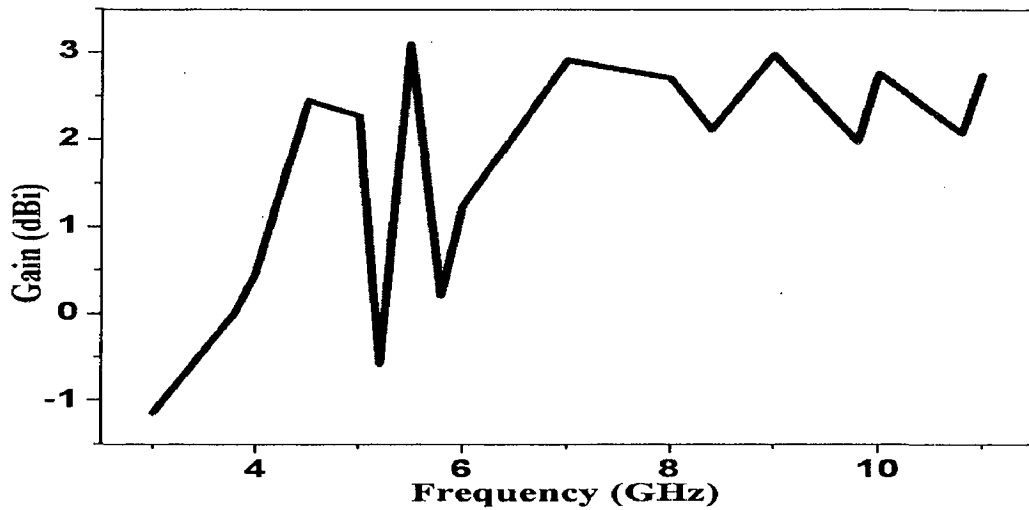
Figure 4.18 Measured gain of the CPW fed monopole antenna with double notch

The measured peak gain of the proposed antenna is plotted in figure 4.18. It can be seen that a gain of 2-3dB is obtained over most of the operating band except the notch frequencies where there is sharp dip in the gain.

The group delay of the antenna is shown in Figure 4.19 where it can be seen that only at the notch frequencies, the group delay is more. At other frequencies, the group delay is relatively small, causing less distortion in the transmitted signal.
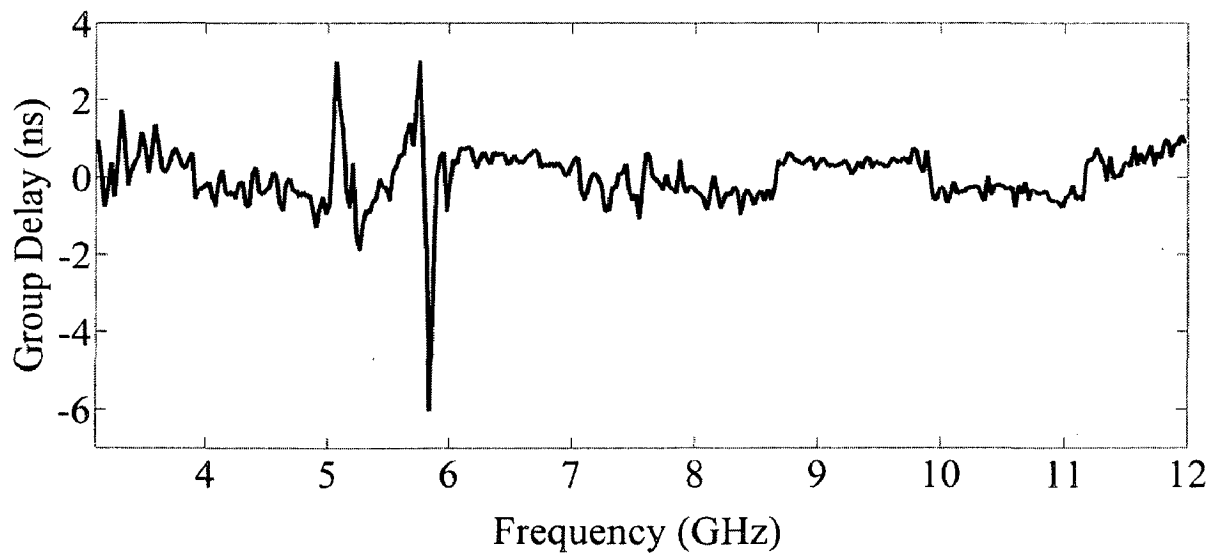


Figure 4.19 Group delay of CPW fed monopole antenna with double notch

## 4.2.2 Time domain characteristics

As mentioned in chapter 3, the UWB communication link can be modelled as the transmitting antenna, the channel and receiving antenna. Two identical CPW-fed monopole antennas were fabricated for studying the time-domain performance of the proposed double band-notched antenna. Measurement of complex S21 was carried out in real indoor scenario by using Rohde & Schwarz ZVM Vector Network Analyzer (VNA). The magnitude of S21 is shown in Figure 4.20 where the two dips at notch frequency can be clearly observed. The phase of S21 varies linearly with frequency except at notch frequencies and is shown in Figure 4.21.
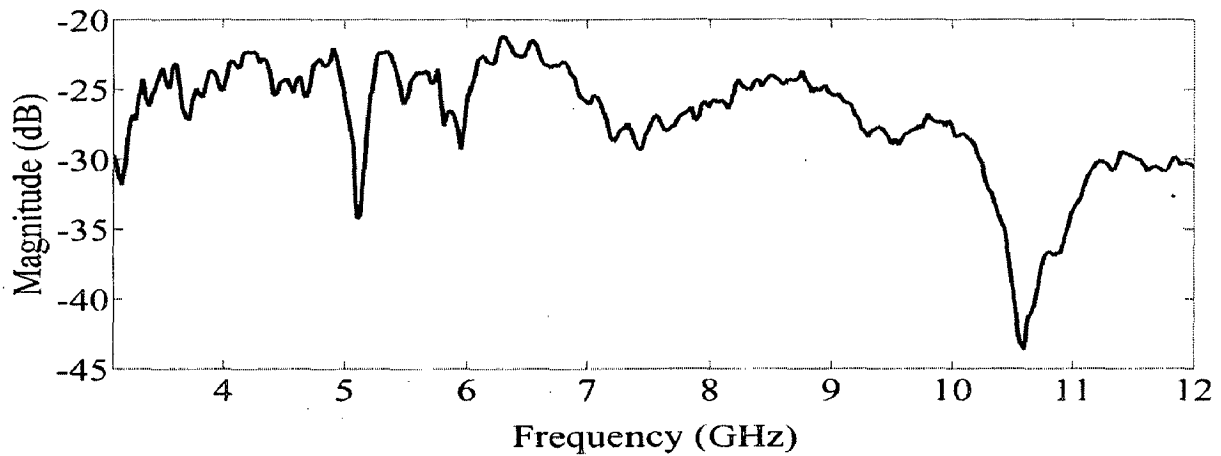


Figure 4.20 Magnitude of measured transfer function of CPW fed monopole antenna with double notch
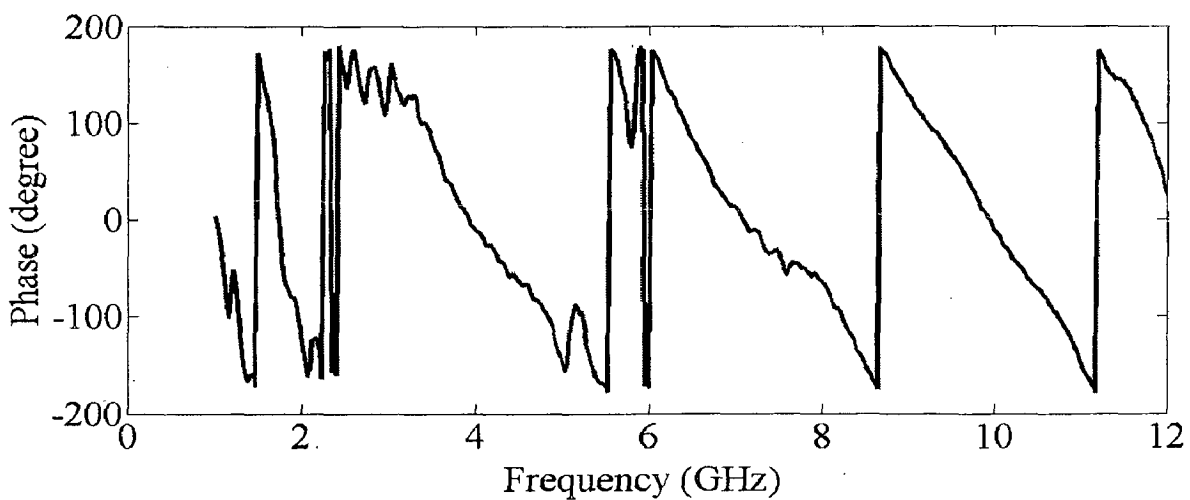


Figure 4.21 Phase of measured transfer function of CPW fed monopole antenna with double notch

## 4.2.2.1 Impulse response

The frequency response of the system (S21) is transformed to time domain using Hermitian processing. First, the pass-band signal is obtained with zero padding from the lowest frequency down to direct current; second, the conjugate of the signal is taken and reflected to the negative frequencies. The resultant double-sided spectrum corresponds to a real signal, i.e. the system impulse response. It is then transformed to the time domain using inverse fast Fourier transform (IFFT) to obtain the impulse response. The impulse response so obtained, is shown in figure 4.22.
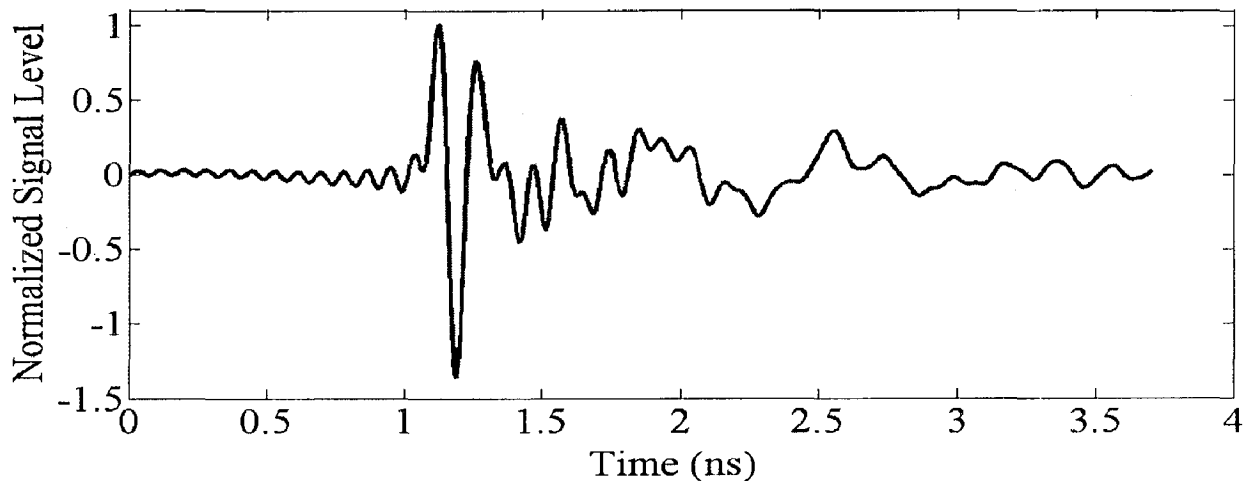


Figure 4.22 Impulse Response of the CPW fed monopole antenna with double notch

## 4.2.2.2 Received signal

The received signal can be obtained by convolving the input pulse with the impulse response of the antenna. The received pulses for modulated Gaussian pulse with fc=8GHz, fourth order Rayleigh pulses and modulated Gaussian pulse with fc=5.2GHz are shown in figure 4.23, figure 4.24 and figure 4.25, respectively. The main energy of modulated Gaussian input signal with fc=8GHz lies from 7GHz to 9GHz (Figure 3.43) which is not affected by the double notch. So the measured fidelity factor is near to 0.9767 and the received signal is almost distortion less. For fourth order Rayleigh pulse, the measured fidelity factor has slightly reduced to 0.8406 as its PSD (Figure 3.47) includes notch bandwidth. Thus UWB antenna just acts as a band-pass filter and does not reshape the signal.
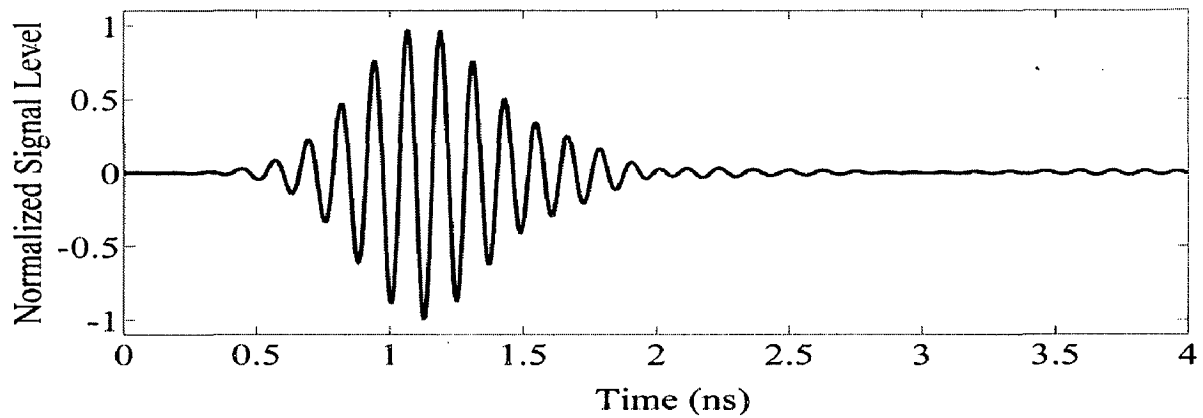
Figure 4.23 Received Pulse for Modulated Gaussian pulse with fc=8GHz
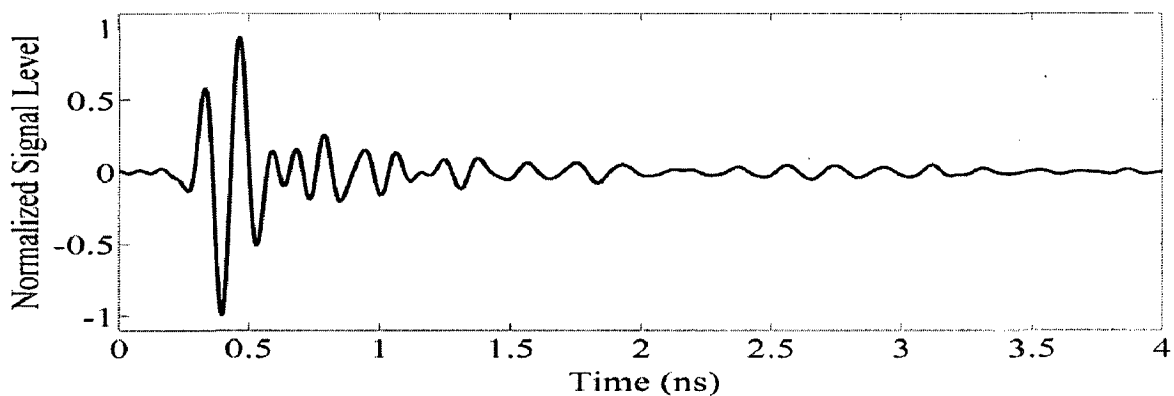


Figure 4.24 Received Pulse for Rayleigh Fourth order pulse

In order to study the effect of modulation frequency, a Gaussian pulse with modulation frequency fc=5.2GHz has been chosen in order to analyze the operation when a source pulse is transmitted around the notch bandwidth. The received signal is severly distorted as shown in figure 3.89 and the fidelity is reduced to 0.9209. This shows that a proper choice of modulation frequency is important for distortion less transmission.
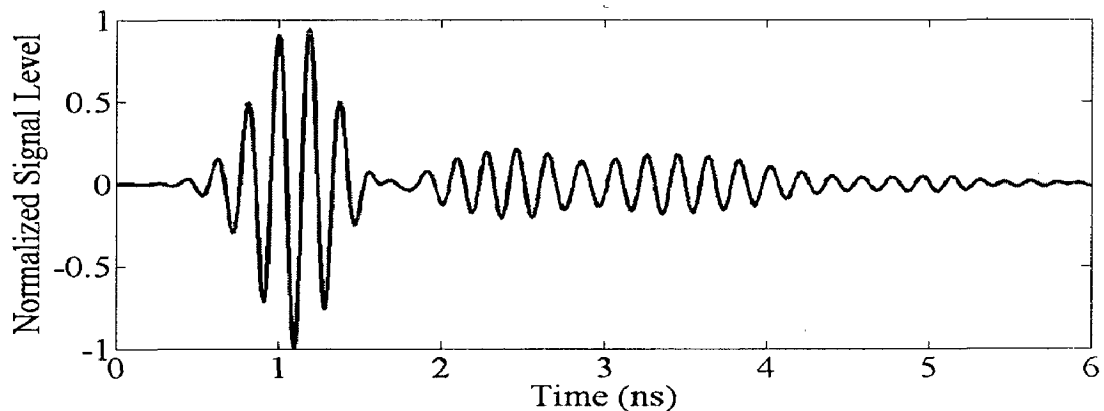


Figure 4.25 Received Pulse for Modulated Gaussian pulse with fc=5.2 GHz

# 5. CONCLUSION AND FUTURE SCOPE

## 5.1 Conclusion

New designs for microstripline-fed and CPW-fed UWB monopole antennas with a capability to reject WLAN bands have been presented. Different types of tapers are investigated to achieve the impedance match over the desired band. For microstrip line fed monopole antenna Klopfenstein taper is found to give better impedance matching. For CPW fed monopole antenna a linear taper has been found to give better impedance matching. A parametric study of various dimensional parameters is carried out on CST Microwave Studio with the aim of understanding their effect on antenna characteristics.

The overlapping of closely spaced resonances results in ultra wideband. It is observed that microstrip line fed and CPW fed monopole antennas proposed in this dissertation are capable of supporting multiple resonances.

The operating principle of microstrip line fed and CPW fed monopole antenna is discussed with the help of H-field distribution over the antenna. At low frequencies, antenna size is comparable to the wavelength of operation. This causes the standing wave to dominate at low frequencies. When the frequency is increased a hybrid mode of standing wave and travelling wave appears over the antenna. As frequency increases, the antenna size became large compared to the wavelength of operation. Hence, the wave travels a longer distance before getting reflected from the tip of the antenna structure. At high frequency end of UWB band, the travelling wave dominates over the standing wave.

UWB operating bandwidth overlaps with the WLAN operating frequencies. In order to avoid interference with WLAN devices, it is desirable to have band-rejection notches at 5.2GHz and 5.8GHz. A microstripline-fed monopole antenna with single notch is proposed in this dissertation. The effect of notch bandwidth on the ringing effect is discussed.

The single band notching method prevents the usage of the spectrum between 5.2GHz and 5.8GHz. To use the band effectively, a UWB antenna with double notch at 5.2GHZ and 5.8GHz is proposed. This antenna allows the usage of frequency spectrum between the WLAN bands. As the notches are closely spaced, mutual coupling between them must be reduced. In the microstrip line fed monopole antenna double notch has been introduced by

combining a T-shaped parasitic strip in the ground plane and CSSRR in the patch. In CPW fed monopole antenna double notch has been introduced by combining a slot in the patch and a pair of CSSRR in the ground plane.

The E-plane and H-plane radiation patterns are measured for all of the proposed antennas at three different frequencies wide distributed over the UWB spectrum. The H-plane radiation patterns are reasonably omnidirectional over the operating bandwidth. The tilting of E-plane radiation pattern at high frequencies is negligible in CPW-fed monopole antennas. The measured peak gain of the proposed antennas is plotted. For double notch antennas, a gain of 2-4dB is obtained over most of the operating band except at the notch frequencies where there is a sharp dip in the gain.

The group delay is used to find the nonlinearity in the system. Only at the band notched frequency, group delay is more while group delay is less minimal at other frequencies, causing less distortion to the transmitted pulse. The importances and design of source pulses are explained in detail.

The frequency response of the system, S21, has been measured by fabricating two identical antennas and by using network analyzer. The impulse response of the UWB system has been found using Hermitian processing. Later, the received pulse is obtained by performing discrete convolution between source pulse and the impulse response.

The microstrip line fed monopole antenna with double notch gives fidelity of 0.99 and 0.85 for modulated Gaussian pulse and fourth order Rayleigh pulse respectively. The CPW fed monopole antenna with double notch gives fidelity of 0.98 and 0.84 for modulated Gaussian pulse and fourth order Rayleigh pulse respectively. It is clearly observed that both the microstrip line fed monopole antenna and the CPW fed antenna have better time domain performance.

## 5.2 Future Scope

The UWB antenna performance embedded with portable devices like pen drive has to be investigated. The performance has to be investigated in the presence of a human body. As UWB antenna is integrated with portable devices, further size reduction has to be done.

Some applications require UWB antenna with directive nature. So UWB antennas with high gain have to be designed. UWB antenna with circular polarization should be investigated to reduce the losses due to orientation.

The E-plane radiation patterns at high frequencies are distorted in microstripline-fed monopole antennas. Methods to improve the stability of radiation patterns at high frequencies have to be investigated. UWB antenna with low ringing effect should be further analyzed.

# References

[1] First Report and Order in the Matter of Revision of Part 15 of the Commission's Rules Regarding Ultra-Wideband Transmission Systems Apr. 22, 2002, ET Docket 98-153, Federal ommunicationsCommission, FCC 02-48.

[2] J. G. Proakis, *Digital Communications*, New York: McGraw-Hill, 1989.

[3] J. R. Andrews, "UWB signal sources, antennas & propagation," Application note AN-14a, Picosecond Pulse Labs, Boulder, Colo, USA, August 2003.

[4] Nguyen Duy Thong Vu Van Yem," Combining two methods to enhance band-notch characteristic of Ultra Wide Band antenna", *International Conference on Advanced Technologies for Communications*, Oct.2009.

[5] Binggang XIAO, Xiumin WANG, Jixiang ZHAO, "A Band Notched Ultra-wideband Antenna Using Complementary Split Ring resonator" *Wireless Communications, Networking and Information Security (WCNIS), 2010 IEEE International Conference* on 25-27 June 2010.

[6] Ki-Hak-Kim and Seong-Oak-Park, "Analysis of the small bandrejected antenna with parasitic strip for UWB," *IEEE Transactions on Antennas and propagation*, Vol 54, Issue 6,p. 1688-1692, june2006.

[7] S. W. Su, K. L. Wong, and C. L. Tang, "Ultra-wideband square planar monopole antenna for IEEE 802.16a operation in the 2–11-GHz band," *Microw. Opt. Technol. Lett.*, vol. 42, no. 6, pp. 463–466, Sept. 2004.

[8] V.H. Rumsey, "Frequency Independent Antennas," *1957 IRE National Convention record*, pt. 1, pp. 114-118.

[9] H. Schantz, *The Art and Science of Ultra wideband Antennas*, Artech House Inc., 2005.

[10] http://www.tuc.nrao.edu/~demerson/bose/bose.html

[11] C. A. Balanis, *Antenna Theory Analysis and Design*, 2nd ed. New York: John Wiley and Sons, 1997.

[12] Y. Mushiake, "Self-Complementary Antennas", *IEEE Antennas and Propagation Magazine*, vol. 34, no. 6, December 1992, pp. 23-29.

[13] Choi, S. H., J. K. Park, S. K. Kim, and J. Y. Park, "A new ultra-wideband (UWB) antenna for UWB applications," *Microsystem Group, Materials and Devices Lab, LG Electronics Institute of Technology, Wiley Periodicals*, Inc., 2004.

[14] J. Liang, C.C.Chiau, X. Chen, and C.G.Parini, "Printed circular disc monopole antenna for ultra wideband applications", *Electronics Letters*, vol. 40, no. 20, pp. 1246-1248,30th September 2004.

[15] J. Jung, W. Choi, and J. Choi, "A small wideband microstrip-fed monopole antenna," *IEEE Microw. Wireless Compon. Lett.*, vol. 15,no. 10, pp. 703–705, Oct. 2005.

[16] A.A. Eldek, "Numerical Analysis of a small Ultra Wideband Microstrip-fed Tap Monopole antenna, " *Progress in Electromagnetics Research*, Vol. 65, pp 59-69,2006.

[17] J. R. Verbiest and G. A. E. Vandenbosch, "A novel small-size printed tapered monopole antenna for UWB WBAN," *IEEE Antenna Wireless Propag. Lett.*, vol. 5, pp. 377–379, 2006.

[18] K. Chung, J. Kim, and J. Choi, "Wideband microstrip-fed monopole antenna having frequency band-notch function," *IEEE Microw. Wireless Compon. Lett.*, vol. 15, no. 11, pp. 766–768, Nov. 2005.

[19] R. Zaker, C. Ghobadi, and J. Nourinia, "Novel modified UWB planar monopole antenna with variable frequency band-notch function," *IEEE Antenna Wireless Propag. Lett.*, vol. 7, pp. 112–114, 2008.

[20] Chen, Z.-N., See, T.-S., and Qing, X, "Small printed ultrawideband antenna with reduced ground plane effect", *IEEE Trans. Antennas Propag.*, 2007, vol 55, no 2, pp. 383–388.

[21] H.-W. Liu and C.-F. Yang,"Miniature hook-shaped monopole antenna for UWB applications," *Electron.Lett.*, Vol. 46, No. 4 18th February 2010.

[22] H. Schantz, M. Barnes, "The COTAB UWB Magnetic Slot Antenna," *IEEE APS 2001* (July 2001).

[23] H. Schantz, "UWB Magnetic Antennas," *IEEE APS 2003*.

[24] Guillanton, E., Dauvignac, J.Y., Pichot, C., and Cashman, J.: 'A new design tapered slot antenna for ultra-wideband applications', *Microw.Opt. Tech. Lett.*, 1998, vol 19, issue 4, pp. 286–289.

[25] E. Gazit, "Improved Design of the Vivaldi Antenna," *Proc. Inst.Elect. Eng.*, Vol. 135, Pt. H, No. 2, 1988, pp. 89-92.

[26] T.-G. Ma and S.-K. Jeng, "A novel compact ultra-wideband printed dipole antenna with tapered slot feed," in Proc. *IEEE Antennas Propagation Soc. Int. Sym.*, vol. 3, Jun. 2003, pp. 608–611.

[27] X. Qing, M. Y. W. Chia, and X. Wu, "Wide-slot antenna for UWB Applications," in Proc. *IEEE AP-S Int. Symp.*, Jun. 2003, vol. 1, pp.834–837.

[28] J. Y. Sze. K.L. Ong, "Bandwidth Enhancement of a Microstrip-Line-Fed Printed Wide-Slot Antenna." *IEEE Trans Antenna and Propagation*, vol. 49, pp.1020-1024, July 2001.

[29] N. Arsusiri, O. Sangaroon, S. Puntheeranurak and N. Anantrasirichai, "A Study on Tuning-Stub of Slot Antenna for Ultra-Wideband Applications," *International Conference on Control, Automation and Systems*, Oct. 27-30, 2010.

[30] J. Y. Sze and C. C. Chang, "Circularly polarized square slot antenna with a pair of inverted-L grounded strips," *IEEE Antennas Wireless Propag. Lett.*, vol. 7, pp. 149–151, 2008.

[31] J. Pourahmadazar, Ch. Ghobadi, J. Nourinia, Nader Felegari, and Hamed Shirzad, "Broadband CPW-Fed Circularly Polarized Square Slot Antenna With Inverted-L Strips for UWB Applications," *IEEE Antennas Wireless Propag. Lett.,*, VOL. 10, 2011.

[32] Y. Ranga, L. Matekovits,P. Esselle and R. Weily,"Enhanced Gain UWB Slot Antenna with Multilayer Frequency-Selective Surface Reflector,"Antenna Technology (iWAT), 2011 International Workshop on 7-9 March 2011 On page(s): 176.

[33] H.-D. Chen, J.-S. Chen and J.-N. Li, "Ultra-wideband square-slot antenna", *Microw. Opt. Technol. Lett.*, vol. 48,no. 3, pp.500-502, Jan. 2006.

[34] H. G. Booker, "Slot aerials and their relation to complementary wire aerials," *Proc. IEE*, pt. IIIA, 90, 4, pp. 620-629, April, 1946.

[35] A. Saitou, T. Iwaki, K. Honjo, K. Sato, T. Koyama, and K. Watanabe, "Practical realization of self-complementary broadband antenna on low-loss resin substrate for UWB applications," in *IEEE MTT-S Int.Microw. Symp. Dig.*, Jun. 2004, pp. 1265–1268.

[36] L. Guo, X. Chen and C.G.Parini, "A printed Quasi-Self-Complementary Antenna for UWB Applications", *2008 IEEE AP-S International Symposium on Antenna and Propagation*, San Diego, U.S.A, July 5-12, 2008.

[37] L. Guo, S. Wang, X. Chen and C.G.Parini, "A Printed Miniature Antenna for UWB Applications", *2010 IEEE AP-S International Symposium on Antenna and Propagation*, Toronto, Canada, July 11-17, 2010.

[38] Kerkhoff A., and Ling H., "Design of a planar monopole antenna for use with ultrawideband (UWB) having a band-notched characteristic," *IEEE Antennas and Propagation Society International Symposium 2003*, Vol.1, pp.830-833, 22-27 June 2003.

[39] Schantz H.G., Wolenec G., and Myszka E.M., "Frequency notched UWB antennas," *IEEE Conference on Ultra Wideband Systems and Technologies 2003*, pp.214-218, 16-19 Nov. 2003.

[40] Tharaka Dissanayake and Karu P. Esselle, "Design of Slot Loaded Band-Notched UWB Antennas" *Antennas and Propagation Society International Symposium*, Vol 1B, pp 545-548 , 2005.

[41] H. Yoon, H. Kim, K. Chang, Y. J. Yoon, and Y. H. Kim, "A study on the UWB antenna with band-rejection characteristic," in *Proc. IEEE AP-S Int. Symp.*, Jun. 2004, vol. 2, pp. 1784–1787.

[42] I. J. Yoon, H. Kim, K. Chang, Y. J. Yoon, and Y. H. Kim, "Ultra wideband tapered slot antenna with band-stop characteristic," in *Proc. IEEE AP-S Int. Symp.*, Jun. 2004, vol. 2, pp. 1780–1783.

[43] K. H. Kim, Y. J. Cho, S. H. Hwang, and S. O. Park, "Band-notched UWB planar monopole antenna with two parasitic patches," *Electron.Lett.*, vol. 41, no. 14, pp. 783–785, Jul. 2005.

[44] C. Hong, C. Ling, I. Tarn, and S. Chung, "Design of a planar ultrawideband antenna with a new band-notched structure," *IEEE Trans.Antennas Propagat.*, vol. 55, pp. 3391–3397, Dec. 2007.

[45] Y.L. Cai and Z.H. Feng, "A UWB antenna with novel L-branches on ground for band-notching application," IEEE, ICMMT2008 Proceedings,vol. 4, 2008, pp. 1654–1657.

[46] J.Kelly ,P.Hall,P.Gardner, "Band-Notched Ultra-Wideband Antenna Incorporating a Microstrip Open-Loop Resonator", *IEEE Trans. Antennas and Propagation*, issue 99, pp. 1, May 20011.

[47] Y. Zhu, F.S. Zhang, C. Lin, Y.C. Jiao and R. Zou,"Design of band-notched structure for UWB applications," *Electron.Lett.*, Vol. 47, No.4, Feb2011.

[48] Lin Peng,  Cheng-Li Ruan , "UWB Band-Notched Monopole Antenna Design Using Electromagnetic-Bandgap Structures", *IEEE Transactions on Microwave Theory and Techniques*, vol. 59, issue 4, pp. 1074-1081, April 20011.

[49] Ming-Chun Tang, Shaoqiu Xiao, Tianwei Deng, Duo Wang, Jian Guan, Bingzhong Wang, and Guang-Ding Ge,"Compact UWB Antenna With Multiple Band-Notches for WiMAX and WLAN," *IEEE Trans. Antennas and Propagation* ,VOL. 59, NO. 4, APRIL 2011.

[50] Zamel, H.M. Attiya, A.M. Hashish, E.A. , " Design of a Compact UWB Planar Antenna with Band-Notch Characterization", *National* Radio Science Conference, pp. 1-8 ,Mar.2010.

[51] D. M. Pozar, *Microwave Engineering*, third edition, John Wiley, 2005

[52] http://www.mathworks.de/matlabcentral/fileexchange/22996-rf-utilities-v1-2

[53] H. Celebi, M. E. Sahin, H. Arslan, J. Haque, E. R. Prado, and D. P. Markell, "Ultrawideband design challenges for wireless chip-to chip communications and interconnects," in *Proc. IEEE Aerosp. Conference* Big Sky, MT, 2006.

[54] B.Allen, M.Dohler, E.E.Okon, W.Q.Malick, A.K.Brown and D.J.Edwards, *Ultra-wideband Antennas and propagation for communictions, Radar and Imaging*, John Wiley, 2007.

[55] Y.Duroc, A.I.Najam, T.P Vuong and S.Tedjini, " Modeling and State Representation of Ultrawideband Antennas" *IEEE TRANSACTIONS ON ANTENNA AND PROPAGATION,* VOL.57, NO.9, September 2009.

[56] Zhi Ning Chen, Xuan Hui Wu, Hui Feng Li, Ning Yang and Michael Yan Wah Chia, "Considerations for Source Pulses and Antennas in UWB Radio Systems", *IEEE Transactions on Antennas and Propagation*, vol.52, no.7, July, 2004, pp.

[57] J. Kunisch and J. Pamp, "UWB radio channel modeling considerations," in Proc. Int. 'Conf *Electromagnetics Adv. Applications (ICEAA)*,Turin, Sep. 2003.

[58] Jianxin Liang, *Antenna Study and Design for Ultra Wideband Communication Applications*, Thesis, Department of Electronic Engineering Queen Mary, University of London United Kingdom, July 2006.

[59] Ian Oppermann, Matti Hamalainen and Jari Iinatti, *UWB Theory and Applications*, John Wiley & Sons, Ltd,2004.

[60] Alan V. Oppenheim, Alan S. Willsky, and S. Hamid Nawab, *Signals & systems (3nd ed.)*, Prentice-Hall, Inc., 2007.

# Publication

S.Theepak and S.N.Sinha, " A Compact UltraWideBand OmniDirectional Antenna With Double Notch At 5.2GHz and 5.8GHz Including Time Domain Analysis" IEEE COMCAS 2011( review results awaited).

# APPENDIX

## MATLAB PROGRAMMES

### 1 MATLAB program for Klopfenstein taper

```
function Zlist=bklop(Zo,Zload,N,RdB)
```

%       Calculate impedance list for a Klopfenstein taper of unit length.

%       Zlist=bklop(Zo,Zload,N,RdB)

%       Zo..Characteristic impedance (Ohms) ,

%       Zload...Load impedance to match to (Ohms)

%       N..Number of sections used to approximate taper (integer) ,

%       RdB.....Operating band ripple (dB)

%       e.g. Zlist=bklop(50,100,60,-25) % Match a 100ohm load to a 50ohm line

%       with operating band ripple at -25dB , Taper defined as list of 60 sections

%       Matches a load impedance Zload to a standard line impedance Zo using Klopfenstein

%       taper.

%       Impedance Values  Zo --->  [ Z1 ] [ Z2 ] ....   [ ZN ]   <-- Zload


```
Tld=log(Zload/Zo)*0.5;              % Reflection coefficient of load
Trip=10.^(RdB/20);                  % Lin value of ripple in operating band
A=acosh(Tld/Trip);                  % Intermediate variable in calculation
z=0;                                % Fractional distance along taper
dz=1/(N-1);                         % Incremental distance
Zx=zeros(1,N);
for c=1:N                           % Loop for impedance values along taper
M=round(z*100+25);                  % Number of steps for the numerical integration
PsiXA=0;
y=0;
dy=((2*z-1)/(M-2));                 % Increment for numerical integration
for d=1:M                           % Loop for PsiXA numerical integration
PsiXA=PsiXA+besseli(1,A*sqrt(1-y.^2))/(A*sqrt(1-y.^2))*dy;
y=y+dy;
end
% Calculate impedance as a function of distance along the unit length transformer
LNZx=0.5*log(Zo*Zload)+(Tld/cosh(A))*(A.^2)*real(PsiXA);
```

```
Zx(1,c)=exp(LNZx);

z=z+dz;

end

Zlist=[Zo,Zx,Zload];          % Assemble the list of impedances for output
```

## 2 MATLAB program for mapping impedance to width of the microstrip antenna

```
function out=impedtoline(z0)

er=3.38;

%z0=50;

d=1.524;

A=((z0*sqrt((er+1)/2))/60)+(((er-1)/(er+1))*(0.23+(0.11/er)));

B=(188.5*pi)/(z0*sqrt(er));

temp=(8*exp(A))/(exp(2*A)-2);

temp1=B-1-log(2*B-1);

temp2=((er-1)/(2*er))*(log(B-1)+0.39-(0.61/er));

temp3=(2/pi)*(temp1+temp2);

if temp<2

   w=temp*d;

else

   w=temp3*d;

end

out=[w];
```

## 3 MATLAB program for modulated Gaussian pulse, Rayleigh fourth order and Rayleigh first order

```
clc;    close all;    close all;    /

%%%%%%    Modulated Gaussian pulse    %%%%%%

dt=1/79.035;

t=0.7:0.012653:1.3;

t=t*(1E-09);

a=67E-12;

temp1=12/(a*a*a*a);
```

```matlab
temp2=(48/(a*a*a*a*a*a))*((t-(1E-09)).*(t-(1E-09)));

temp3=(16/(a*a*a*a*a*a*a))*((t-(1E-09)).*(t-(1E-09)).*(t-(1E-09)).*(t-(1E-09)));

temp4=exp(-(  ((t-(1E-09))/a).*((t-(1E-09))/a)  ));

temp=((temp1-temp2+temp3).*temp4)/6E41;

Fs = 79.035*(1E+09);

[freq value]=periodogram(temp,[],'onesided',512,Fs);hold on;grid on;

freq=10*log10(freq);

freq=freq-max(freq)-41.3;

figure1=plot(value(1:5:150)/1E+09,freq(1:5:150),'--rs','LineWidth',3);hold on;

xlabel({'Frequency (GHz)'},'fontsize',30);

ylabel({'Power Spectral Density (dBm/MHz)'},'fontsize',24);

legend(figure1, 'Modulated Gaussian Pulse');


%%%%%%    Rayleigh Fourth order    %%%%%%
dt=1/79.035;

t=0.1:dt:1.9;  %0.012653

t=t.*1E-09;

a=350*1E-12;

y=exp(-power(((t-1E-09)/a),2));

fc=8E+09;

temp=sin(2*pi*fc*(t-1));

temp2=temp.*y;

Fs = 79.035*(1E+09);

[freq1 value1]=periodogram(temp2,[],'onesided',512,Fs);hold on;

freq1=10*log10(freq1);

freq1=freq1-max(freq1)-41.3;

figure1=plot(value1(1:150)/1E+09,freq1(1:150),'b','LineWidth',3);

legend(figure1,'Rayleigh Fourth order Pulse');


%%%%%%    Rayleigh First order    %%%%%%
dt=1/189.035%79.035;

t=0.7:dt:1.3;

t=t*(1E-09);

a=30E-12;
```

```matlab
temp1=-(2*(t-(1E-09)))/(a*a);

temp2=exp(-( ((t-(1E-09))/a).*((t-(1E-09))/a) ));

temp=(temp1.*temp2);

temp=temp/max(abs(temp));

Fs = 189.035*(1E+09);

[freq1 value1]=periodogram(temp,[],'onesided',512,Fs);hold on;

freq1=10*log10(freq1);

freq1=freq1-max(freq1)-41.3;

xlabel({'Frequency (GHz)'},'fontsize',30);

ylabel({'Power Spectral Density (dBm/MHz)'},'fontsize',24);

figure1=plot(value1(1:150)/1E+09,freq1(1:150),'b','LineWidth',3); hold on;

legend(figure1, 'Rayleigh Fourth order Pulse');
```

## 4 MATLAB program for impulse response, received signal and fidelity

```matlab
clc;     close all;     clear all;

S21=importdata('I:\ s21.mat');

mag=S21(:,2);          freq=S21(:,1);

plot(freq/1E+09,mag,'LineWidth',3);

xlabel({'Frequency (GHz)'},'fontsize',30);

ylabel({'Magnitude (dB)'},'fontsize',30);     figure;

mag=10.^(mag/20);

mag=mag/(max(abs(mag)));

s21r1=mag.*(cosd(S21(:,3))+sqrt(-1)*sind(S21(:,3)));

n1=length(s21r1);

DC=36;

s21r(1:DC)=zeros(1,DC);

s21r(DC+1:DC+n1)=s21r1;

N2 =length(s21r);

s21r(N2+3000)=0;

N =length(s21r);

s21=zeros(1,2*N-1);

s21(1:N)=s21r(1:N);

s21c=conj(s21r);

s21(N+1:2*N-1)=s21c(N:-1:2);
```

```
N7=length(s21);

H=ifft(s21);

dt=1/(189.035*(1E+09));

N8=floor(N7/2);

H1=circshift(H,[0 N8]);

plot((0:dt:700*dt)/1E-09,H1(3300:4000)/max(H1(3300:4000)),'LineWidth',3);

xlabel({'Time (ns)'},'fontsize',28);

ylabel({'Normalized Signal Level'},'fontsize',28);

[sig,tim]=gaussianmodulated;%rayleigh;%

Fs = 189.035*(1E+09)%79.035*(1E+09);%

con=conv(H1,sig);

N4=length(con);

T=N4*dt;

t=0:dt:T-dt;

con1=[ con(3500:4800) ];

t1=t(3500:4799)-t(3500)

diffsc=diff(con1);

diffsc=diffsc/max(abs(diffsc));

plot(t1/1e-09,diffsc,'LineWidth',3);

ylabel({'Normalized Signal Level'},'fontsize',28);     xlabel({'Time (ns)'},'fontsize',28);

diffs=diff(sig);

diffs=diffs/max(abs(diffs));

x1=diffs;

y=con;

m=length(con);

m1=length(x1);

x=[x1 zeros(1,m-m1)]

temp=x.*x;

engs=sum(temp);

temp1=y.*y;

engo=sum(temp1);

eng=sqrt(engs*engo);

n1=length(x);

n2=length(y);
```

```matlab
a=zeros(1,n1+n2-1);
m=n1;
for j=1:n1
  k=j;
  for i=n1:-1:m
     a(j)=a(j)+(x(i)*y(k));
     k=k-1;
  end
  m=m-1;
end
m=n1;
for j=length(a):-1:n1+1
  k=1;
  for i=m:n1
   a(j)=a(j)+( x(k)* y(i));
   k=k+1;
  end
  m=m-1;
end
a=a/eng;
max(a)
```